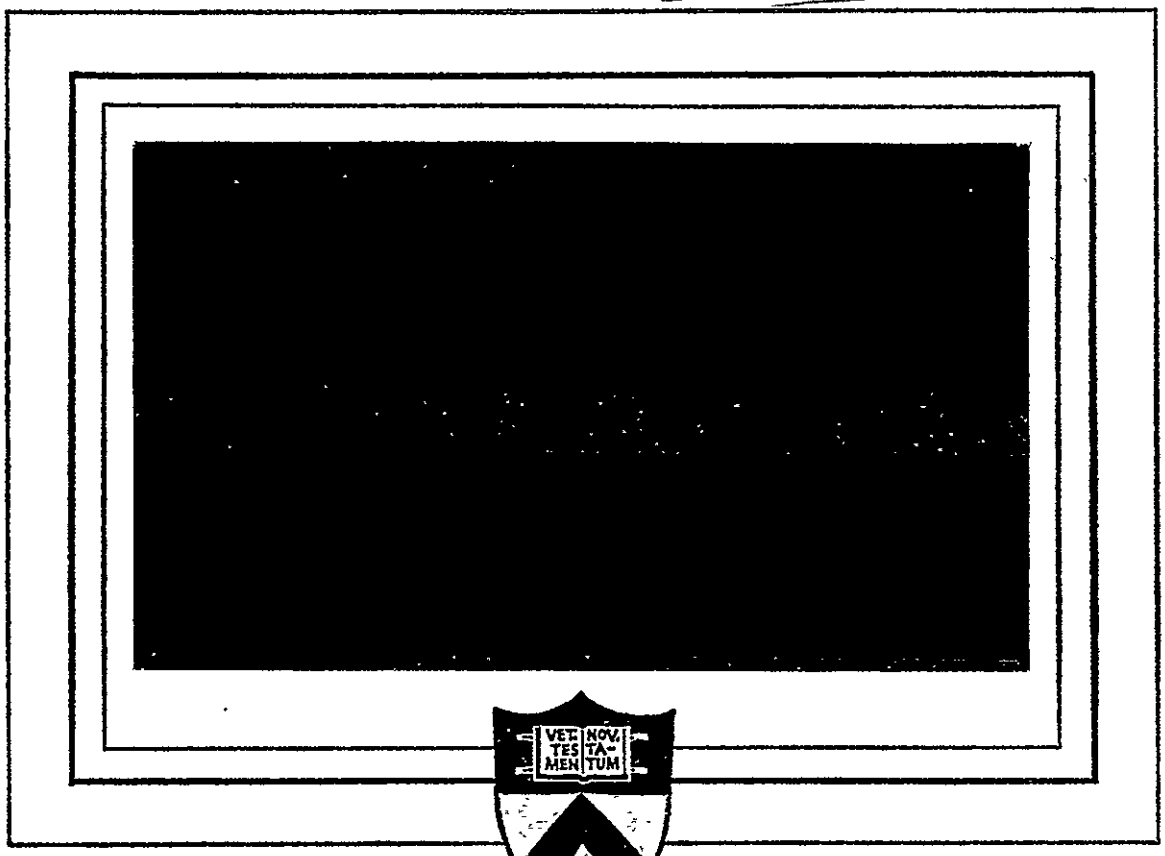

PRINCETON UNIVERSITY

DEPARTMENT OF

AEROSPACE AND MECHANICAL SCIENCES

Prepared for
National Aeronautics
and Space Administration
NASA Research Grant NGL 31-001-005

ANODE PHENOMENA IN HIGH-CURRENT DISCHARGES

R. C. Oberth and R. G. Jahn

Report 961*

Prepared by Ronald C. Oberth
RONALD C. OBERTH

Approved by Robert G. Jahn
ROBERT G. JAHN
Professor of Aerospace Sciences
and Principal Investigator

*This report is a reproduction in entirety of the Ph.D. dissertation of Mr. Ronald C. Oberth. It is submitted to the sponsor and to the distribution list in this form both as a presentation of the technical material, and as an indication of the academic program supported by this Grant.

December 1970

School of Engineering and Applied Science
Department of Aerospace and Mechanical Sciences
Guggenheim Aerospace Propulsion Laboratories
PRINCETON UNIVERSITY
Princeton, NJ 08540

ABSTRACT

An experimental investigation of a large-radius pinch discharge has revealed that the cylindrical current sheet develops a broad and diffuse anode attachment which, under certain conditions, divides into two distinct regions of high current density. Furthermore, the existence of precursor current conduction at downstream anode locations was inferred from data which showed a substantial increase in arc voltage in response to insulation of the central portions of the pinch anode. Other experiments indicated that both of the above noted anode phenomena occur in a parallel-plate accelerator, and also that the analogous cathode processes arise at somewhat later times in the discharge history. Experimental study of various anode processes in a quasi-steady MPD arc has clarified certain aspects of the current conduction and power loss mechanisms in these devices. Measurements of anode fall voltage and local anode current density at "matched" operating conditions have defined an overall inverse relationship between these two quantities which is reciprocal in form. This result translates into a significant decrease in fractional anode power loss for quasi-steady MPD arc operation in the megawatt range of pulse power. For matched and overfed mass flows, anode current conduction in this device is accomplished by random thermal flux of electrons from the adjacent arc plasma; for underfed conditions, substantial electric fields develop around the anode in order to support anode current conduction at this low plasma density situation.

CONTENTS

LIST OF ILLUSTRATIONS

TABLE

CHAPTER I

INTRODUCTION

By detailed mission analysis, and by consideration of the equation of motion for a rocket, it has been shown that interplanetary space missions can only be effectively carried out by space thrusters which provide specific impulses of over 1000 sec; i.e., propellant exhaust velocities in excess of 10,000 m/sec. Exotic chemical and nuclear rockets have been extended to specific impulses in the 800 sec range, but it is becoming increasingly apparent that a different propulsion concept is required to achieve those values of specific impulse demanded by future space missions. The acceleration of gases by electrical heating and/or by electric and magnetic body forces has demonstrated a very high specific impulse capability at relatively low thrust densities, and now defines a promising new propulsion system known as electric space propulsion. The penalty of low thrust capability is not severe in the weak gravitational fields of interplanetary space; and is more than counterbalanced by the much higher ratio of payload mass to initial rocket mass achievable by means of the high exhaust velocities of electric space thrusters.

Jahn[1] subdivides the field of electric propulsion into three classes:

1. Electrothermal propulsion, wherein the propellant gas is heated electrically, then expanded in a suitable nozzle.

2. Electrostatic propulsion, wherein the propellant is accelerated by direct application of electric body forces to ionized particles.

3. Electromagnetic propulsion, wherein an ionized propellant stream is accelerated by interactions of external and internal magnetic fields with electric currents driven through the stream.

Both electromagnetic as well as certain electrothermal plasma accelerators consist basically of a high-current arc discharge passing through a streaming plasma between two suitably designed and insulated electrodes. The thermal arcjet, operating on the electrothermal principle, takes advantage of very high arc column temperatures to increase the enthalpy of the propellant gas, and then converts this enthalpy to streaming energy by expanding the gas through a nozzle which also functions as the anode. At low mass feed rates and high arc currents, the propellant flow becomes almost totally ionized and the magnetic fields become sufficiently strong to enable the electromagnetic mode of plasma acceleration to take over, causing significant increase in specific impulse. Devices with coaxial electrode configuration, in which the interaction of high arc currents with self- or imposed-magnetic fields directly accelerates an ionized flow of plasma, became known as magnetoplasmadynamic (MPD) arcjets.

In general the electromagnetic class of plasma accelerators can be further subdivided into those that operate in the steady or continuous mode and those that operate in the unsteady or pulsed mode. Steady accelerators, of which the MPD arcjet has demonstrated the best performance, employ a dc power supply capable of delivering at least 3000 A of continuous current at kilowatt power levels; but, are restricted to operation in this low power range because of severe heat transfer to the electrode and limitations of the dc power supply. Unsteady plasma accelerators normally have pulse times on the order of μsecs with current levels above 10^4 A and employ a variety of electrode configurations: parallel rail, parallel plate, coaxial, and cylindrical z-pinch. The acceleration process begins when the voltage of a capacitor network is suddenly transferred to the accelerator electrodes causing the ambient gas-

fill to ionize and conduct current in a narrow region at the position of minimum inductance. The narrow current distribution, or current sheet, the shape of which depends on the accelerator geometry, is then acted upon by the $\vec{j} \times \vec{B}$ magnetic interaction forces which drive the sheet along the electrode channel, forcing it to entrain and accelerate the ambient gas to interesting propulsion velocities. Because of the very short duration of the driving-current pulse, devices of this type do not suffer from serious electrode heating and hence can operate at extremely high-power levels which appear to entail high specific impulses and high thermal efficiencies. However, pulsed accelerators are limited to a thrust efficiency of about 50% because of the inelastic piston behavior of the current sheet.[2] Furthermore, the extremely short pulse times place severe demands on the gas-feeding and power-switching systems if the accelerator is to be effectively operated in a repetitive manner.

Recent studies[3] have demonstrated the feasibility and advantages of utilizing the so-called quasi-steady mode of accelerator operation, wherein self-field MPD arcjets are operated in a pulsed manner but essentially steady, high-power operation is achieved over 100 μsec to several msec pulse durations. The overall concept involves repetitive pulsing of the accelerator at repetition rates commensurate with available space power supplies, thereby affording the opportunity for variable thrust accomplished via simple duty cycle adjustment. These devices, known as quasi-steady MPD arcjets, promise high thermal efficiencies and high specific impulses,[4] both inherent to the high power regime; as well as high thrust densities along with tolerable heat transfer and mean power demands. Much of the work reported here was carried out on a quasi-steady MPD arc which is described briefly in Chap. III and with more detail in references 3 and 5.

Considerable experimental work has been done on thermal and MPD arcjets to assess the thermal efficiencies of these devices.[6–10] The results indicate that thermal efficiencies

range from 10 to 70%, with most of the power loss appearing at the anode, and also that these efficiencies tend to improve at high power levels. The investigations also indicate that most of the anode heat transfer is due to the flux of current-carrying electrons which deposit energy gained in the anode fall sheath at the anode. Hence, the magnitude of the anode fall voltages which arise in steady and quasi-steady MPD arc discharges determine, to a large extent, the amount of anode power loss, and thus the thermal efficiency of these devices. Part of this thesis, therefore, is devoted to an investigation of the anode voltage drop in a quasi-steady MPD arc.

Much of the early work on the electrode regions of the arc discharge[11] concentrated on the cathode, as it was considered to be the electrode most critical for the maintenance of the discharge. Furthermore, most of the arc discharge studies reported in the literature have been carried out on so-called classical arcs, distinguishable by currents in the ampere range and pressures near one atmosphere, conditions far removed from those of interest to electric propulsion. In recent years, studies of the anode region have been extended to thermal arcjets and steady, low-power MPD arcs where the introduction of streaming plasmas, strong magnetic fields, and coaxial geometry has added considerable complexity to the problem.[12–14] Extension of MPD arc operation into the multimegawatt power range, through the application of the quasi-steady concept, incorporates a host of new physical processes at the anode region which cannot be inferred from studies on low-power MPD arcs. Thus, in order to further the understanding of the microscopic and macroscopic processes prevailing at the anode of quasi-steady, high-power MPD arcs, in particular those of current conduction and heat transfer, this experimental research program was undertaken on the quasi-steady MPD device at Princeton.

Interest in anode phenomena in this laboratory grew originally from the early experiments of Black on an 8-in. pinch discharge employing currents of over 10^5 A for μsec pulse

durations.[15] Among other contributions, these studies pointed out the occurrence of a peculiar current sheet bifurcation; i.e., an apparent splitting of the current sheet at the midway point of its rapid collapse towards the chamber center. Later experiments revealed that the anomalous behavior was, in fact, related to a broad, diffuse, and sometimes divided current sheet anode attachment.[16] Further investigations of this phenomena uncovered a precursor conduction current at the anode surface which bears a strong influence on the resistive voltage of the pinch discharge. These studies were later extended to a pulsed parallel-plate accelerator where several modifications in electrode phenomena were observed. The results of these investigations are presented in Chap. IV and V of this thesis.

The experiments on the pinch and parallel-plate devices were concluded when it became evident that better understanding of the current sheet anode attachment and anode precursor conduction would require detailed investigations of various plasma instabilities and surface phenomena, somewhat beyond the scope of this work. At the same time, it was decided that the previously described quasi-steady MPD arc would be a more interesting facility in which to study anode processes. The electrode geometry, along with the quasi-steady nature of this MPD discharge, facilitate detailed study of the anode region with electrostatic and magnetic probes; while the present interest in quasi-steady plasma acceleration further emphasizes the importance of extending anode studies to this device. As a result, the focus of this thesis shifts after Chap. V to experiments on and analysis of the anode region of the quasi-steady MPD arc. Thus, the present investigation of anode phenomena includes experimental study at various discharge geometries: cylindrical pinch, linear parallel-plate, coaxial; and at two different operation conditions: unsteady and quasi-steady.

CHAPTER II

REVIEW OF ANODE PROCESSES IN ARC DISCHARGES

A. INTRODUCTION

The term, electric arc, is used to define a particular kind of electrical discharge characterized by high current and very low impedance. Electric arc discharges have been studied extensively for many years, and have recently become relevant to the concept of plasma acceleration because of their ability to conduct very high currents at reasonably low voltages, while producing very high plasma temperatures. High arc currents along with their attendant strong magnetic fields can be used to accelerate ionized gases to very high velocities by means of the magnetic interaction, or $\vec{j} \times \vec{B}$ body forces. Another class of accelerators, the electrothermal variety, capitalize on the high temperatures produced in the arc column, up to 50,000 ^{o}K, to increase the enthalpy of the propellant gas which is subsequently expanded through a nozzle. This chapter will acquaint the reader with some of the physical processes which participate at the anode-plasma junction of conventional electric arcs; and will also examine several more recent studies carried out on the thermal arcjets and MPD arcs referred to in Chap. I.

B. DESCRIPTION OF THE CLASSIC ELECTRIC ARC

The electric arc is distinguished from other types of gas discharges such as the corona, abnormal glow, and normal glow, by the fact that the cathode is sufficiently heated by ion bombardment to enable the thermionic emission of electrons to occur, and this mechanism permits the arc discharge to attain its very low impedance.

The classical electric arc can be roughly broken down into three regions, each of which plays an important and distinct role essential to the overall physical process:

1) A positive column, which extends over most of the arc length and whose purpose is the conduction of current through the main body of the gas. The electric fields are rather weak in this part of the arc, and the plasma, usually in thermal equilibrium, consists of a strongly radiating mixture of electrons, ions, and neutral atoms at nearly the same temperature, from 5000 ^{o}K to 50,000 ^{o}K; having corresponding degrees of ionization from a few percent to essentially 100 percent. The random thermal velocities of the electrons in this region far exceed their mean drift velocities in the weak field along the column, and thus the predominant ionization mechanisms are thermal electron-atom collisions and photoionization. Current conduction is mainly via a diffusion-dominated drift of the electrons.

2) A cathode fall, which exists at the cathode surface and whose function is the transfer of current across the gas-cathode junction. This requires high electric fields relative to those in the column and results in a positive space-charge accumulation. The cathode fall is typically less than 20 V and the cathode surface emits electrons prolifically (10^3 to 10^7 A/cm^2) by a combination of thermionic, photoelectric, and field emission processes. Only in this part of the arc do ions contribute significantly to the current conduction during their acceleration through the cathode fall.

3) An anode fall, which exists at the anode surface and whose function is the transfer of current across the gas-anode junction, also requiring high electric fields. The anode fall is roughly of the same magnitude and spatial extent as the cathode fall (on the order of the dominant collision mean free path), and the principle ionization processes involve the field-accelerated electrons. In general, the anode does not emit ions, and current conduction is almost entirely by electrons which leave the positive column via a diffusion-

dominated drift and are accelerated towards the anode by the anode fall. On the other hand, ions move from the anode towards the cathode due to the electric field and hence a negative space charge develops. To maintain this steady flow of ions required for electrical neutrality of the column, and to guarantee that the spatial extent of the space-charge region be small, ions must be produced in a thin sheath contiguous to the anode surface. According to Hocker and Bez[19] the ion production in this sheath may occur either by field ionization, wherein the electrons fall freely through the anode fall space and ionize neutral atoms at collision only after they have acquired an energy at least as great as the ionization energy of the gas or vapor, or by thermal ionization, wherein the electrons undergo several collisions in the anode fall so that their directed energy becomes thermalized and only the electrons in the high energy "tail" of the energy distribution engage in ionizing collisions with neutrals. The value of the anode fall voltage is then determined by the energy requirements for ion production.

A major difference between the cathode fall and the anode fall lies in the amount of charge carrier production required in the two regions. It can be shown that I_i/e ions and electrons per second must be generated at the anode fall whereas I_e/e electrons per second must be produced at the cathode, where I_i and I_e are the ion and electron components of the total arc current in the quasi-neutral plasma of the column.[17] Moreover, near the anode the current is almost entirely electronic and hence only about I_i/I_e (proportional to the ratio of the relative drift velocities in the column of the two species, about 10^{-2}) ionizations per incident electron are needed. Hence, almost all of the current-carrying electrons reach the anode without undergoing inelastic collisions and deliver the energy they have gained in the fall directly to the anode. This results in a large arc power loss at the anode (see Sec. E).

C. PLASMA COOLING AT THE ANODE

According to Bez and Höcker,[18] the thickness of the anode fall sheath is of the order of the electron mean free path in the anode-adjacent plasma. This calculated thickness agrees with experimental measurements of Block and Finkelnburg[23] who found, from moving probe measurements, a sheath thickness of 2 μ for the carbon arc at atmospheric pressure. Adjacent to this fall sheath, a second region exists in which the field intensity is lower than in the fall but still a factor of approximately 50 to 100 higher than in the column. Experimental evidence[23] shows that this region extends at most to a distance ϵ = 0.1 mm from the anode surface. It is caused by the cooling effect of the anode surface which decreases the electrical conductivity in this zone; it will be referred to as the ϵ - layer.

The temperature dependence of the electrical conductivity of argon at a pressure of 1 atm, as calculated by Busz and Finkelnburg,[24] is shown in Fig. 2-1. Two regions exist in the σ - T variation, one in which σ rises very rapidly with temperature, and a second in which σ is roughly constant for increasing plasma temperature. An approximate value of the temperature separating these two regions is T $\approx$ 10,000 ^{o}K, which is also very close to the temperature of the plasma at the outer edge of the ϵ - layer ($y = \epsilon$). Obviously at $y > \epsilon$ the temperature drop due to the cooling of the plasma by the anode has no effect upon the electrical conductivity, and hence the field intensity in the outer region of the thermal boundary layer ($\delta_T > y > \epsilon$) is comparable to that in the arc column; i.e., relatively low. In the region $0 < y < \epsilon$, however, where the electrical conductivity decreases rapidly with decreasing wall distance and thus decreasing plasma temperature, the electric field intensity must increase sharply in order to maintain current continuity. Thermal equilibrium between electrons and heavy gas particles no longer exists at this high field intensity because of the strong energetic coupling between the electric field and the electrons, and the

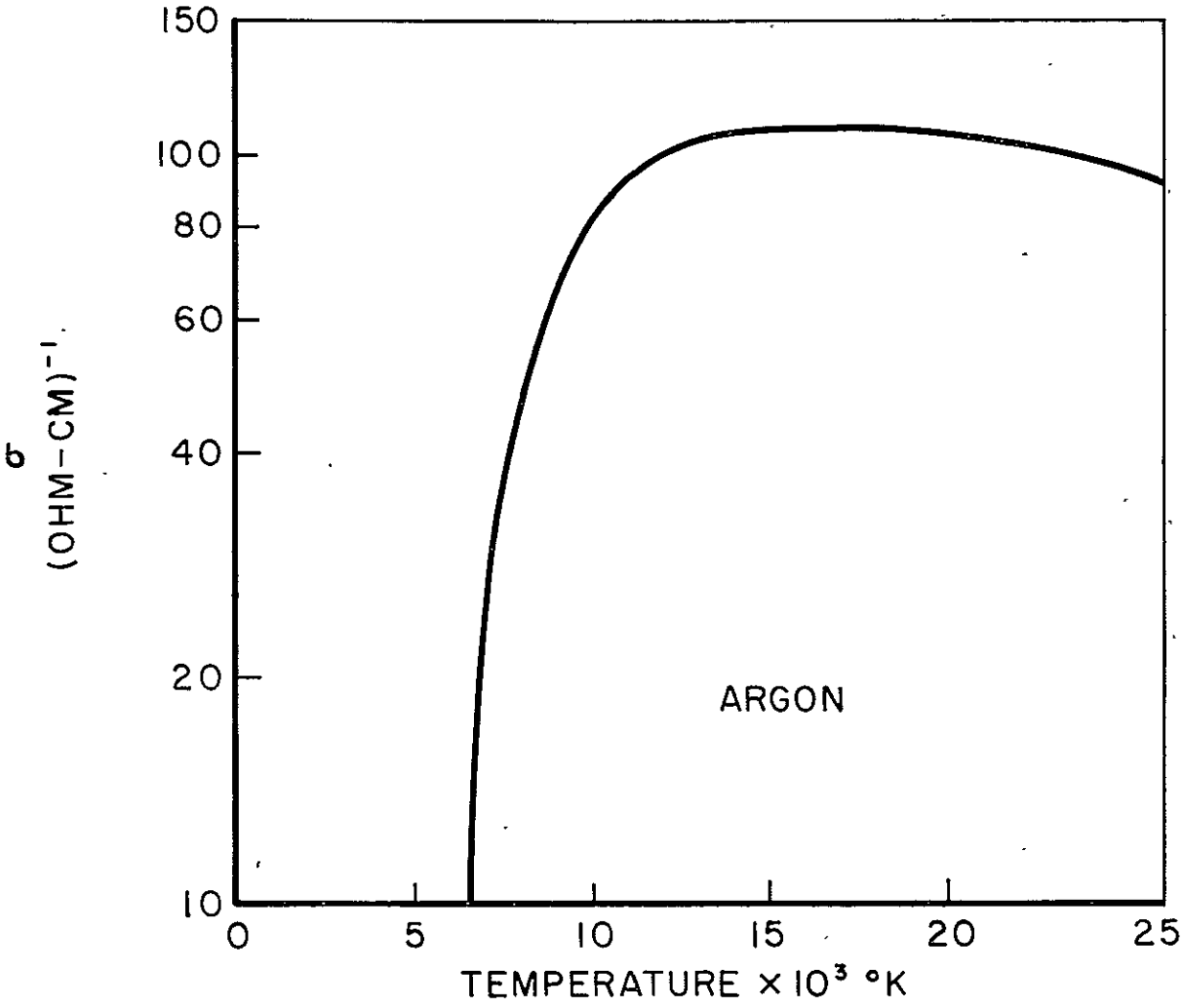

TEMPERATURE DEPENDENCE OF ELECTRICAL CONDUCTIVITY AT A PRESSURE OF 1 atm. (AFTER BUSZ-PEUCKERT & FINKELNBURG (24))

FIGURE 2-1

weak coupling between the heavy particles and both the field and the electrons. Thus, the electrons receive additional energy from the field which they cannot transfer to the heavy particles, resulting in an increase in the electron temperature T_e above that of the heavy particles T_g in the ϵ - layer. A qualitative representation of the distribution of temperature, voltage, and electric field is given in Fig. 2-2[25], where the thermal boundary layer thickness, δ_T , is used as a reference distance. The anode fall thickness is too small to be shown on this scale. Henceforth the combination of the anode fall and the ϵ -layer shall be referred to as the anode voltage drop. Electrostatic probe measurements in the pinch discharge and quasi-steady MPD arc, presented in Chap. IV and VI, were taken at distances from the anode which are too great to allow for a distinction between the anode fall and the ϵ -layer. Hence, the voltage measured at the anode surface will include contributions from both of these regions, and therefore can only be used to define the anode voltage drop rather than the anode fall voltage specifically.

D. ANODE FALL THEORIES

The only detailed theoretical investigation of the anode fall region is that developed in a series of papers by Bez and Höcker.[18-22] They cited three main functions of the anode fall:

1) The production of ions which then diffuse through the cross section of the column towards the cathode.

2) The directed velocity of the ions, accelerated towards the column by the anode fall, must be converted into a thermal velocity distribution corresponding to the thermal temperature of the positive column or to that of the adjacent ϵ -layer.

3) The accomplishment of the transition from the relatively low temperature anode to the high temperature of the positive column or adjacent ϵ -layer; to this end the fall probably heats the cold gas adjacent to the anode surface.

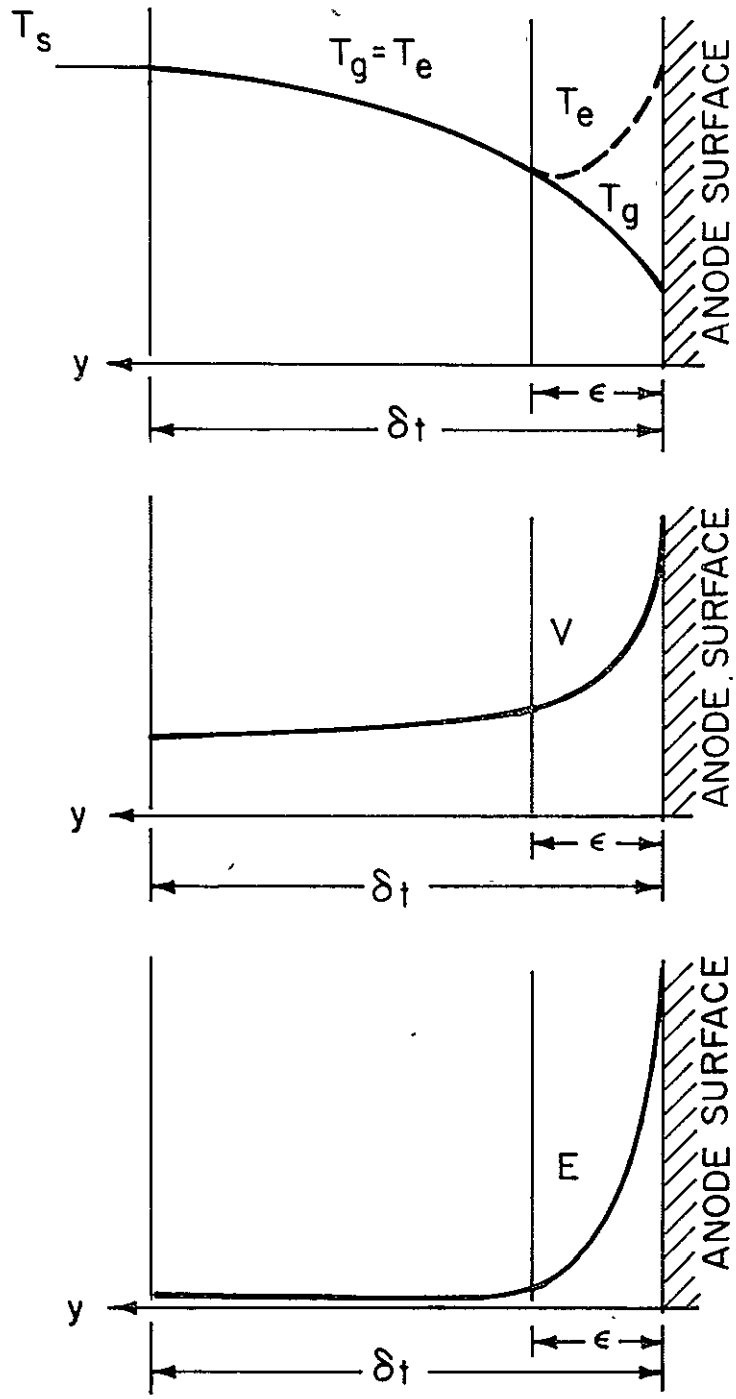

TEMPERATURES, VOLTAGE AND ELECTRIC FIELD INTENSITY NEAR THE ANODE SURFACE (REF.25)

FIGURE 2-2

It is known that, with equal energy, the differential coefficient of ionization of electrons is appreciably larger than that of the ions. For this reason, only electrons are taken into consideration in the ionization processes. Bez and Höcker have distinguished two different types of ionization by electrons in the fall region: field ionization and thermal ionization. Their characteristics are discussed below.

1. Field Ionization

The term, field ionization, applies to the state of affairs in which electrons fall freely through the anode fall space using the energy thus acquired to ionize gas or vapor atoms at collision. To investigate this possibility, Bez and Höcker divided the anode space-charge zone into two different model zones, an "acceleration zone" and an "ionization zone." The "acceleration zone" is that part of the anode fall zone in which the voltage, starting from the column, grows to the ionization voltage of the gas, V_I, while the "ionization zone" is described by the region in which the voltage grows from the ionization voltage to the anode fall voltage, V_A. For the special case of a carbon arc burning freely in air at atmospheric pressure, the authors calculate the extent of these areas as 0.4×10^{-3} cm and 1.8×10^{-3} cm, respectively.

As Bez and Höcker consider the extent of the anode fall area, for this type of ionization, as less than one electron mean free path, they calculate the motion of the electrons in the acceleration zone in accordance with the laws of free fall. If one further ignores the thermal energy at entry into the acceleration zone, then the electrons will have at point x the energy corresponding to the potential V(x).

To describe the ionization zone, from $X = X_o$ to $X = X_A$, the authors use the following expression for the ion production over a distance dx

$$d j_i(x) = - C_I (V(x) - V_I)\, j_e(x)\, \frac{dx}{\lambda_e^I} \qquad (2\text{-}1)$$

where $C_I(V(x) - V_I)$ is an approximation of the coefficient of differential ionization, and λ_e^I is the electron mean free path for ionization. This expression can be integrated to give an exponential form, and since $dx/\lambda_e^I \ll 1$ the exponential can be approximated by a linear form yielding

$$j_i(x) = j_i(x_o) - j_e(x_o) \frac{C_I}{\lambda_e^I} \int_{x_o}^{x} (V(x) - V_I)\, dx \qquad (2\text{-}2)$$

It is assumed that the ion current vanishes at the anode surface, $x = x_A$; the above expression then gives

$$j_i(x_o) = j_e(x_o) \frac{C_I}{\lambda_e^I} \int_{x_o}^{x_A} (V(x) - V_I)\, dx \qquad (2\text{-}3)$$

By ignoring the ion current density and the counter field diffusion of ions toward the anode, Bez and Höcker[18] approximate the voltage V(x) in both the acceleration and ionization zones by a "generalized Langmuir formula"

$$V(x) = a_1 \cdot 3 \left(\frac{3 m_e \pi^2 j_e^2}{2e} \right)^{1/3} x^{4/3} \qquad (2\text{-}4)$$

in which a_1 is an adjustable parameter used to fit the experimental anode fall data. Application of the Langmuir formula, derived from a collisionless model, to the ionization zone is based on the assumption that this region is much smaller than an electron collision mean free path, and thus most electrons fall freely through the ionization zone to the anode surface.

Equation (2-3) can now be readily integrated by using the above expression for the voltage variation in the fall

zone. The result is

$$\frac{j_i}{j_e^{1/2}}(3a_1)^{3/4}\left(\frac{3\,m_e\pi^2}{2e}\right)^{1/4}\frac{\lambda_e^I}{C_I} = \frac{3}{7}\left(V_A^{7/4}-V_I^{7/4}\right) - V_I\left(V_A^{3/4}-V_I^{3/4}\right) \qquad (2\text{-}5)$$

where the authors use $j_e(x_o) \approx j_e$ and $j_i(x_o) \approx j_i$ which are respectively the electron and ion current densities at the anode end of the positive column. When j_e and j_i are written in terms of the electron and ion mobilities, the following expression for V_A, as an implicit function of T, is derived

$$\left(\frac{m_e}{m_i}\cdot\frac{\pi 3^{3/2} e^{3/2} a_1^{3/2} E}{2^{1/2} k^{1/2}}\right)^{1/2} \cdot \frac{m_e^{1/2}\,\lambda_e^I\,\lambda_{ia}}{C_I\,\lambda_{et}^{1/2}\,T^{1/4}} =$$

$$\frac{3}{7}\left(V_A^{7/4}-V_I^{7/4}\right) - V_I\left(V_A^{3/4}-V_I^{3/4}\right) \qquad (2\text{-}6)$$

where T is the temperature of the plasma at the anode end of the column (assumed to be in local thermodynamic equilibrium), and λ_{ia} and λ_{et} are the ion-atom and electron-heavy particle collision mean free paths.

By adjusting the value of a_1, Eq. (2-6) can be used to predict the correct anode fall voltage, V_A = 20 V, for the low current carbon arc burning in nitrogen at atmospheric pressure with a gas temperature of about 6000 °K. However, the authors noted that the calculated anode fall voltages rise sharply at temperatures beyond about 9000 °K. This results mainly because of the rapid decrease of λ_{et}, due to increasing electron-ion collisions, as the degree of ionization begins to rise (see Fig. 2-3). In fact, Eq. (2-6) predicts an anode fall voltage of 35 V for the above described

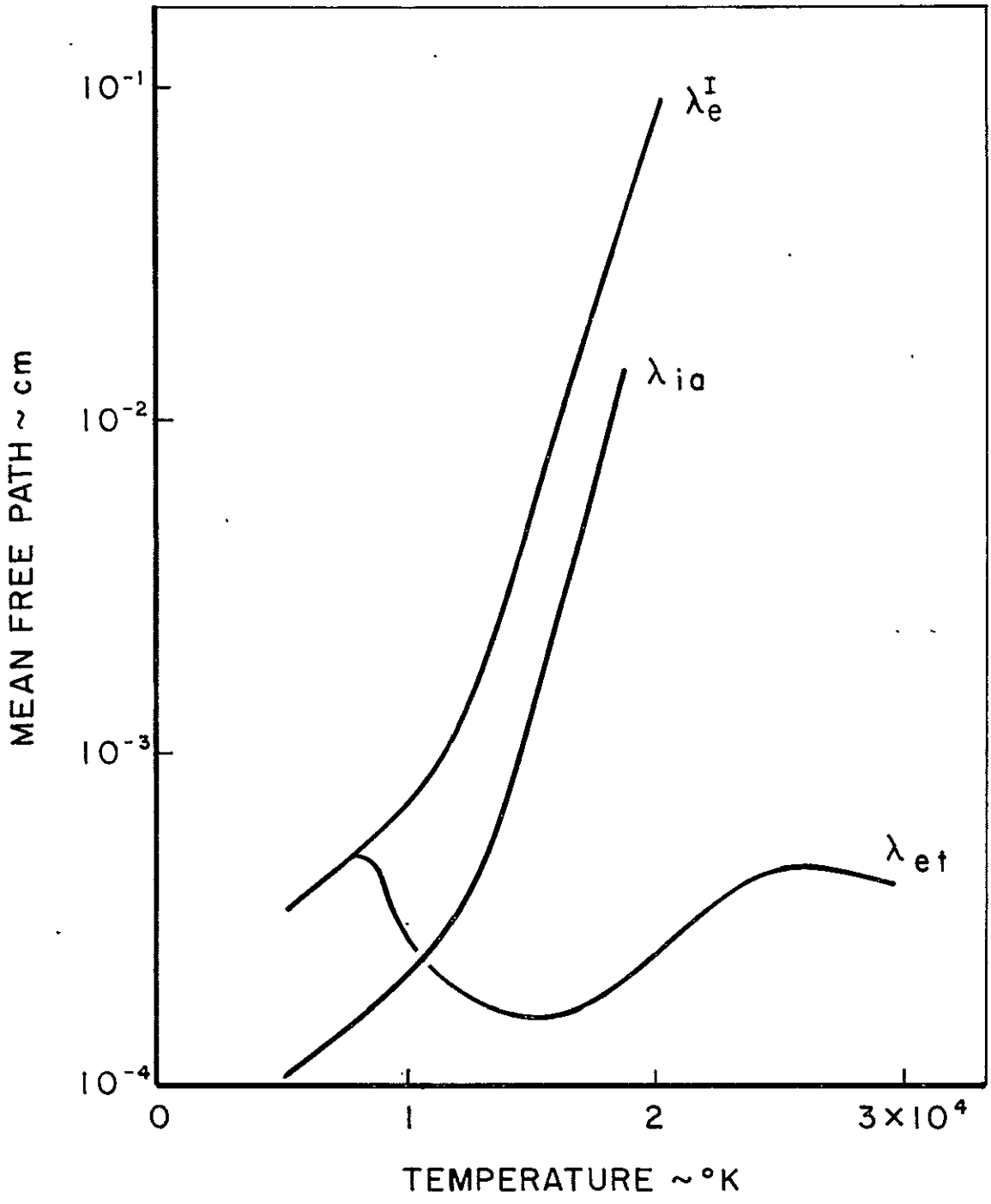

TRANSPORT MEAN FREE PATHS IN NITROGEN AT ATMOSPHERIC PRESSURE AS A FUNCTION OF GAS TEMPERATURE (AFTER HÖCKER & BEZ (19))

FIGURE 2-3

arc when the nitrogen temperature is raised to 10,000 °K. Since this result contradicts the experimental data, Bez and Höcker claim, therefore, that the field ionization model cannot describe the ion production in the anode fall zone for arc column temperature beyond about 9,000 °K. Instead, ion production at the anode fall of high temperature arcs proceeds via the thermal ionization mechanism which is described next.

Since Joule-heating of the column plasma depends upon the square of the current density (j^2/σ), it follows that high arc temperatures are normally associated with high-current density arcs. Therefore, the distinction between field and thermal ionization in the anode fall can also be made on the basis of current density. For example, the low current carbon arc, with an anode current density of 40 A/cm^2 and anode fall of 20 V, exhibits the properties of field ionization at the anode, whereas the high-current carbon arc, with an anode fall 8 to 10 V lower, is characterized by the thermal ionization mechanism.[17]

2. Thermal Ionization

The term, thermal ionization, denotes the state of affairs in which electrons undergo several collisions in the anode fall so that their velocities are randomized and approximately thermal with an electron temperature, T_{eA}, somewhat above that of the heavy particles. There are sufficient electrons in the high energy "tail" of the energy distribution to produce the necessary ionizing collisions and resulting positive ions; hence, the anode fall need not be as large as when field ionization prevails, where it must be at least as large as the first ionization potential of the vapor or gas. The anode fall thickness will be greater than for field ionization because the electrons must now make several collisions in this region, and therefore the fall zone must be larger than λ_{et}.

A simple energy balance for the thermal production

of ions takes the form

$$j_{V_A} = j_i V_I + j_e/e \left(5/2 \, k T_{eA} \right) \qquad (2\text{-}7)$$

where j_{V_A} is the power density deposited in the anode fall, j_i is the ion current density leaving the cathode end of the fall, and the last term represents the power delivered to the anode surface by the current-carrying electrons, which have become thermalized in the fall at a temperature T_{eA}. From Eq. (2-7), the following estimate of the anode fall voltage requirement can be derived,

$$V_A = \left(\frac{m_e}{m_i} \right)^{1/2} \frac{\lambda_{ia}}{\lambda_{et}} V_I + \frac{5}{2} \frac{k T_{eA}}{e} \qquad (2\text{-}8)$$

where j_e and j_i have again been expressed in terms of the relative mobilities of the electrons and ions in the column plasma. For this type of ionization, the mean thermal electron energy, $k T_{eA}$, can be much smaller than the ionization energy of the gas or vapor; in addition, the ratio $(m_e/m_i)^{1/2}$ keeps the first term small even at high gas temperatures where the ratio $\lambda_{ia}/\lambda_{et}$ becomes large (see Fig. 2-3). Thus, Eq. (2-8) demonstrates that the anode fall voltage requirement for ion production by the thermal ionization process can, indeed, be considerably less than the ionization potential of the gas.

E. ANODE ENERGY BALANCE

An anode heat transfer model for steady plasma accelerators, formulated by Shih, Pfender, Ibele, and Eckert,[9] includes a variety of transfer processes such as energy transfer by electrons carrying the current, heat transfer by combined conduction and convection, and by radiation. The

electrons carry to the anode surface an amount of energy, 5 $kT_e/2$ per electron, corresponding to their thermal energy in the neighboring column plasma, plus the amount of energy gained through the anode fall, V_A. In addition, an amount of energy proportional to the work function of the anode material, ϕ_A, appears also as heat input. There has recently been some discussion about whether the contribution due to the electron thermal energy in the column should be 5 $kT_e/2$ or 2 kT_e. This question is taken up in the Appendix with the conclusion that 5 $kT_e/2$ is the better representation of this effect. The convective heat transfer from the plasma to the anode surface can be expressed in terms of the enthalpy difference between the plasma stream and the anode surface.[27] The total heat input to the anode is then given by

$$P_A = h_i A_A (i_s - i_A) + P_{RA} + J\left(\frac{5}{2}\frac{kT_e}{e} + V_A + \phi_A\right) \quad (2\text{-}9)$$

where
- h_i = heat transfer coefficient at the anode surface based on enthalpies
- i_s = enthalpy of the gas outside the boundary layer
- i_A = enthalpy which the gas assumes in the immediate proximity of the anode surface
- A_A = surface area of the anode
- P_{RA} = radiative heat transfer from the cathode and neighboring plasma to the anode
- J = total arc current
- T_e = electron temperature at the anode end of the column

The total arc current is used in this expression rather than the electron current specifically because, at the anode, the arc current is carried almost entirely by electrons. Furthermore, as was noted in Sec. B, only about 0.1 to 1.0 percent of electrons entering the anode fall give up their

energy in ionizing collisions with neutral atoms, therefore this energy need not be subtracted from the electron contribution to the anode energy flux.

A confirmation of the proposed anode heat transfer model was obtained experimentally by measuring the total heat transfer to the anode for various arc currents,[9,12] with the result that plots of P_A vs J gave a straight line, indicative of constant values of T_e and V_A. It was concluded from this data that the dominant contribution to the anode energy loss is due to the electron current, particularly at high arc currents, and hence the equation for anode heat transfer can be approximated by

$$P_A \approx J\left(\frac{5}{2}\frac{kT_e}{e} + V_A + \phi_A\right) \qquad (2\text{-}10)$$

The expression for heat transfer to the cathode contains a similar term which is linear in the ion current, J_i.[9] Since for high-current arcs $J \gg J_i$, and since electron emission at the cathode is an endothermic process, it is evident that the cathode power loss is much less significant than anode power loss. There is also considerable empirical evidence supporting this claim.[9] Hence, it follows that most of the attempts to improve the thermal efficiency of plasma accelerators have been focused on alleviating the anode power loss.

Much experimental work has been devoted to the measurement of anode heat losses in high-current arcjets and MPD arcs. It has been reported that the relative heat losses at the anode depend on arc parameters such as current, mass flow rate, and applied magnetic field. Without detailing the dependence of the anode losses on these quantities, the average results quoted by a number of investigators will now be given. Schoeck[6] found that the total heat flow to the anode for a high pressure thermal arcjet, operating between 50 and 150 A

at a pressure of 1 atm, was between 75 and 90% of the total arc power. Schneiderman and Patrick,[7] as well as Ducati, Muehlberger, and Treat,[8] also working with thermal arcjets, observed that as much as 60 to 70% of the input power was lost to the anode. Shih et al.[9] reported anode power losses from 30 to 60% in argon and amonnia-fed MPD arcs. Finally, Nerheim and Kelly,[10] in a review of MPD arc technology, found that the more technically promising engines had a median range of thermal efficiency of around 50 to 70%, with most of the power losses appearing at the anode.

F. TRANSPIRATION COOLING OF THE ANODE

In view of the substantial heat load which must be carried by the anode of high-current plasma accelerators, attempts were made both to cool the anode and to lower the net anode heat loss by a process known as transpiration cooling of the anode; i.e., the injection or forcing of a suitable coolant through an anode which has been fabricated from a porous material. The transpiring gas readily provides the cooling needed to prevent ablation of the anode and, in addition, feeds a large portion of the energy normally lost to the coolant back into the arc region where it may serve a useful purpose. Schoeck et al.[25] injected argon gas through a porous graphite anode back into their high intensity argon arc, and observed that, although between 50 and 80% of the arc input power was transferred to the anode, up to 80% was recoverable by this process. In fact, thermal efficiencies as high as 80% were attainable. Pfender et al.[28] employed a constricted, wall-stabilized argon arc, with power inputs from 2.5 to 16 kW, to compare a water-cooled copper anode and a porous graphite transpiration-cooled anode. They found that the anode heat losses were reduced by a factor of two, from 20% to only 10% of the total input power, when transpiration cooling was used. Hence, it would appear that transpiration cooling of the anode is an effective means of improving the thermal efficiency of low power arc thrusters. However, as

will be shown in Chap. VI, high-power, quasi-steady MPD arcs promise high thermal efficiencies, in the 80% range, without the complications of this anode cooling procedure.

G. ANODE PRECURSOR PHENOMENA IN PULSED ACCELERATORS

Lie, Ali, and Chang[29] have observed precursor effects along the anode surface ahead of the main current sheet in both parallel-plate and coaxial accelerators. They used monochrometers to detect preionization in the ambient gas ahead of the current sheet, and observed that the level of preionization was much higher at the anode than at the cathode for helium, nitrogen, and argon prefilling pressures of 0.05 to 0.5 Torr. In addition, they observed that this preionized gas near the anode carried a considerable fraction of the discharge current, particularly when the filling pressures were low. It was concluded that the anode preionization and precursor conduction are related neither to the initial high-current discharge near the back insulator, nor to the radiation emitted by the main discharge current, but rather, are a vestige of the breakdown conduction processes which occur along the entire electrode surface.

The existence of this anode surface current was used by Lie et al. to explain the incline of the current sheet towards the anode in parallel-plate and rail accelerators. This so-called, current sheet tilt, wherein the anode attachment runs ahead of the main portion of the current sheet, has been well documented in previous works,[30–32] and was also observed in the present experiments (see Chap. V). Since the current sheet near the anode has a forward axial current component, due to precursor surface conduction, this part of the sheet experiences a $\vec{j} \times \vec{B}$ force directed toward the cathode, and this tendency amplifies itself as the current sheet travels down the electrode gap resulting in a tilt of the sheet as a whole.

It is instructive to note that Lovberg[33] has observed

a planar, untilted current sheet in the case of a hydrogen-filled (0.3 Torr) parallel-plate accelerator; and also that Lie et al. found no appreciable preionization and no axial current along the anode of their accelerator when hydrogen was used. These two observations suggest that the phenomena of current sheet tilt and precursor anode conduction are indeed causally related as proposed by Lie et al..[29] In addition, it can be postulated that these two related phenomena are somehow associated with the large ion Larmor-radii of the heavier gases, such as nitrogen and argon, which in some cases approach inter-electrode dimensions. Hydrogen, on the other hand, which produces planar current sheets and no appreciable preionization, indicates ion Larmor-radii at least an order of magnitude smaller.

Other experiments, performed by Lovberg on a parallel-plate accelerator with hydrogen-filling, showed that a 100 V anode sheath was present, with the cathode sheath being much smaller.[33] This large anode sheath voltage was explained in terms of a current sheet model, in which ions are presumed to be the major current carriers, and for which Lovberg found supporting experimental evidence.[32] The small Larmor-radii predicted for the hydrogen ions support this conclusion, since the hydrogen ions will be therefore able to make complete revolutions within the current sheet, and thus may drift towards the cathode, carrying current in the process. With ions carrying the current and moving away from the anode, a large excess of electrons will be left there, and the resulting negative space charge causes the large voltage drop at the anode surface. The rather small cathode sheath voltage arises because the current sheet is an effective ionizing agent, thus making electron emission at the cathode and ionization in the cathode fall unnecessary.

Kislov et al.[34] have mapped the potential contours in a quasi-steady coaxial plasma accelerator, operating at current levels from 20 to 50 kA and nitrogen mass flow rates from 1 to 3 g/sec. They also observed large potential drops at the

anode surface (30 to 110 V), or about 40% or more of the total discharge voltage, while the drop near the cathode was relatively small. Working with a similar device, Kovrov et al.[35] measured the magnetic fields and current distributions, and discovered that the discharge current pattern appeared to "slide" along the anode surface and thus extend well downstream of the cathode current zone. Kislov et al.[34] attempted to explain the sizable anode voltage drop by suggesting that the electrons are prevented from reaching the anode by virtue of their large Hall parameters, which enable them to undergo a cross-field drift parallel to the anode surface in response to the electric and magnetic fields, which are respectively perpendicular and parallel to the anode. Hence, rather than being absorbed at the anode, the electrons form a negative space-charge layer there, resulting in a substantial anode voltage drop. Furthermore, it was proposed by Kovrov et al. that the electron Hall drift parallel to the anode in the downstream direction causes the current distribution to extend along the forward portion of the anode, the so-called "anodic sliding." The measured values of electron temperature and density at the anode of this device confirm that the electron Hall parameters are indeed large enough for this effect to occur.

The conclusions of Kislov et al.,[34] which relate the anode voltage drop in their accelerator to the large electron Hall parameters, correlate well with earlier experiments of Karkosok and Hoffman,[36] in which electrode voltage drops in a MHD channel, with a current of only 1 A and a pressure of 1 atm, were measured. Their results indicate that the anode voltage drop doubled, from 20 V to 40 V, for an increase in the electron Hall parameter from very small values to about 2.5.

More recently, Dammann et al.[37] have observed a precursor in a thin layer near to the anode in front of the convergent cylindrical shock wave of z-pinch discharges in helium and argon. The precursors, which were investigated

by interferometric methods, appear to separate from the shock wave at higher filling pressures, and then run ahead along the anode toward the chamber center. The authors have attempted to explain their observations in terms of gasdynamic effects.

H. REMARKS

In this chapter a discussion of plasma cooling at the anode and a theory of the anode fall zone have been presented. The physical understanding developed in these sections will be employed in later chapters to explain certain experimental results pertaining to the anode region of pinch and quasi-steady MPD discharges. In addition, the anode heat transfer model is applied to the quasi-steady MPD arc in order to compute the anode power loss and thermal efficiency. Finally, the discussion of the anode precursor phenomena aids our attempts to understand and explain similar phenomena in our pulsed accelerators.

CHAPTER III

EXPERIMENTAL FACILITIES AND DIAGNOSTIC TECHNIQUES

A. INTRODUCTION

The study of anode phenomena in high-current discharges was carried out, for reasons stated previously, under a variety of discharge geometries and operating conditions. For example, pulsed or unsteady discharges, employing a propagating current sheet as a plasma acceleration mechanism, were studied in both cylindrical z-pinch and linear, parallel-plate geometries at current levels from 100 to 300 kA and pulse times from 3.5 to 20 μsec. The quasi-steady mode of electromagnetic plasma acceleration was investigated in a coaxial device employing current levels from 4.4 to 42 kA and pulse durations from 60 to 600 μsec. Argon was used as the operating gas for each of these experiments because it is relatively inexpensive and because its relatively high molecular weight affords the opportunity for high thrust density.

B. CYLINDRICAL Z-PINCH FACILITY

The large-radius linear pinch discharge is characterized by the early formation of a uniform cylindrical current sheet at the outer chamber radii, the configuration of lowest inductance, followed by the rapid collapse of this current structure towards the chamber center as it is driven by self-field, $\vec{j} \times \vec{B}$ forces.[15,38] The main components of the discharge apparatus are the cylindrical discharge chamber, a gas-triggered switch,[39] and a series of high-voltage capacitors distributed along a transmission line.[15] Briefly, the discharge chamber is 8-in. in diameter and 2-in. high; the electrodes, of 3/4-in. aluminum, are separated by a 1/4-in. thick, 2-in. high Pyrex

sidewall (Fig. 3-1). The switch unit consists of a similar 8-in. pinch chamber fitted with a gas-feeding Plexiglas insert. The discharge is initiated by injecting argon into the previously evacuated switch chamber, thereby causing the switch to break down and transfer the capacitor bank potential to the electrodes of the prefilled main discharge chamber. The chamber electrodes are both held at ground potential during the charging of the capacitor bank by means of a 1 kΩ ballast resistor. The electrical energy is initially stored in a bank of 20 capacitor units, each with nominal 2.5-μf capacitance and 15-nH inductance, rated to 10 kV. The capacitors are arranged along an LC transmission line.[15] The driving-current waveform can be altered by simply changing the distribution of the capacitor units along the line. The discharge chamber is normally prefilled to 100 μ argon; and the entire system is evacuated to several μ after each discharge by means of a mechanical pump and then flushed with argon gas. Chamber pressures are monitored with a standard Pirani gauge. The discharge current is measured with a Rogowski coil of standard design[40] connected to a passive RC integrator circuit. Data were generally recorded photographically from a Tektronix Type 555, dual-beam oscilloscope.

C. PARALLEL-PLATE ACCELERATOR

The parallel-plate experiments are, in many respects, similar to the cylindrical pinch; the only major differences are in the geometry and dimensions of the apparatus (Fig. 3-2). In the present arrangement 3/4-in. aluminum electrodes, 6-in. wide and 48-in. long, are separated and supported by 2-in. high Plexiglas sidewalls.[41] A rectangular gas-triggered switch is employed to initiate the discharge sequence. Electrical energy is stored in a capacitor bank consisting of 40 3.2-μF capacitors rated at 30 kV. The four rows of 10 capacitors each can be arranged in either parallel or series to vary the magnitude and shape of the driving-current waveform; from 120 kA x 20 μsec to 4.4 kA x 600 μsec. The discharge is again initiated when

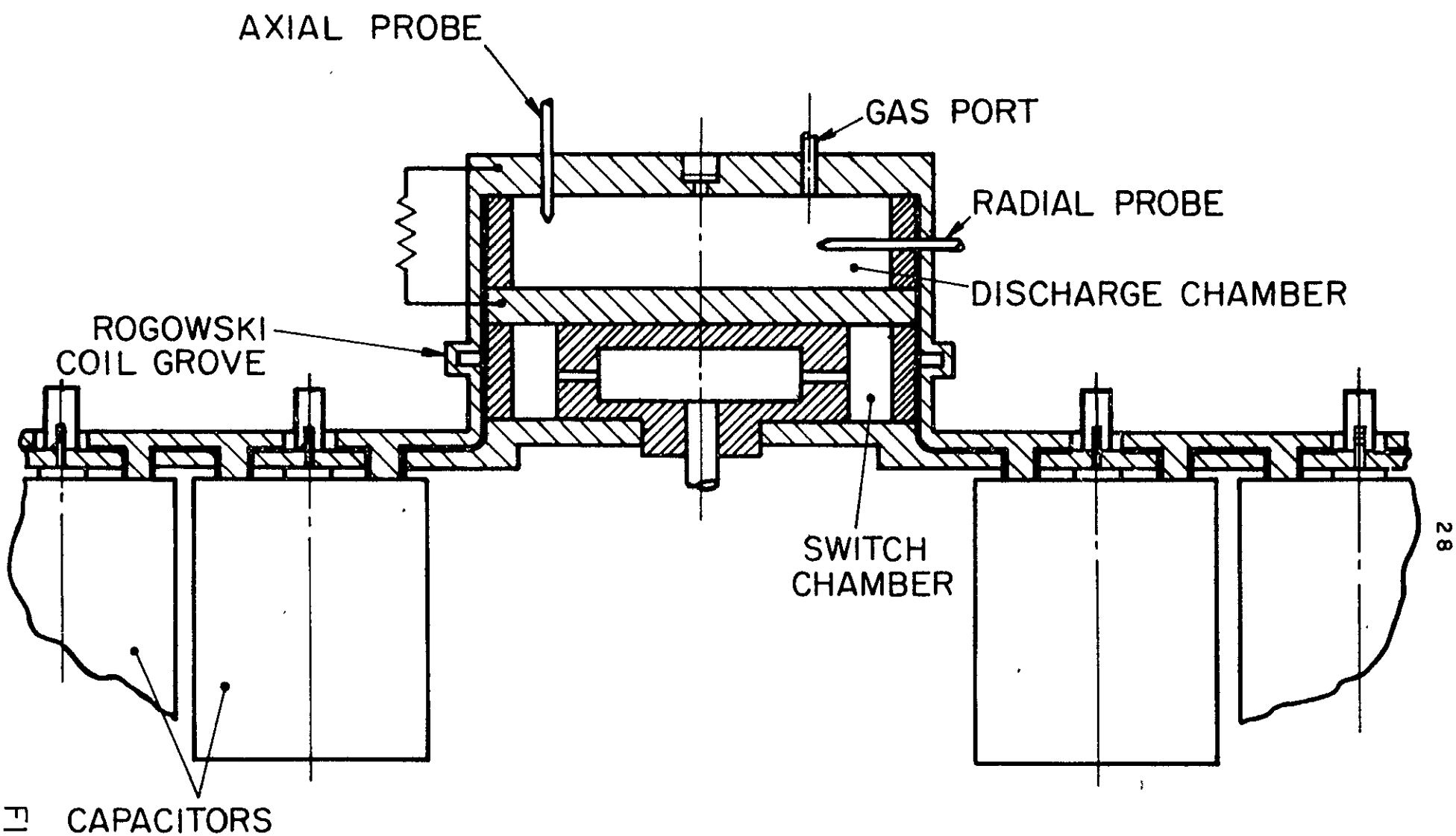

FIGURE 3-1

DIAGRAM OF 8-in PINCH DEVICE

FIGURE 3-2

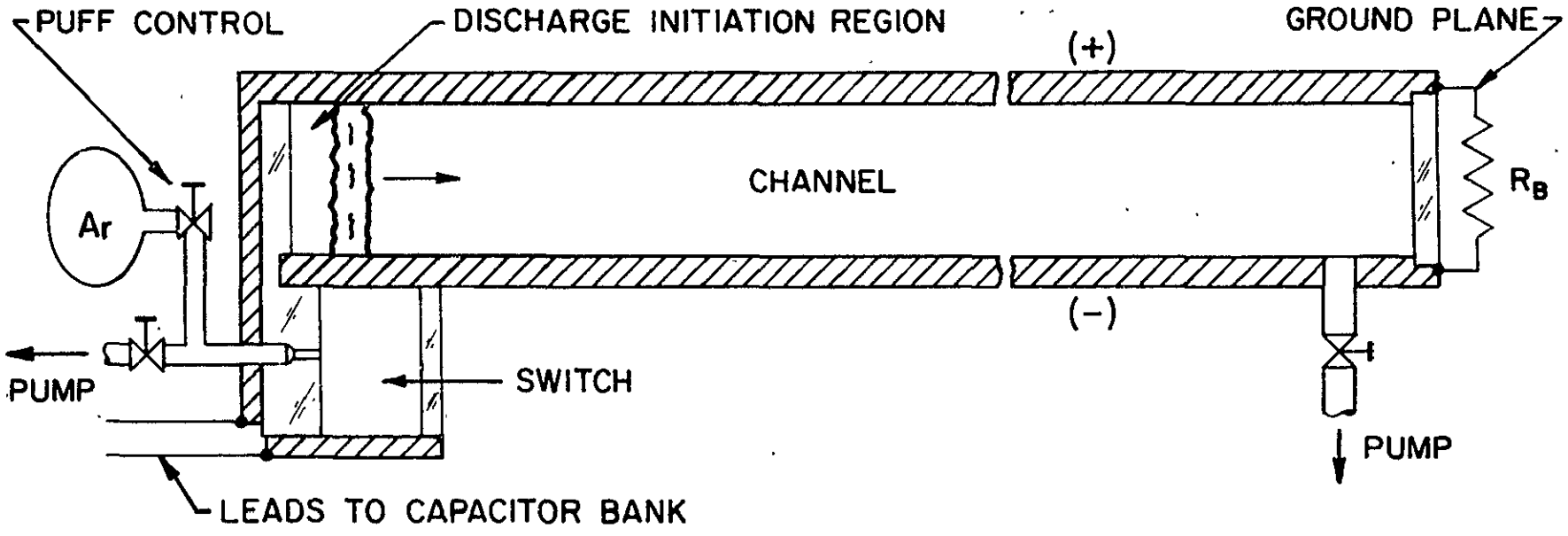

DIAGRAM OF PARALLEL PLATE ACCELERATOR

the switch is injected with argon, causing it to break down and transfer the 10 kV bank potential to the accelerator electrodes. A uniform, planar current sheet is initially established at the back insulating wall, the position of lowest inductance; and then propagates down the length of the electrode channel, driven by self-magnetic forces. The total discharge current and accelerator width are such that the resulting current densities are sufficiently high to guarantee, at least in the early phases of the discharge, a well-defined current sheet. In some experiments,[42] nylon insulation was inlaid along the electrodes in order to arrest the propagating current sheet and induce a stabilized current pattern.

The supporting apparata employed with this facility are similar to those associated with the 8-in. pinch device: a mechanical pump to evacuate the system after each discharge, a Pirani gauge, a Rogowski coil, and a Type 555 dual-beam oscilloscope. The accelerator channel is normally prefilled to 100 μ argon. This device affords several diagnostic advantages over the 8-in. pinch facility: longer streamwise dimensions, longer time scales, and easier photographic observation. The disadvantages are: a less reproducible discharge and greater three-dimensionality of the current sheet, both caused by the side-wall distortion of the magnetic field lines.

D. QUASI-STEADY MPD ARC FACILITY

The quasi-steady mode of arc operation affords distinct diagnostic advantages over the unsteady operation of the 8-in. pinch and parallel-plate facilities. The pulse duration is sufficiently long that the troublesome transient and inductive effects can subside, yet is sufficiently short to permit the application of simple unsteady diagnostic techniques. In addition, problems of probe destruction, encountered in the hostile environments of steady-flow MPD arcs, are not serious in the quasi-steady operating regime. The other attractive features of the quasi-steady MPD arc have already been discussed in Chap. I, and therefore will not be restated here.

The quasi-steady MPD arc facility, employed in the present investigation of anode phenomena, is described in detail in reference 5. This device closely replicates the conventional magnetoplasmadynamic arc configuration, but on a scale one order of magnitude larger to permit detailed interior diagnostics. A schematic diagram of this apparatus is shown in Fig. 3-3. Briefly, it consists of a cylindrical discharge chamber with a 3/4-in.-diameter conical tungsten cathode, and an aluminum anode with a 4-in.-diameter orifice, driven by a 130 μF x 10 kV capacitor line, arranged to provide a variety of rectangular current pulses ranging from 4.4 kA x 600 μsec to 140 kA x 20 μsec. Propellant gas, normally argon, is injected through six calibrated orifices in the arc chamber endplate from a high pressure reservoir, abruptly established by the end wall stagnation of the flow in a simple shock tube. An adjustable bleed line from the same shock tube triggers the discharge circuit switch, similar to the one described in Chap. III, Sec. B, thereby permitting correlation of the mass flow pattern with the arc current profile. The arc chamber and thruster assembly are mounted in a 3-ft. diameter x 6-ft. long Plexiglas vacuum tank,[43] which is evacuated down to pressures of about 10^{-5} Torr by a 6-in.-diameter oil diffusion pump.

The operation sequence of the system begins with the pressurization of the shock tube driver section to 45 psig, normally, and the charging of the capacitor line to 10 kV. The shock tube diaphragm is ruptured, and the pressure wave is first bled into the evacuated switch and then establishes a pressure reservoir at the end wall of the driven section, which in turn feeds the argon gas into the chamber through the six end-wall orifices. The bleed-line length is adjusted so that the switch breaks down and transfers the 10-kV bank potential to the accelerator electrodes, only after steady mass flow has been established in the arc chamber. The steady phase of operation, when both current and mass flow patterns have become stabilized, can be achieved over a large portion of the driving-current pulse; all arc data are collected during

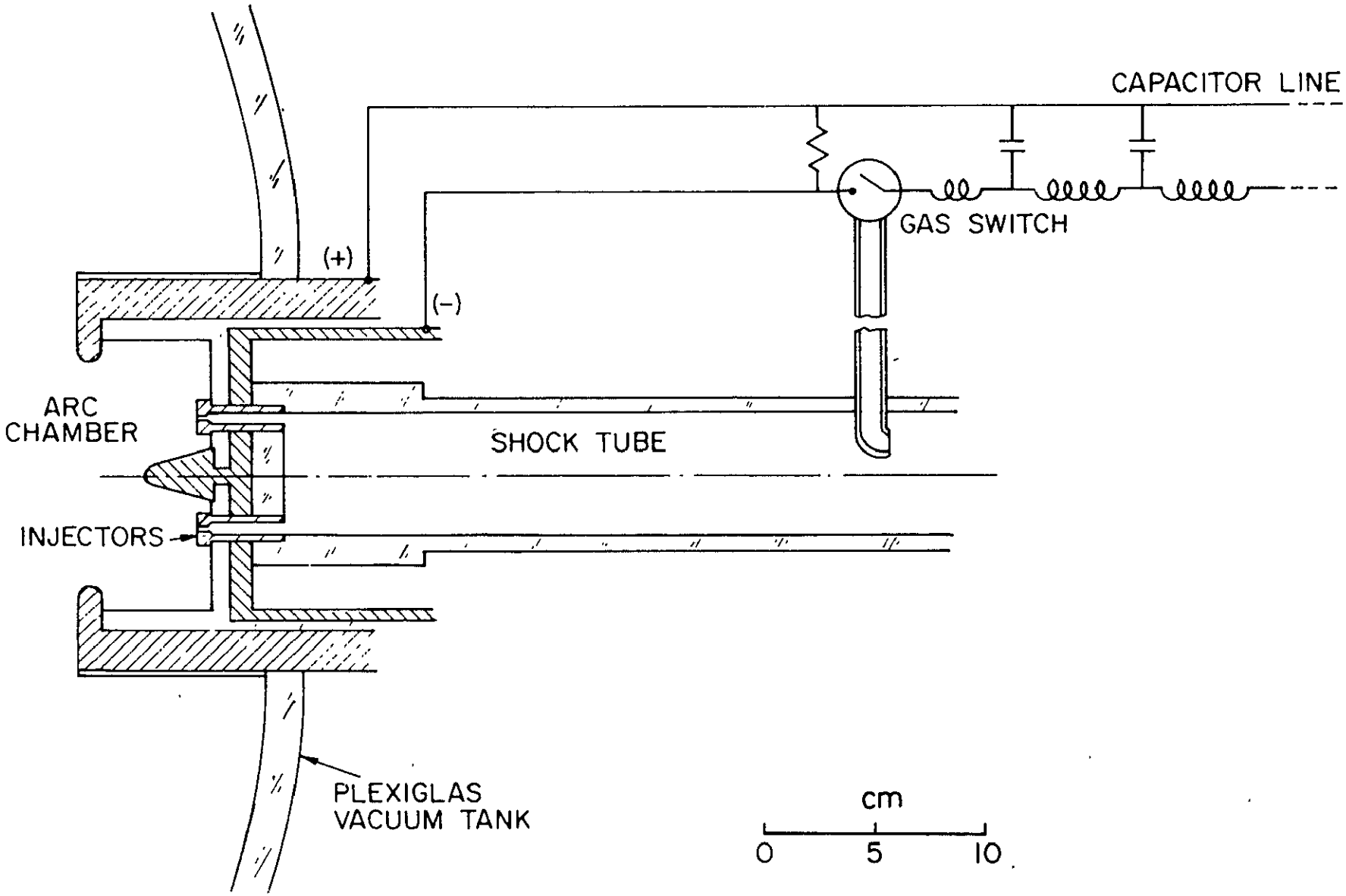

FIGURE 3-3

SCHEMATIC OF QUASI-STEADY MPD ARC FACILITY

this steady phase. The experiments on this quasi-steady MPD arc facility are carried out at currents from 4.4 to 42.0 kA and argon mass flow rates from 1.2 to 36.0 g/sec.

E. MAGNETIC PROBE DIAGNOSTICS

Magnetic probes, or magnetic induction coils,[40] have been employed to measure the magnetic field patterns in each of the previously described experimental facilities. These probes consist of small, multi-turn coils of insulated wire, which generate a voltage across their leads in response to a change in the magnetic flux threading the coil. The probe signal, by Faraday's law, is proportional to the rate of change of magnetic field at the sensor location. Integration of the probe signal by a passive RC integrator circuit provides a record of the magnetic field over the discharge history. By assuming azimuthal symmetry of the discharge, Ampere's law can be used to relate the local magnetic field strength to the total current enclosed within a radius defined by the coil location in the discharge chamber. Hence,

$$\int_S \nabla \times \vec{B} \cdot d\vec{S} = \int_S \mu_o \vec{j} \cdot d\vec{S} \qquad (3\text{-}1)$$

where S is the plane circular surface defined by rotating the radius of the probe location through 360°. Thus

$$\int_{r=r_p} \vec{B} \cdot d\vec{\ell} = \mu_o J_{ENCLOSED} \qquad (3\text{-}2)$$

where r_p is the radius of the probe location; and assuming azimuthal symmetry, this integral yields

$$2\pi r_p B = \mu_o \cdot J_{ENCLOSED} \qquad (3\text{-}3)$$

which relates the local magnetic field strength, B, at a radius r_p, to the total current closed by that radius, $J_{enclosed}$. Thus, contours of equal enclosed current can readily be plotted from a knowledge of the magnetic field distribution; these contours can then be used to deduce the distribution of current density in the arc discharge.

Several turns of thin Formvar wire, wound on a 1/8-in.-diameter coil, provide sufficiently large signals and sufficiently fine spatial resolution to accurately measure the strong magnetic fields of the high-current, pinch and parallel-plate devices. However, in order to measure the weak magnetic fields at the anode of the quasi-steady MPD arc, much more sensitive probes are required. The probes used for this purpose consist of 100 turns of #40 Formvar wire wound on a 3/16-in.-diameter nylon spool. The probes are bent to allow access to the back portions of the anode; and the signals are fed to a Type 555 dual-beam oscilloscope through an integrator circuit with RC = 1500 μsec, a time one order of magnitude longer than the current pulse in order to avoid excessive droop in the integrated signal.

F. INNER VOLTAGE DIVIDER

Voltage studies were carried out on both the cylindrical pinch and parallel-plate facilities, wherein the resistive voltage drop across the current sheet must be separated from the inductive voltage contribution associated with the rapidly propagating current distribution. The pure resistive component of the discharge voltage can be monitored by the proper placement of an inner divider voltage tap; i.e., an insulated metal rod which completes a circuit between the two electrodes such that no magnetic flux is enclosed. In the pinch geometry, the voltage top must be located at the chamber center, whereas a voltage top inserted at the downstream end of the parallel-plate accelerator serves the same purpose. Magnetic fields fold out behind the propagating current sheet; i.e., interior to the current sheet and the return conductor path. Hence, it can readily

be seen that a measuring circuit consisting of the current sheet, the two electrodes, and a downstream voltage tap, will not enclose any magnetic flux (see Fig. 3-4). A Tektronix Model 6013 voltage probe is used to monitor the total voltage drop of this measuring circuit, which is simply the resistive voltage across the current sheet neglecting the voltage drops along the electrodes and metal voltage tap.

G. TWIN LANGMUIR PROBE TECHNIQUE

Twin Langmuir probes have been successfully employed to measure the electron temperature and number density at several locations inside the arc chamber, and adjacent to the anode of the quasi-steady MPD facility. These probes consist of two separately shielded, and biased, 1/8-in. long exposed tips of 3-mil tungsten wire, oriented parallel to the flow axis to minimize streaming effects, and placed sufficiently close together to sense essentially the same plasma. The probe radius is less than the anticipated electron-ion mean free path in the region to be probed and larger than the Debye length, in order to minimize the effects of particle collisions and sheath size on the measurements.[44]

The twin probe technique involves the attachment of different resistor pairs to the two probe tips, and the monitoring of the voltage developed across these resistors with Tektronix P6006 voltage probes (Fig. 3-5). A differential Type G pre-amplifier is used with a Tektronix Type 555 dual-beam oscilloscope to record the voltage difference between the two probe tips. In this way, a single discharge of the accelerator will provide sufficient information for the determination of local electron temperature, provided that both probes operate in the electron retarding portion of the Langmuir probe characteristic. This simple calculation is based on the following reasoning. The electron current to a probe tip, which is biased to retard electron flux, is given by

$$I_e = e A_p \left(\frac{m_e \bar{C}_e}{4}\right) \exp\left(\frac{e V_p}{k T_e}\right) \qquad (3\text{-}4)$$

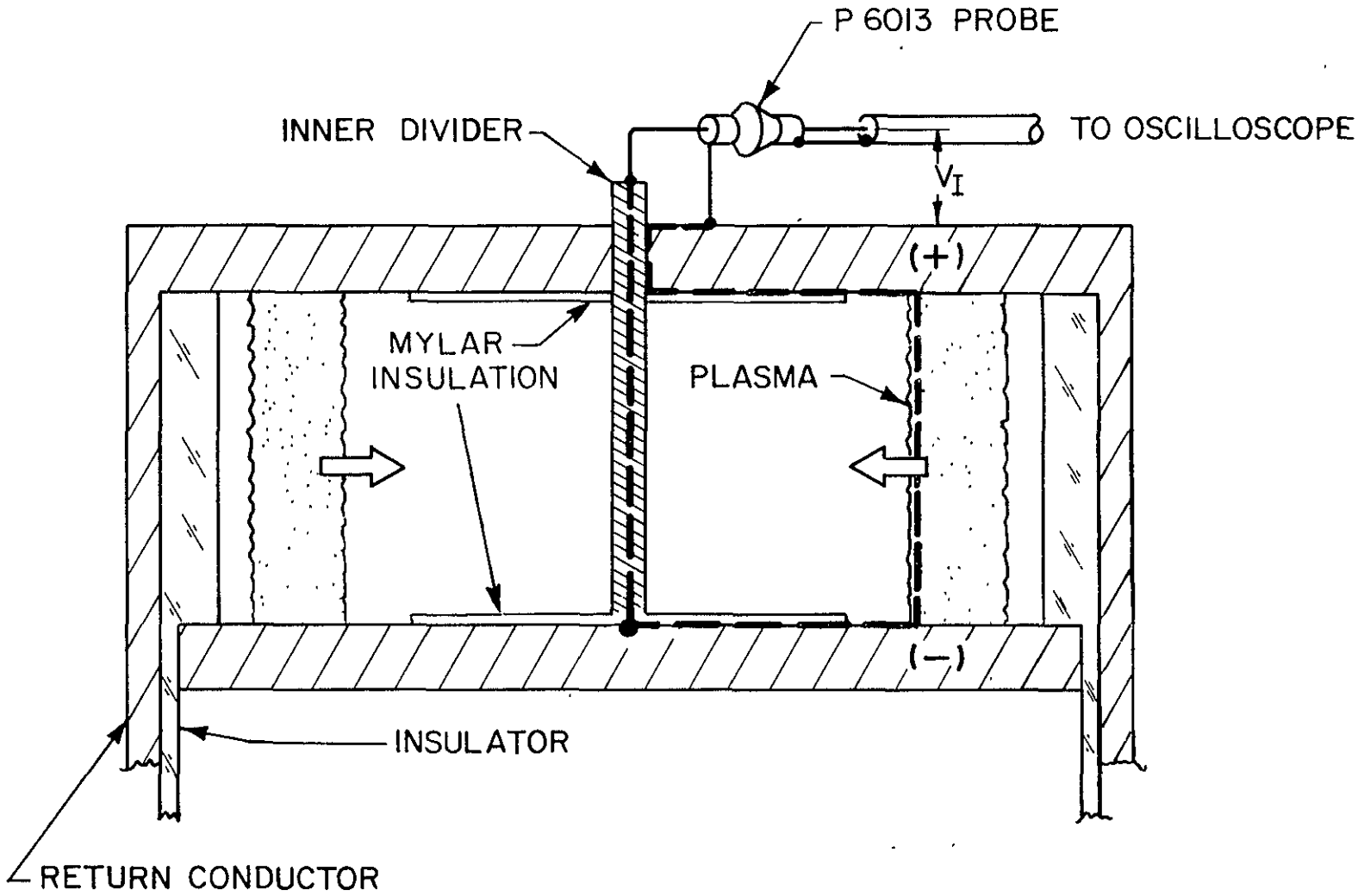

INNER DIVIDER VOLTAGE MEASUREMENT

FIGURE 3-4

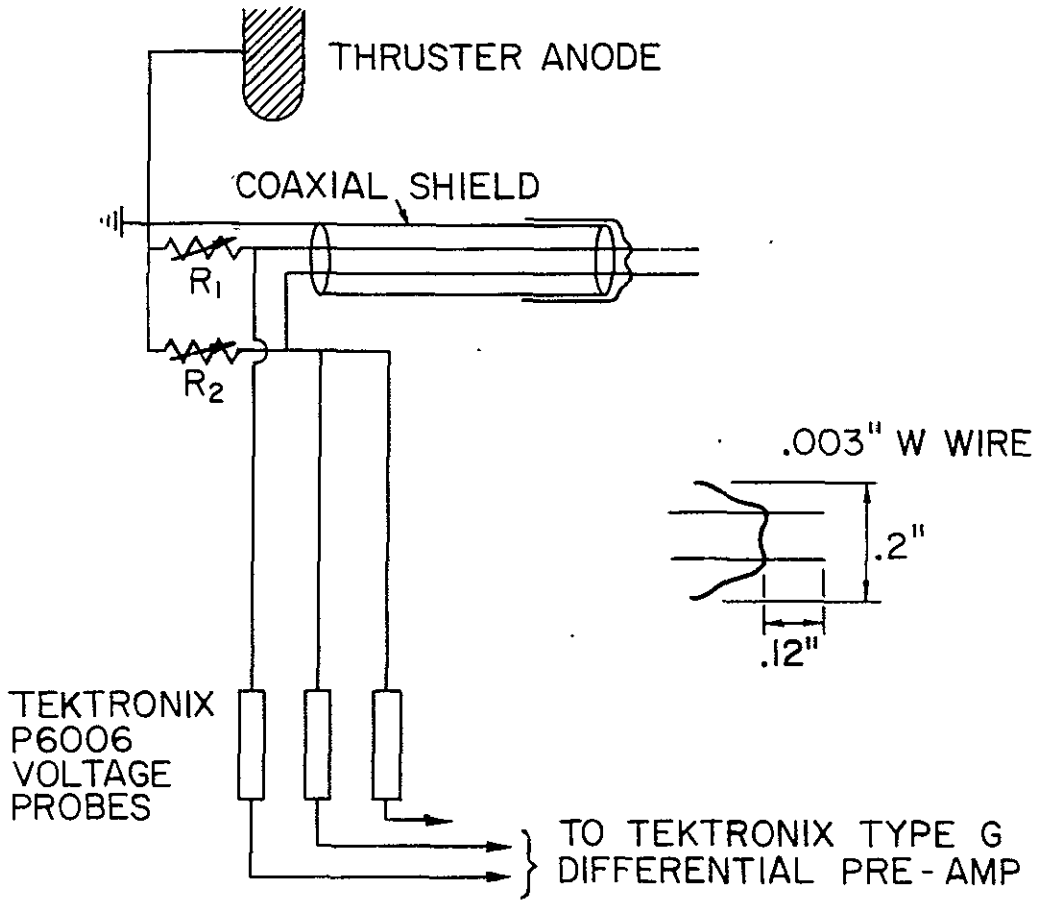

SCHEMATIC OF TWIN LANGMUIR PROBE AND CIRCUITRY

FIGURE 3-5

where A_p is the area of the probe tip, n_e and T_e are the electron number density and temperature respectively, $\bar{C}_e$ is the mean thermal electron speed, and V_p is the probe potential relative to plasma potential. When both probe tips operate on the electron retarding branch of the characteristic, the ratio of the relative electron currents is

$$I_{e1}/I_{e2} = \exp\left(\frac{e}{kTe}(V_1-V_2)\right) \qquad (3\text{-}5)$$

where V_1 and V_2 refer to the actual probe tip voltages since the plasma potential value cancels out of the difference. The advantage of the twin electrostatic probe technique rests with the fact that I_1, I_2, V_1, and V_2 are measured at the same time in the same discharge, thus assuring that n_e and $\bar{C}_e$ will cancel precisely in the above ratio, and thereby eliminating the problem of shot-to-shot fluctuations in electron density. Furthermore, it is required that the probe tips draw a sufficiently large electron current that the ion current to the probe can be neglected, therefore

$$I_{e\,1,2} \approx I_{1,2} = V_{1,2}/R_{1,2} \qquad (3\text{-}6)$$

where $I_{1,2}$ are the actual currents drawn by the respective probe tips, calculated from the measured probe voltages, $V_{1,2}$, and known resistor values, $R_{1,2}$. Thus, taking the logarithm of Eq. (3-5) and using the above approximations yields

$$Te = \frac{e}{k}(V_1-V_2)/\ln(I_1/I_2) \quad {}^{\circ}K$$

or

$$kT_e = e\Delta V_{12} / \ln(I_1/I_2) \quad eV \qquad (3\text{-}7)$$

To reiterate, this expression for electron temperature is valid only when both probes are retarding the electron flux and the electron flux to the probe still greatly exceeds the ion flux. Probe data must be collected for a number of different resistor pairs in order to establish when the proper domain of probe operation has been achieved, and when the probes cease to retard electrons and pass over onto the electron-collecting branch of the probe characteristic. This transition occurs when the probe potential becomes equal to the plasma potential and results in a noticeable change in probe behavior. At this special condition, the probe current is given by

$$I^* = e A_p (n_e \bar{c}_e / 4)$$

$$= e A_p \left(\frac{kT_e}{2\pi m_e} \right)^{1/2} m_e \qquad (3\text{-}8)$$

The electron number density, n_e, is thus readily obtained from the previously determined electron temperature, T_e, the probe surface area, A_p, and the measured probe current at the transition from the electron-retarding to the electron-collection regions, I^*.

Figure 3-6 displays a typical plot of twin Langmuir probe data for 17.5 kA x 5.9 g/sec operation of the quasi-steady MPD arc; the twin probe was located at a chamber radius of 3/4 in., and axial position 1 in. upstream of the front anode

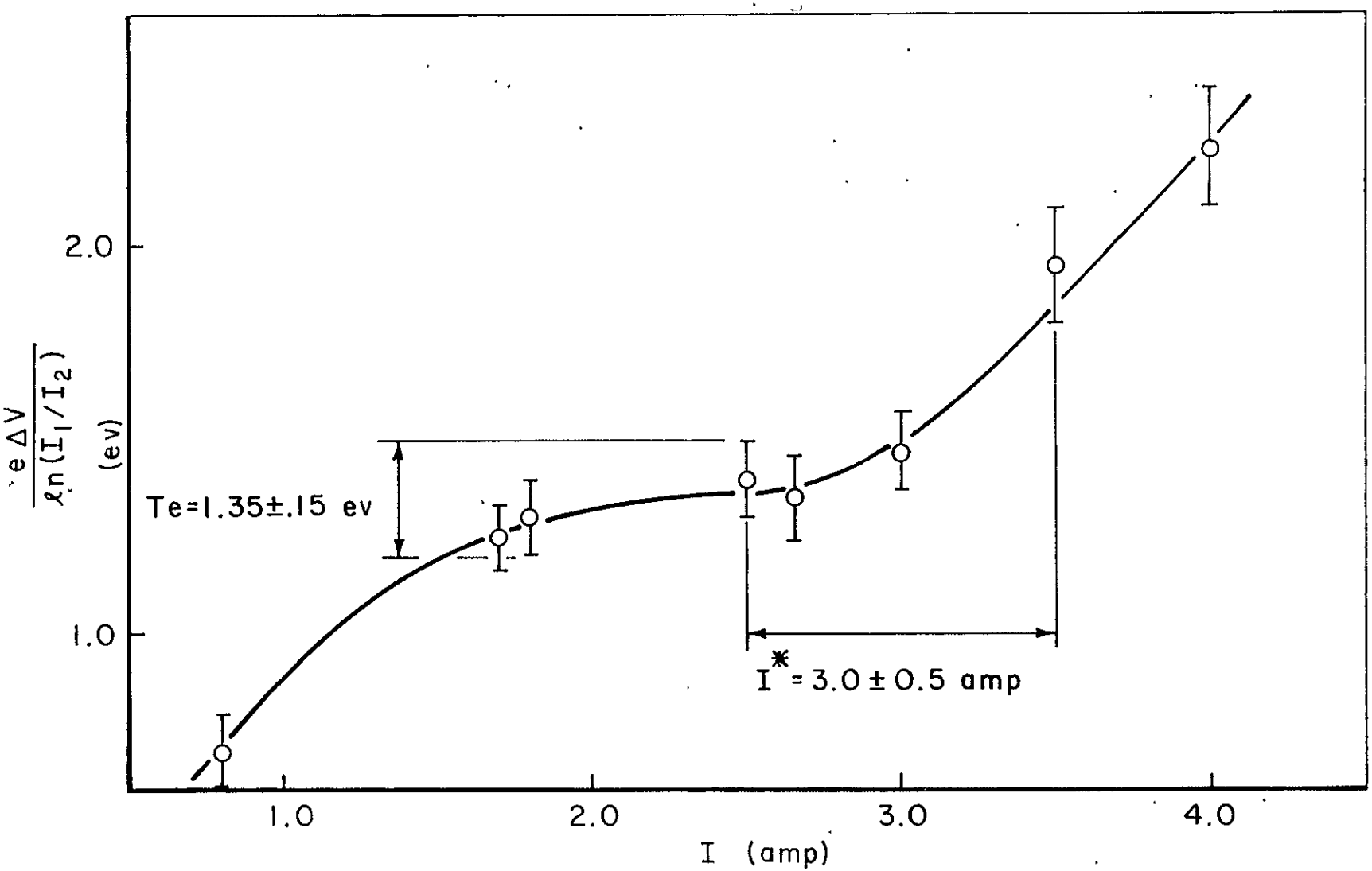

TWIN LANGMUIR PROBE DATA AT r=3/4 in, z=-1 in.
AND 17.5 kA × 5.9 g/sec

FIGURE 3-6

face. The quantity $e\Delta V_{12}/\ln(I_1/I_2)$ is plotted against the larger of the two probe currents for several different resistor pairs. Several features of this plot are immediately evident. The plateau between 1.75 and 2.75 A corresponds to probe operation in the high-current portion of the electron retarding branch. In this region of the characteristic, $kT_e = e\Delta V_{12}/\ln(I_1/I_2)$ and therefore the electron temperature is read directly from the ordinate to be

$$kT_e = 1.35 \pm 0.15 \text{ eV}$$

The rise in the curve at around 3.0 A indicates that the probe has reached the transition region and hence has a potential equal to that of the surrounding plasma. At this condition the electron density is given by Eq. (3-8). Substituting $I^* = 3.0 \pm 0.5$ A from the above plot, and inserting $T_e = 1.35 \pm 0.15$ eV into Eq. (3-8), yields the following value

$$n_e = 1.3 \pm 0.4 \times 10^{20} \text{ m}^{-3}$$

The departure from the plateau at the low currents reflects probe operation on the low current portion of the electron-retarding branch where the approximation, $I_e \approx I$ is violated. The quantity $e\Delta V_{12}/\ln(I_1/I_2)$ no longer equals the local electron temperature and begins to decrease as the two probe potentials start to converge.

CHAPTER IV

EXPERIMENTS ON THE 8-INCH PINCH DEVICE

A. BACKGROUND

Early experimental work carried out on the 8-in. pinch device with associated pulse-forming network, described in Chap. III, yielded certain anomalous data on current sheet dynamics which eventually led to the present studies of anode phenomena.[15] These early studies compared the observed current sheet trajectories with those computed from the so-called "snowplow model" of the pinch event. This model considers the current sheet to be an impermeable front, driven by self-magnetic fields, which entrains and imparts substantial velocity to the gas as it sweeps towards the chamber center. The term "inelastic piston" aptly describes this acceleration model. For most situations considered, the agreement between theory and experiment was rather good, except in certain cases where the current sheet appeared to divide spontaneously at about mid-chamber radius into two concentric sheets of like sign, which then followed each other to the center of the chamber. This peculiar event was first observed when a relatively flat current pulse of 200 kA and 5.5 μsec duration was used to drive an 8-in. pinch discharge into 100 μ of ambient argon fill. So-called "current sheet bifurcation" was detected by means of unintegrated magnetic probe records which departed from the normal single peak configuration, representing the passage of a single current sheet, and began to display two distinct maxima, implying the passage of two similar current sheets. After the inception of current sheet bifurcation, the slower of the two signal peaks continued to follow the predicted snowplow trajectory, whereas the leading peak ran forward at

approximately twice the snowplow velocity. Figure 4-1 displays the trajectory plots for the bifurcating-sheet along with the theoretical snowplow trajectory; also shown is the driving-current waveform used in this experiment. It was noted that a factor of approximately two separates the leading sheet velocity from the snowplow velocity. This suggests an "elastic piston" model, wherein particles are elastically reflected off of the moving current sheet, thereby acquiring a velocity which is twice that of the sheet.

B. MAGNETIC PROBE STUDIES

In order to test the elastic piston hypothesis, further magnetic probing of these interesting pinch discharges was carried out. The above quoted data were taken with magnetic probes constrained to the midplane of the pinch device; to explore the axial development of the bifurcation event, magnetic probe readings were taken at several different axial positions in the chamber. Figure 4-2 displays the magnetic probe responses at a chamber radius of 1 in. along with the 400 kA x 3.6 μsec driving-current pulse, also found to produce anomalous sheet behavior. With the probe located 1/4 in. from the anode, Fig. 4-2a, two distinct maxima are seen, implying the passage over the sensing coil of two distinct zones of high-current density. In Figs. 4-2b and 4-2c, the probe is moved from a position 1/2 in. from the anode to one at the chamber midplane, with the result that the $\partial B/\partial t$ (unintegrated probe signal) maxima have moved closer together and appear to coalesce into a single peak similar to that observed at a probe position 1/2 in. from the cathode (Fig. 4-2d). This single maxima class of response is maintained everywhere from this location up to the cathode surface.

Figure 4-2 yields two other important pieces of information. The front-running $\partial B/\partial t$ peak near the anode is ahead of the midplane response, thus agreeing with the previously observed tilt of the current sheet wherein the anode attachment runs ahead of the main portion of the sheet, see

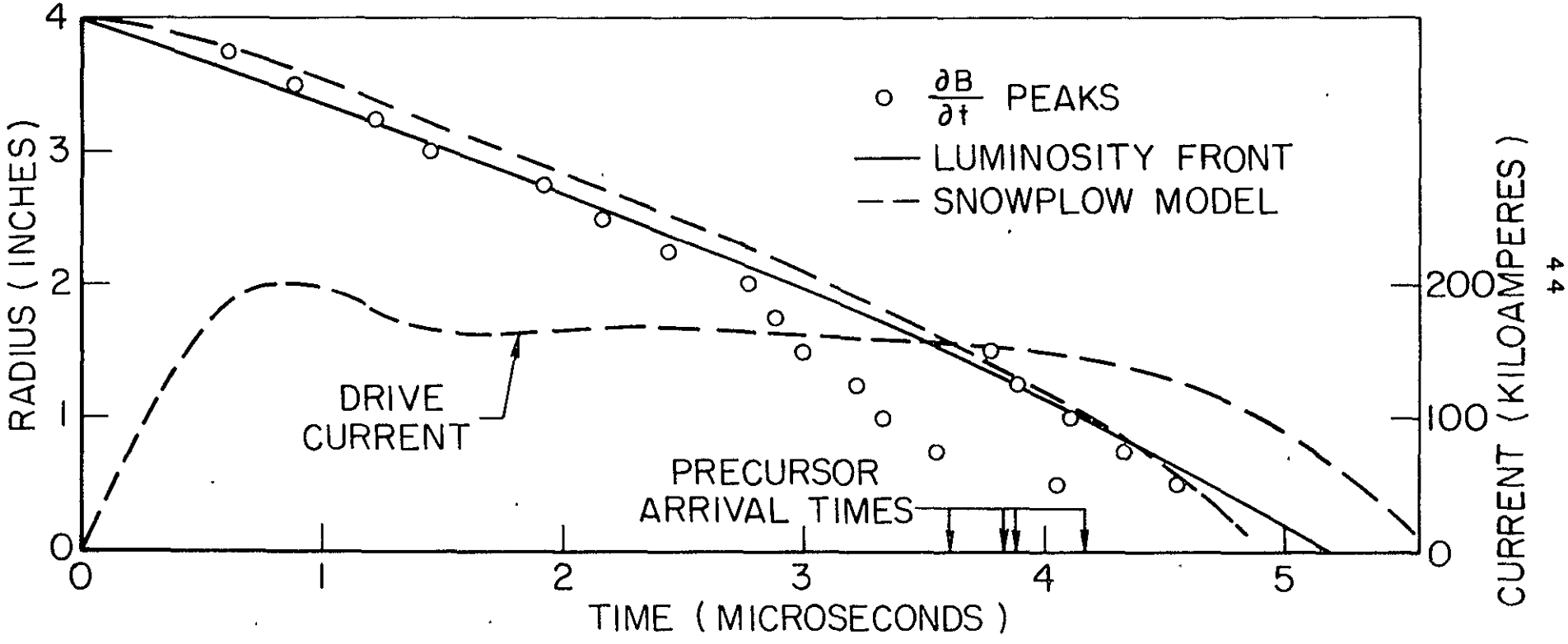

FIGURE 4-1

TRAJECTORIES OF: $\frac{\partial B}{\partial t}$ MAXIMA, LUMINOUS FRONT AND SNOWPLOW MODEL IN 8" PINCH DISCHARGE AT 100μ ARGON (REF. 15)

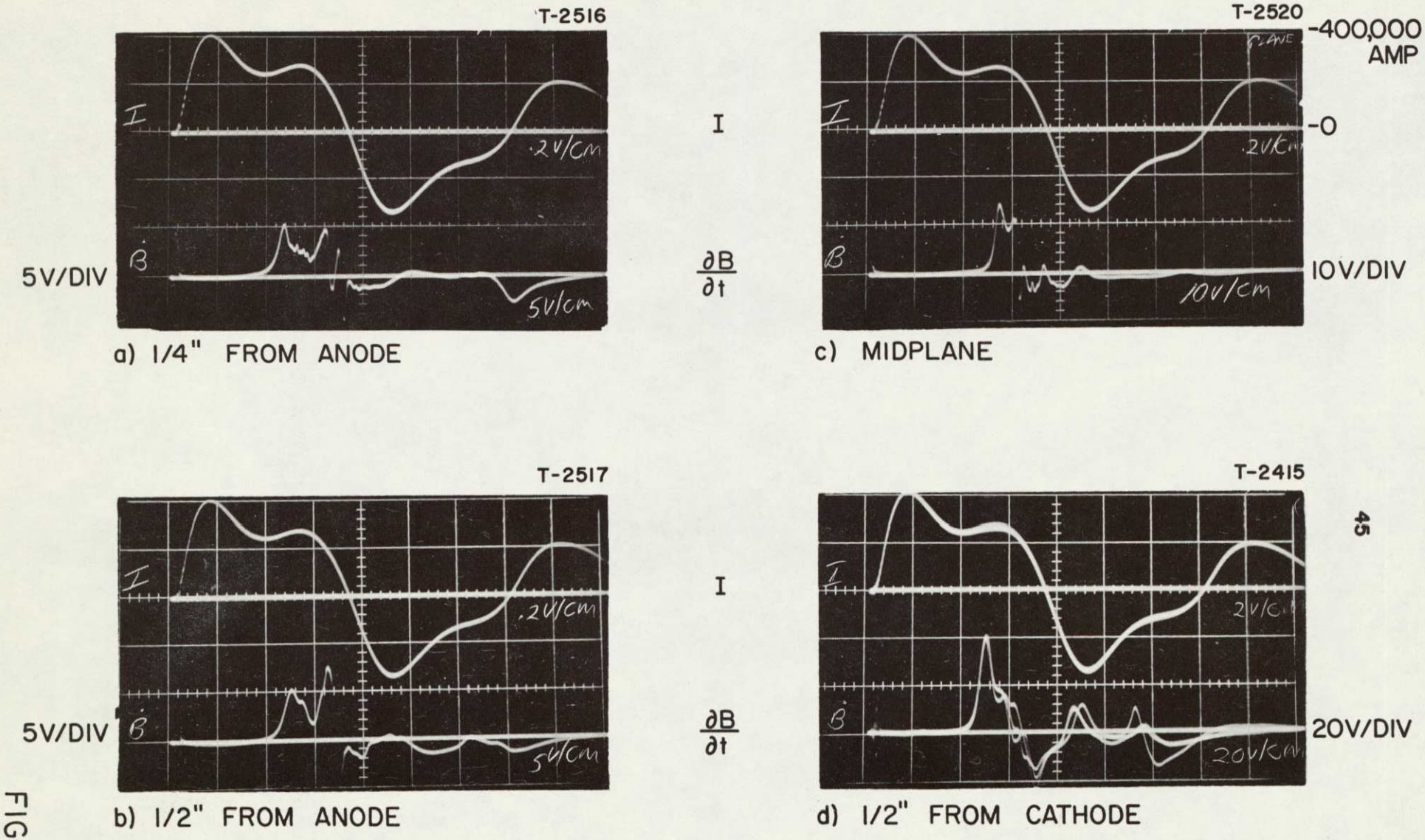

FIGURE 4-2

MAGNETIC PROBE RESPONSES AT VARIOUS AXIAL POSITIONS AND FIXED RADIAL POSITION OF r=1.0" IN A 100μ ARGON DISCHARGE

FIGURE 4-3

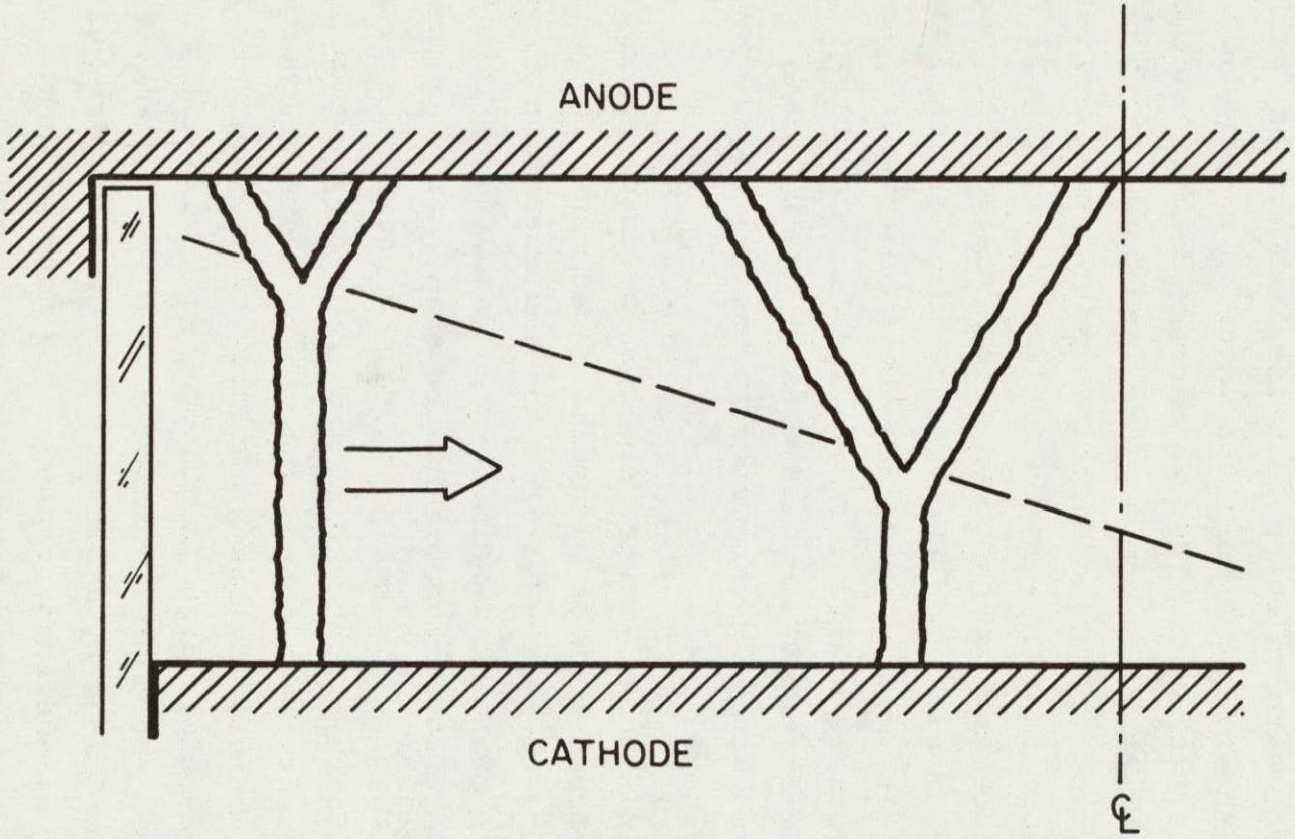

SCHEMATIC REPRESENTATION OF
ANODE FOOT DEVELOPMENT DURING PINCH

Chap. II, Sec. G. Also, the magnitude of the maximum probe response near the anode is about one-half that of the probe near the cathode, and more broadly spread, implying a more diffuse current density structure at the anode.

A collection of data of this type now suggests a substantially different image of the bifurcation process. Namely, that the current extends to the cathode in a single, well-defined current sheet, but enters the anode in a more diffuse, double-humped attachment. The two current density maxima are widely separated at the anode surface, and coalesce to the single sheet structure at some "triple point" away from the surface thus forming a "Y"-shaped configuration, Fig. 4-3. As this structure propagates toward the center of the chamber, the separation of the anode attachment widens and the "triple point" progresses axially away from the anode, steadily eroding more and more of the original single sheet. Magnetic probes placed on the midplane thus would observe a single sheet at large radii, and would be subjected to the well-developed anode bifurcation at small radii, recall Sec. A.

Further studies with magnetic probes have demonstrated that the phenomena of anode bifurcation can occur for a variety of driving-current waveforms and ambient argon chamber pressures. The event is favored by relatively slow rise time pulses of either flat or double-humped shape, and was observed over a broad range of chamber pressure. However, the extent of the anode attachment structure and the rate at which it erodes the current sheet depend on both of these discharge parameters. Furthermore, the anode bifurcation event is peculiar to large-radius pinch discharges with relatively long discharge times. Burton,[45] working with a 5-in.-diameter pinch discharge driven by a 300 kA x 1.2 μsec current pulse, observed only well-defined, reproducible current sheets with no evidence of a broad and divided anode structure. On the other hand, Kolpin[46] observed double maxima in current density in a large-radius inverse pinch, employing 16-in.-diameter electrodes, a 600 kA x 14 μsec current pulse, and ambient

helium at 500 μ. From these observations it would appear that anode bifurcation is also a function of discharge time and geometry. The 1.2 μsec pinch time of Burton's small radius discharge is simply too short for this anode structure to develop to any observable degree.

C. PHOTOGRAPHIC STUDIES OF ANODE BIFURCATION

Following the initial observations of this unusual current sheet behavior, attempts were made to map the current density distribution in the "anode foot" region, but this was precluded by an inordinate scatter in the data, a significant result in itself for these otherwise highly reproducible closed-chamber discharges. The unusual irreproducibility of these measurements is interpreted to indicate that the discharge current experiences considerable difficulty in establishing a viable conduction mechanism near and into the anode surface, and thus is vulnerable to unspecified instabilities and turbulence in this region.

In deference to the above-mentioned irregularity of the process, a systematic photographic study was undertaken to catalog the visual aspects of the domain before attempting further accumulation of electrical data. For this purpose a series of radial-view Kerr-cell photographs were taken of the discharge. This was accomplished by removing a section of the outer return conductor, allowing radial optical access to the interior of the chamber through the glass wall insulation (Fig. 4-4). All of the displayed photographs were taken with a 100 μ argon discharge in a 8-in. diameter chamber driven by a 5.5 μsec x 200 kA current pulse. A magnetic probe, visible in the photographs, was also inserted axially into the chamber to provide $\partial B/\partial t$ records along with Kerr-cell photographs.

The first series of photographs, displayed in Fig. 4-5, shows the progress of the pinching current sheet from 1.4 μsec to 3.8 μsec after initiation of the discharge. These pictures again show that the luminous front does divide and diffuse

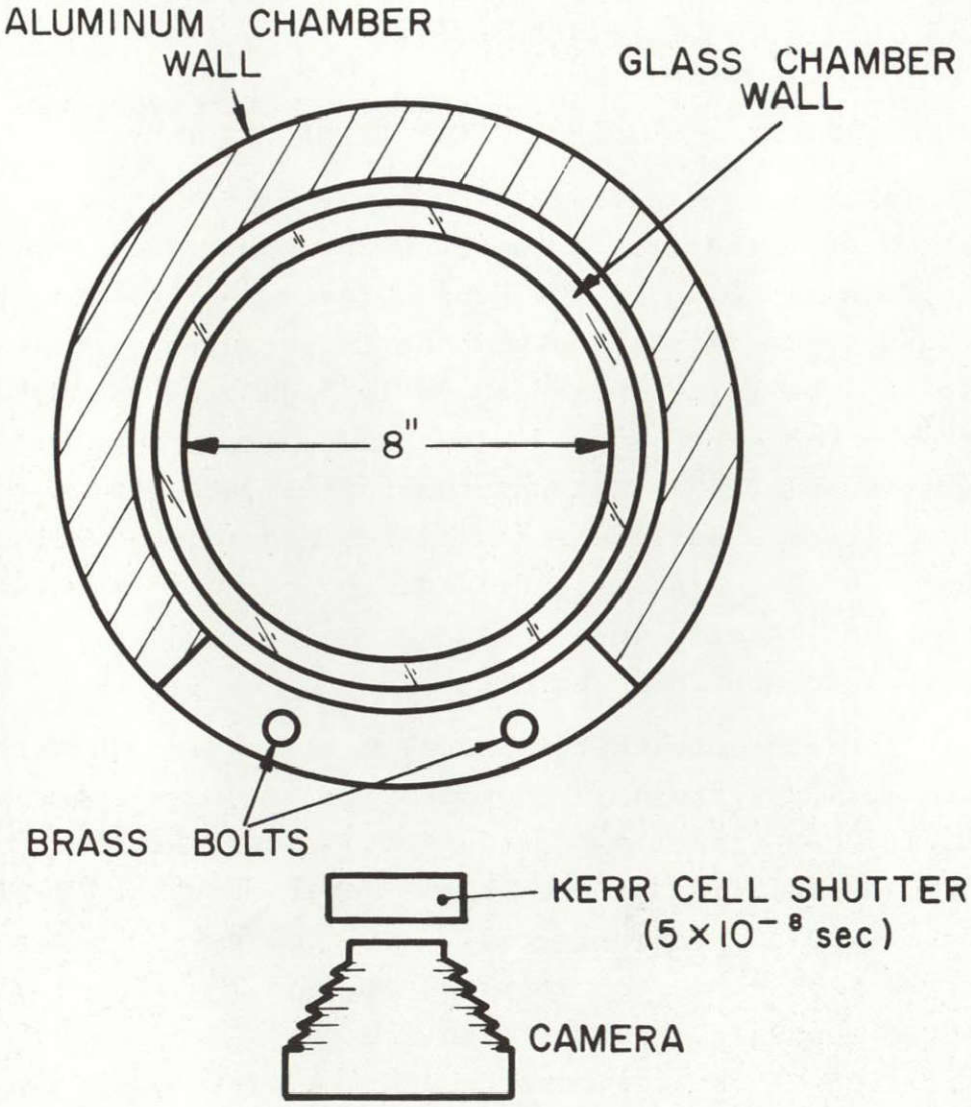

KERR CELL CAMERA ARRANGEMENT
FOR FOLLOWING PHOTOGRAPHS

FIGURE 4-4

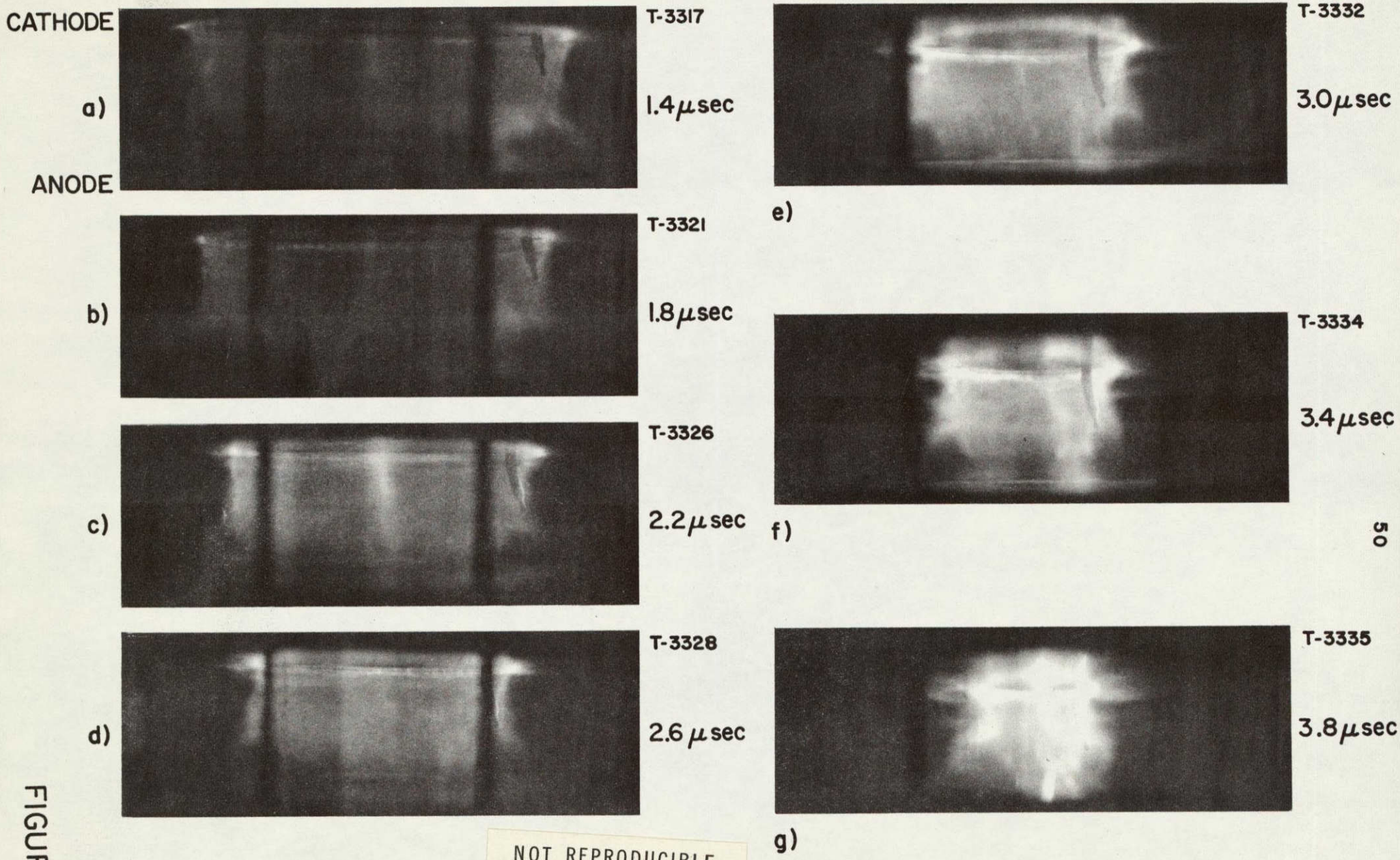

FIGURE 4-5

PROGRESS OF BIFURCATING CURRENT SHEET IN 100 μ ARGON

near the anode, and that the disturbance grows towards the cathode as the current sheet propagates inward.

Correlation of such Kerr-cell photographs with corresponding magnetic probe records allows one to relate the luminosity front to the current conduction regions of the sheet. Figure 4-6 compares photographs with the appropriate magnetic probe records for three different positions of the probe. In Fig. 4-6a, both the luminosity pattern and the magnetic probe data indicate a single current conduction zone at the midplane. For Fig. 4-6b the magnetic probe has been positioned 1/2 in. from the anode. The photograph shows the probe standing between the two "legs" of the bifurcated current sheet. The corresponding probe trace shows that one current conduction region has swept over the probe prior to 1.8 μsec and that a second current zone is about to pass the probe. Apparently, then, each part of the bifurcated luminosity front has a current conduction region associated with it. Figure 4-6c, with the magnetic probe at a position 1/4 in. from the anode, further supports this conclusion.

In the course of this qualitative photographic survey, it seems reasonable to try to establish the pressure dependence of the anode foot processes. Figure 4-7 shows photographs of current sheets propagating into ambient argon at pressures of 50 μ, 100 μ, and 200 μ at approximately the same radial positions. In each case the driving current is constant at about 200 kA for the times indicated. Each photograph shows the familiar current sheet bifurcation near the anode, with little drastic change in scale over the range tested. In fact, the degree of similarity among the three figures would seem to indicate that chamber pressure is not a critical factor in determining the current sheet behavior near the anode.

Under certain conditions another aspect of the anode process has been observed photographically. When a highly polished aluminum electrode is employed, a distinct filamentary "spoking" is found to occur at a random spot on the anode. Figure 4-8 illustrates the situation: at the early

T 3322

1.8 μ sec

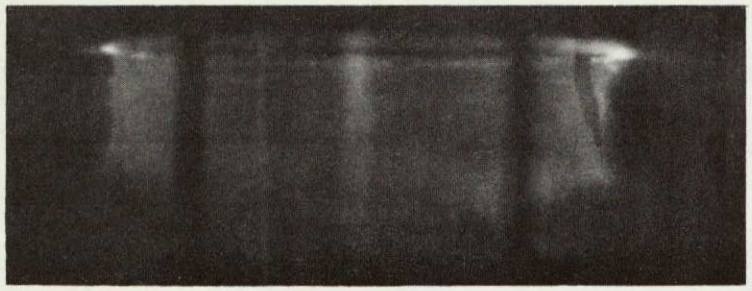

a) ANODE

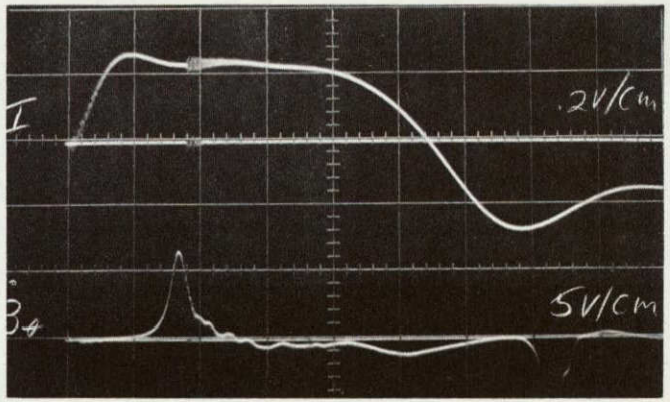

MIDPLANE

T 3323

1.8 μ sec

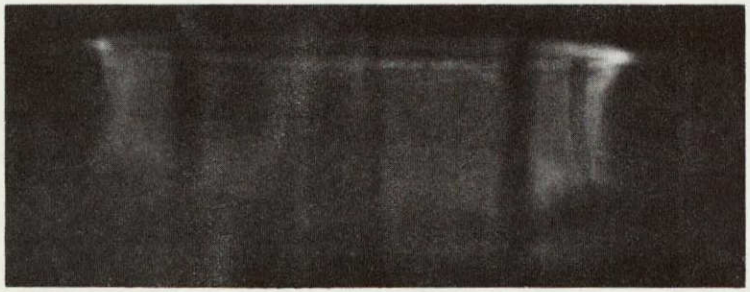

b) ANODE

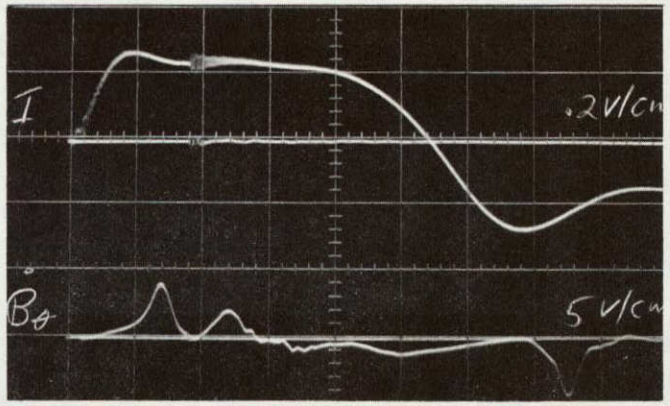

1/2" FROM ANODE

NOT REPRODUCIBLE

T 3324

1.8 μ sec

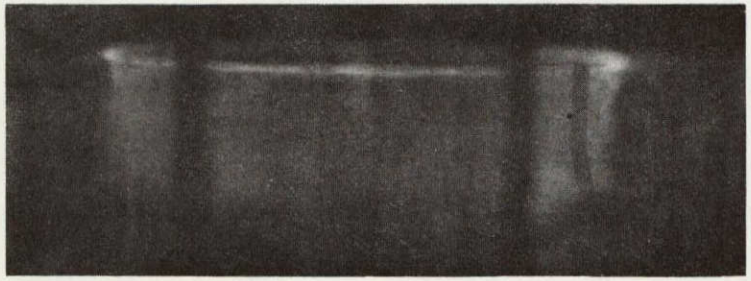

c) ANODE

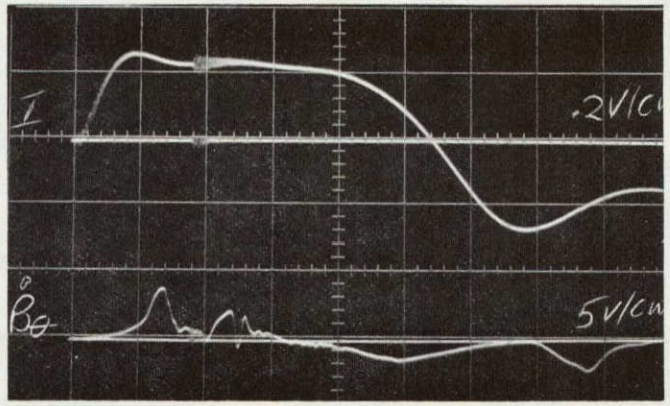

1/4" FROM ANODE

FIGURE 4-6 SIMULTANEOUS KERR CELL PHOTOGRAPHS AND MAGNETIC PROBE RECORDS

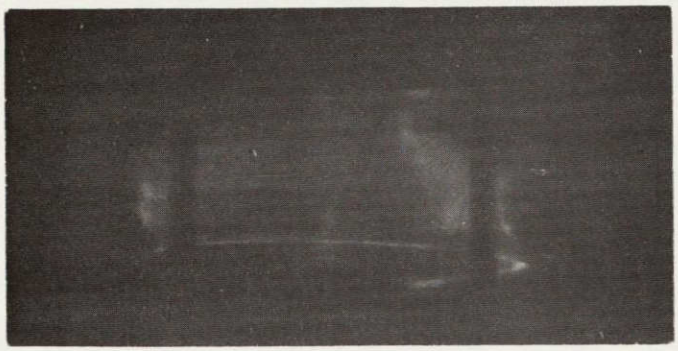

a) 50 μ ARGON

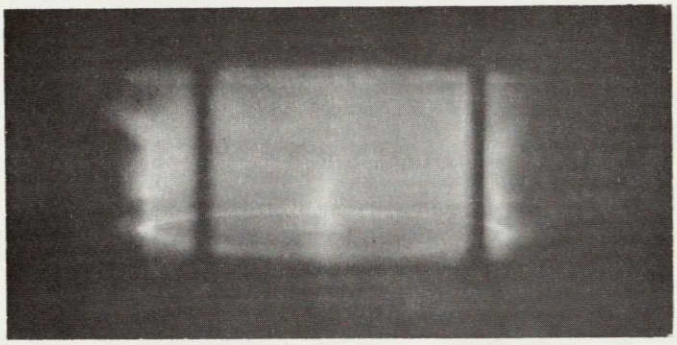

b) 100 μ ARGON

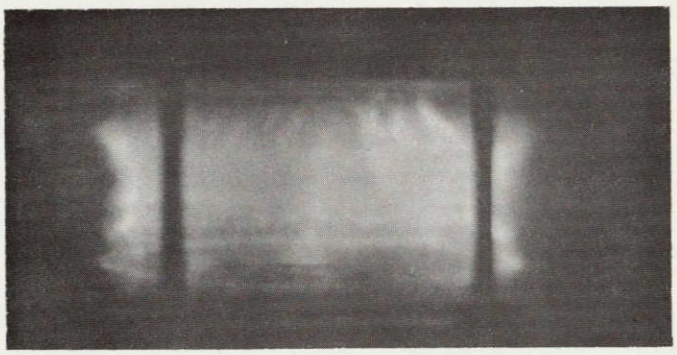

c) 200 μ ARGON

PRESSURE DEPENDENCE OF ANODE FOOT

FIGURE 4-7

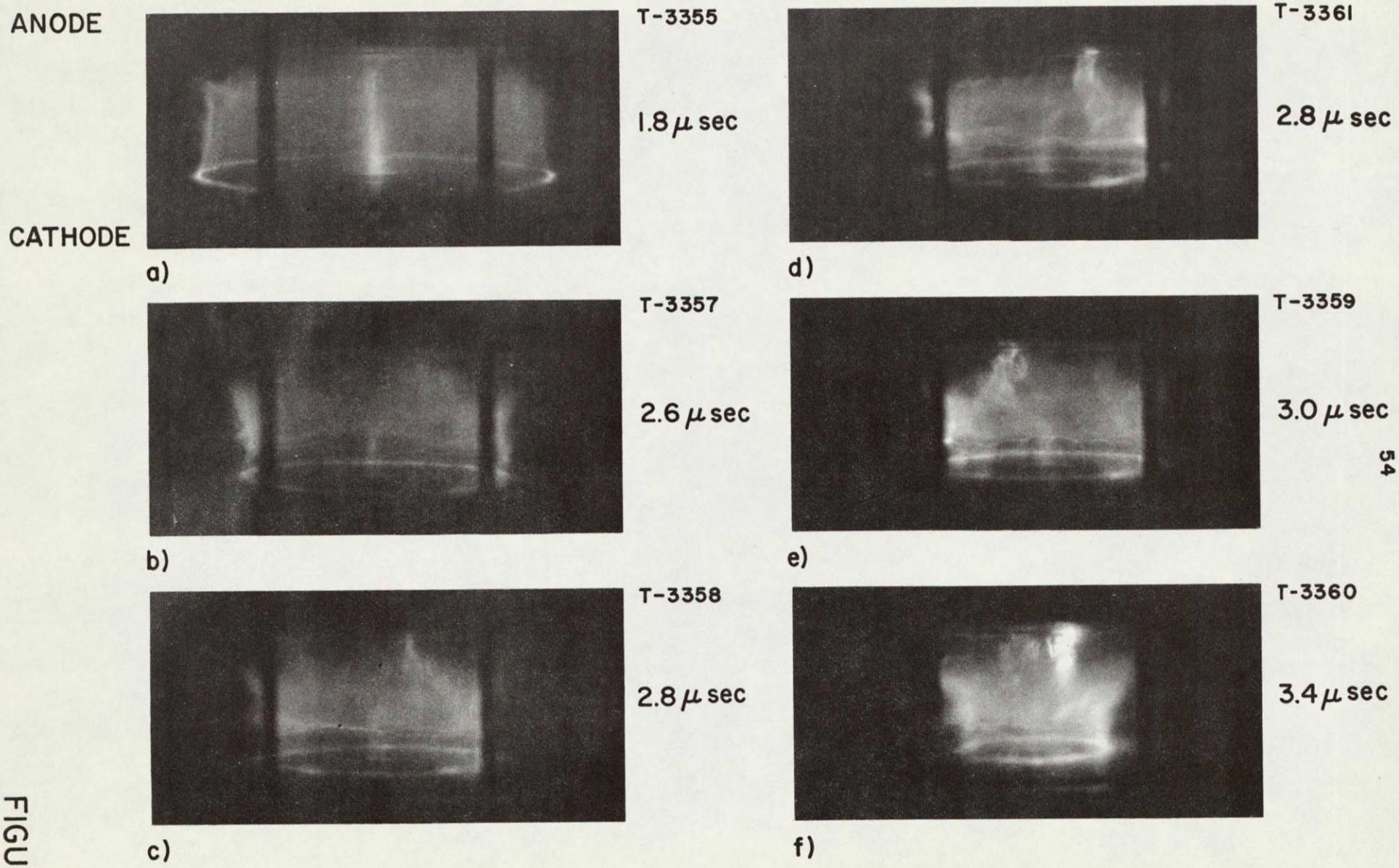

FIGURE 4-8

FORMATION OF ANODE SPOKE

times the familiar bifurcated anode attachment is observed, but later, at about 2.6 μsec, a luminous "spot" is seen to form on the anode surface. This luminous spot intensifies as the current sheet propagates inward. This is not to be confused with the central chamber luminosity, seen in the early photographs, which is caused by a process known as "bleed through," in which some of the intense luminosity produced when the sheet collapses at the chamber center is able to penetrate the nitrobenzene shutter of the Kerr cell and register on the film. From many photographs of this type, it is concluded that the "spoke" does not form at any one particular point on the anode, but seems to attach at a different point for each discharge. Little is presently known about the current densities associated with this "anode spoke" but it seems reasonable, however, that such instabilities give rise to the irreproducible magnetic probe data mentioned earlier. Finally, this "spoking" phenomena may be interpreted to mean that the discharge current is having difficulty establishing a feasible conduction mechanism at the anode, and must therefore resort to unusual and erratic means of making the transition across the metal-plasma interface.

D. ARC VOLTAGE MEASUREMENTS

Further experiments associated with the study of current conduction properties at the anode of the 8-in. pinch discharge have focused on measurements of the arc voltage in this device. Since unsteady discharges of this kind have very large inductive voltage contributions, it is necessary to employ an inner divider voltage probe (see Chap. III, Sec. F) to measure the pure resistive component of the total discharge voltage, referred to as the arc voltage. Since the arc voltage is a good index of the energy delivered to the electrodes and to Joule-heating of the arc plasma, and since the broad and diffuse anode attachment of the pinching current sheet probably involves certain dissipation of energy, it seems reasonable to seek, now, some correlation between the arc voltage and the current distribution near the anode.

For this purpose, the 8-in. pinch discharge was monitored with an inner voltage divider constructed of an insulated metal rod inserted across the chamber electrodes to complete a measuring circuit of which the current sheet is part. The signals were presented to the oscilloscope via a Tektronix Model 6013 voltage probe of 10^8 ohm impedance. The relevance of the current sheet anode attachment, as well as other features of anode current conduction, in determining the resistive voltage drop, or arc voltage, was assessed by a technique of selective electrode insulation. Namely, the 8-in.-diameter pinch electrodes were partially insulated by attaching to them two circular layers of 0.005-in. mylar of diameter 4 in., 6 in., and 7 in., respectively (Fig. 4-9). In one sequence of measurements an electrode with a 6-in.-diameter glass center section was used to provide the desired electrode configuration.

Figure 4-10 shows a series of oscillograms of driving-current waveforms and inner divider voltage signatures, in triple overlays, for the cases where 7-in.-diameter mylar covered, alternately, major portions of the anode, cathode, and both electrodes. The quoted voltage readings were taken at the earliest measurable time, 0.4 μsec, when the driving current has a value of 130 kA and when a viable current sheet is becoming established at the outer wall. Figure 4-10a shows the voltage signature for the normal all-metal electrode situation. The portion of the signature of primary interest lies between 0.4 μsec and 3.0 μsec; i.e., well before the arrival of the current sheet at the center voltage tap. The large signal following at 4.0 μsec is caused by magnetic flux linkage in the measuring circuit after the current sheet collapses at the chamber center. Figures 4-10b and 4-10c demonstrate the different effects on arc voltage caused by cathode and anode insulation, respectively. Figure 4-10b is interpreted as follows: during the first 1.0 μsec after breakdown the narrow cathode attachment has not yet contacted the electrode insulation and, therefore, the arc voltage closely approximates

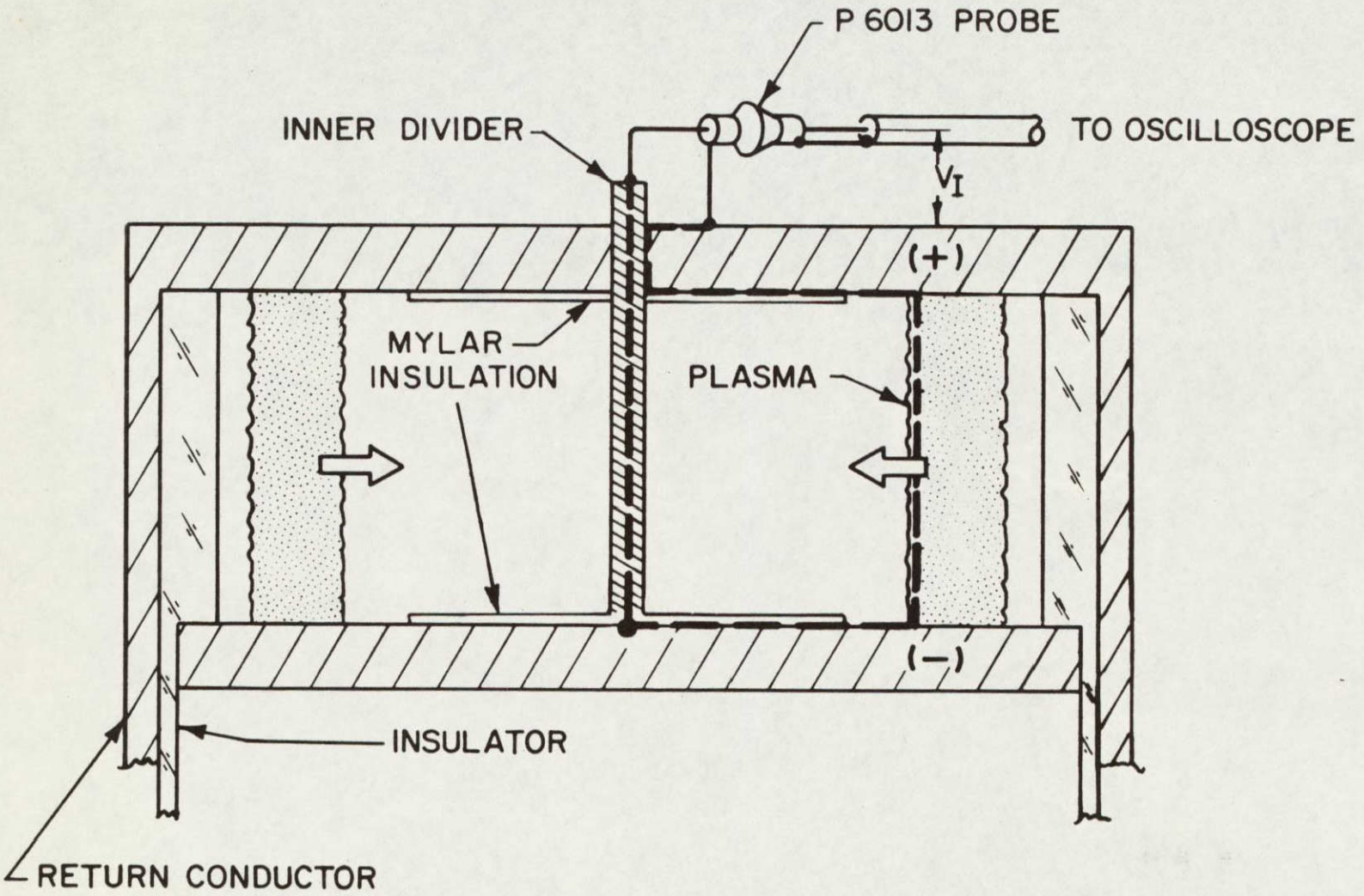

FIGURE 4-9

SELECTIVE ELECTRODE INSULATION EXPERIMENT

T-3819

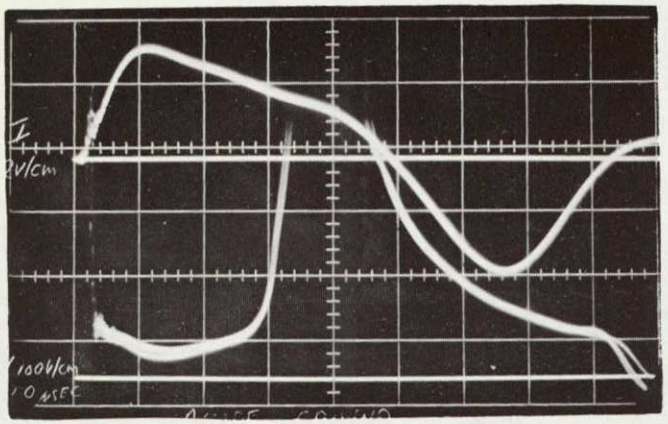

70V—

a) BOTH ELECTRODES METAL

T-3833

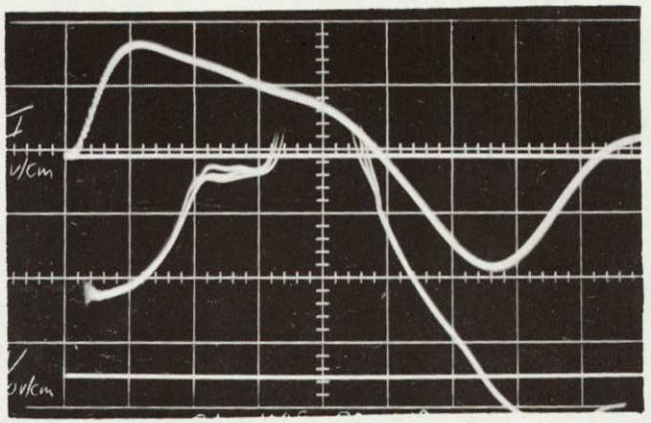

J

130V—

V_I
100V/DIV
1 μsec/DIV

c) ANODE COVERED, r= 3.5" MYLAR

T-3834

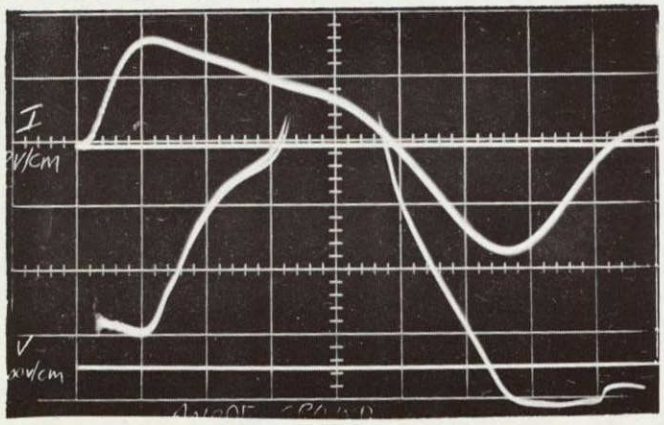

70V—

b) CATHODE COVERED, r= 3.5" MYLAR

T-3835

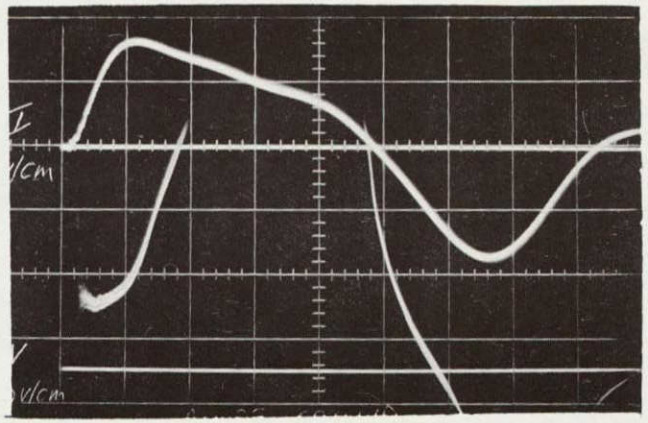

J

120V—

V_I
100V/DIV
1 μsec/DIV

d) BOTH COVERED, r= 3.5" MYLAR

FIGURE 4-10

OSCILLOGRAMS OF CURRENT WAVE FORM
AND INNER DIVIDER VOLTAGE

the all-metal case over this time period. At 1.0 μsec the cathode attachment reaches the insulation and is arrested there, while the bulk of the current sheet runs inward, bending back along the insulation to maintain contact with the exposed cathode. The large voltage rise between 1 μsec and 3 μsec may thus be due to the increasing arc length as the current pattern moves inward, or to some other dissipative effect associated with this distortion of the cathode attachment pattern.

When the experiment is repeated with the anode rather than the cathode insulated, (Fig. 4-10c), the voltage is substantially higher, 130 V compared to 70 V for cathode insulation, at the earliest observable time, 0.4 μsec. It then begins to increase rapidly, indicating that the broader anode attachment is already being distorted by the insulating layer, and is thereafter arrested causing the arc length to increase until the sheet collapses at the chamber center. The failure of the arc voltage to lower to the "all-metal" voltage, even at the earliest observable time, is indicative of the involvement of the interior portions of the anode surface in the early phases of the normal pinch discharge. Once the anode is insulated, little change in the inception or earliest observable arc voltage is affected by additional insulation of the cathode (Fig. 4-10d). This result, along with that for cathode insulation alone (Fig. 4-10b), implies that the interior or central portions of the cathode do not participate, to the same extent as those of the anode, in the early phases of discharge current conduction.

A more complete picture of these results is displayed in Fig. 4-11, which shows the values of the inception arc voltages, measured at 0.4 μsec after breakdown, for various exposed areas of cathode and anode. The inception arc voltages are seen to rise from 65 $\pm$ 5 V to 135 $\pm$ 5 V when the exposed area of the anode is decreased from 50 sq. in. (no insulation) to 12 sq. in. (7-in.-diameter insulation). An equivalent decrease in the cathode area causes the arc voltage to increase

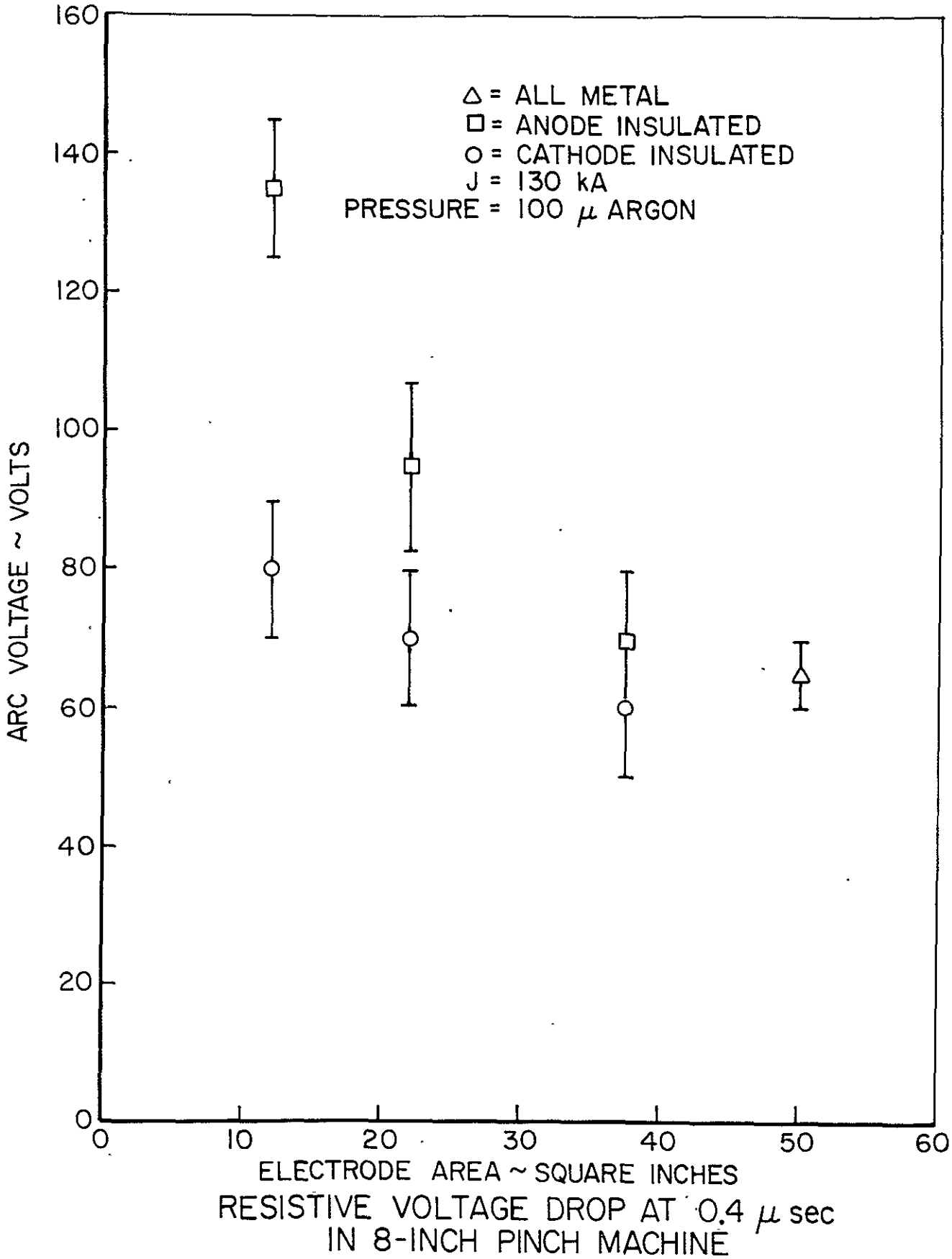
△ = ALL METAL
□ = ANODE INSULATED
○ = CATHODE INSULATED
J = 130 kA
PRESSURE = 100 μ ARGON
ARC VOLTAGE ~ VOLTS
0
20
40
60
80
100
120
140
160
0
10
20
30
40
50
60
ELECTRODE AREA ~ SQUARE INCHES
RESISTIVE VOLTAGE DROP AT 0.4 μ sec
IN 8-INCH PINCH MACHINE

FIGURE 4-11

only slightly to 80 ± 10 V. For all of the above data, the reductions in electrode area were affected by insulating the central portions of the anode or cathode, respectively.

The following qualitative physical model is proposed to explain the anomalous arc voltage data presented in this section. Insulation of substantial central portions of the anode should not interfere with the initial formation of the current sheet at large chamber radii; nor should it obstruct, at 0.4 μsec anyway, the development of the broad current sheet "anode foot" which does not become evident until later times in the discharge history. However, the arc voltage data of Fig. 4-11, corresponding to a time just 0.4 μsec after breakdown, does show a noticeable change in arc voltage for increasing central anode insulation. One must conclude, therefore, that the central portions of the anode are also involved in the initial discharge processes. This involvement probably takes the form of precursor anode current conduction downstream of the current sheet. Although the specified anode insulation does not influence the initial establishment of the current sheet, it clearly precludes the normal development of precursor conduction at the central portions of the anode. If anode precursor conduction is an essential part of the pinch discharge, any obstruction of it will increase the arc impedance, and since the current is determined by the external circuit, this results in an increased arc voltage. On the other hand, it has been shown that similar insulation of the cathode has a much weaker effect on the arc voltage. Therefore, it is presumed that cathode precursor conduction is not substantial during the initial phase of the pinch event.

These indications of anode precursor conduction in the large-radius pinch discharge are in qualitative agreement with recent experiments on similar high-current pulsed discharges (see Chap. II, Sec. G). Namely, anode surface currents, existing well ahead of the current sheet, have been detected in both parallel-plate and coaxial accelerators.[29] In addition, certain unsteady plasma devices have exhibited

charge layers and voltage sheaths at the anode surface downstream of the main current distribution.[33] Hence, anode precursor phenomena, of one form or another, are common to a variety of plasma accelerators employing different electrode geometries, current levels, and ambient gas fills.

At this point insufficient information is available to warrant any attempts at proposing a mechanism for the precursor conduction phenomena. Therefore, the collection of further detailed data in the central portions of the chamber will next be undertaken.

E. ELECTROSTATIC PROBE STUDIES

In an attempt to test the hypothesis concerning precursor anode current conduction, various measurements were made of the local properties of the slightly ionized plasma in the region ahead of the propagating current sheet. For example, sensitive magnetic induction coils were inserted to search for possible central chamber current densities ahead of the main sheet. These experiments proved inconclusive because the leakage magnetic fields due to current sheet asymmetries tend to overshadow those which might be related to possible central chamber current densities.

Since central chamber current density measurements were precluded, a single tip electrostatic probe was then inserted to map the plasma potential profiles in this region. The probe tip was spherical with a diameter of 1/32 in., and was formed such that it could be placed very close to the anode. The measuring circuit had a very high resistance, which forced the probe tip to float at plasma potential less a small sheath drop associated with the electron temperature. A more detailed discussion of the correction from the measured floating potentials to the physically more interesting plasma potentials is given in Chap. VI; it suffices here to state that the displayed floating potential distributions are a good representation of actual plasma potentials.

In its first application, the probe was used to determine the potential distribution between the pinch electrodes at a chamber radius of 1 in. with the current sheet standing at a radius of about 3 inches. The driving-current waveform used in these experiments is the same as that employed in the arc voltage studies; the chamber was prefilled with 100 μ argon. This distribution of potential for all-metal electrodes, shown in Fig. 4-12, reveals that most of the voltage drop occurs within 1/2 in. of the anode with a smaller drop at the cathode. This result relates to the markedly different arc voltage signatures obtained for substantial insulation of the central portions of the anode and cathode, discussed in the previous section. The existence of a substantial voltage gradient near the anode in the region well ahead of the current sheet indicates that some form of precursor current conduction is occurring there. Hence, the placement of insulation on the central portion of the anode must inhibit this part of the current conduction pattern; the discharge responds to this disruption by increasing its arc voltage. Conversely, the near absence of precursor cathode conduction (witness the absence of voltage gradients at the central cathode region) is consistent with the minimal effect of cathode insulation on the arc voltage.

It is instructive to repeat the electrostatic probe measurements at the same 1-in. radius, but with a 7-in.-diameter mylar insulation placed alternately on the anode and cathode. Figure 4-13 shows these potential distributions in comparison with that of the all-metal electrode case. Cathode insulation appears to have a minimal effect on the central chamber potential distribution, not an unexpected result. Anode insulation, on the other hand, gives rise to a much altered potential profile, particularly in view of the large voltage drop, 80 V, which appears adjacent to the insulated anode surface. This observation complies with the substantial increase in the arc voltage of the pinch discharge which results from similar insulation of the anode. The large anode voltage drop

FIGURE 4-12

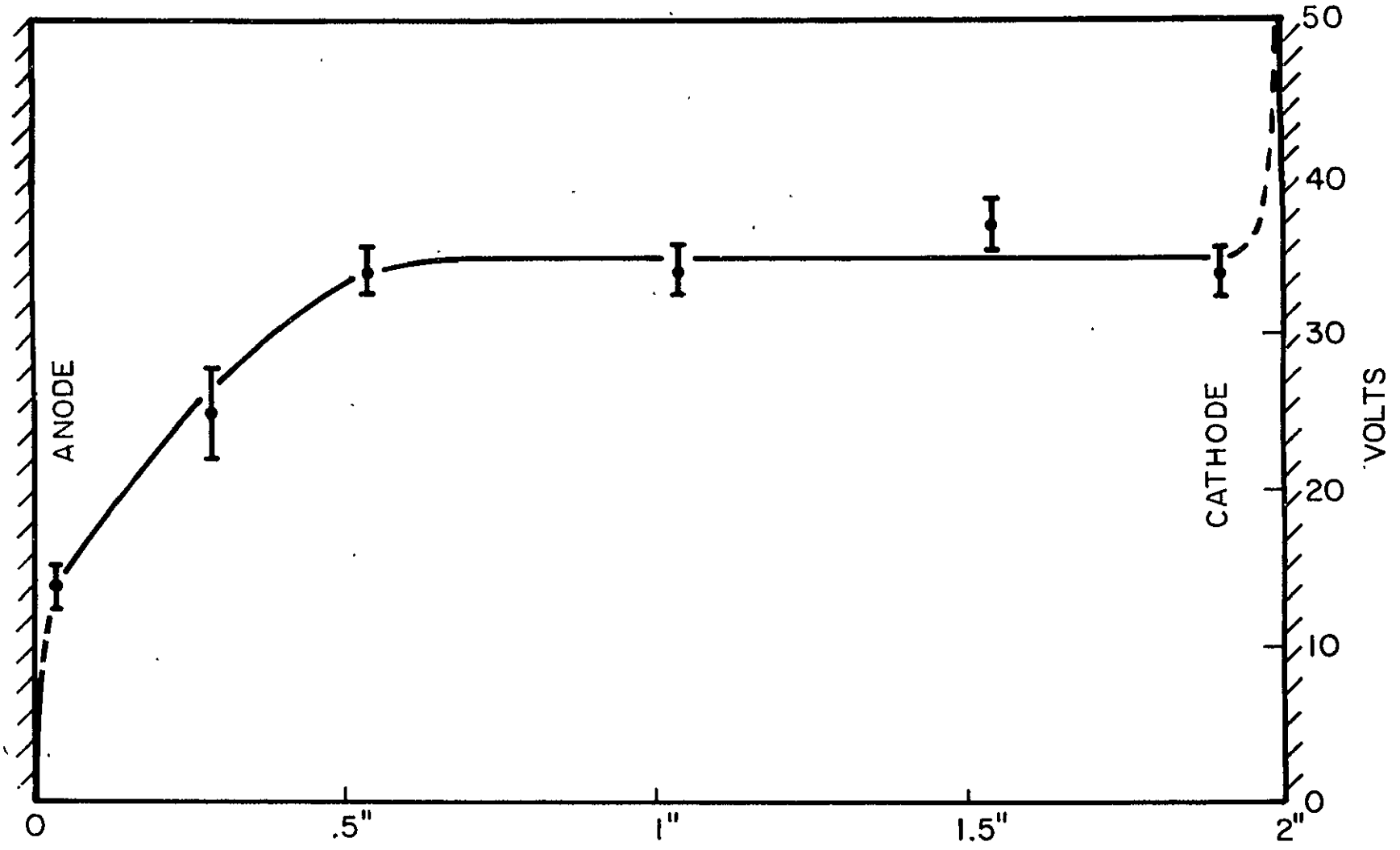

POTENTIAL DISTRIBUTION ACROSS CHAMBER AT 1 INCH RADIUS

$t = 1\ \mu$ sec

CURRENT SHEET AT R = 3"

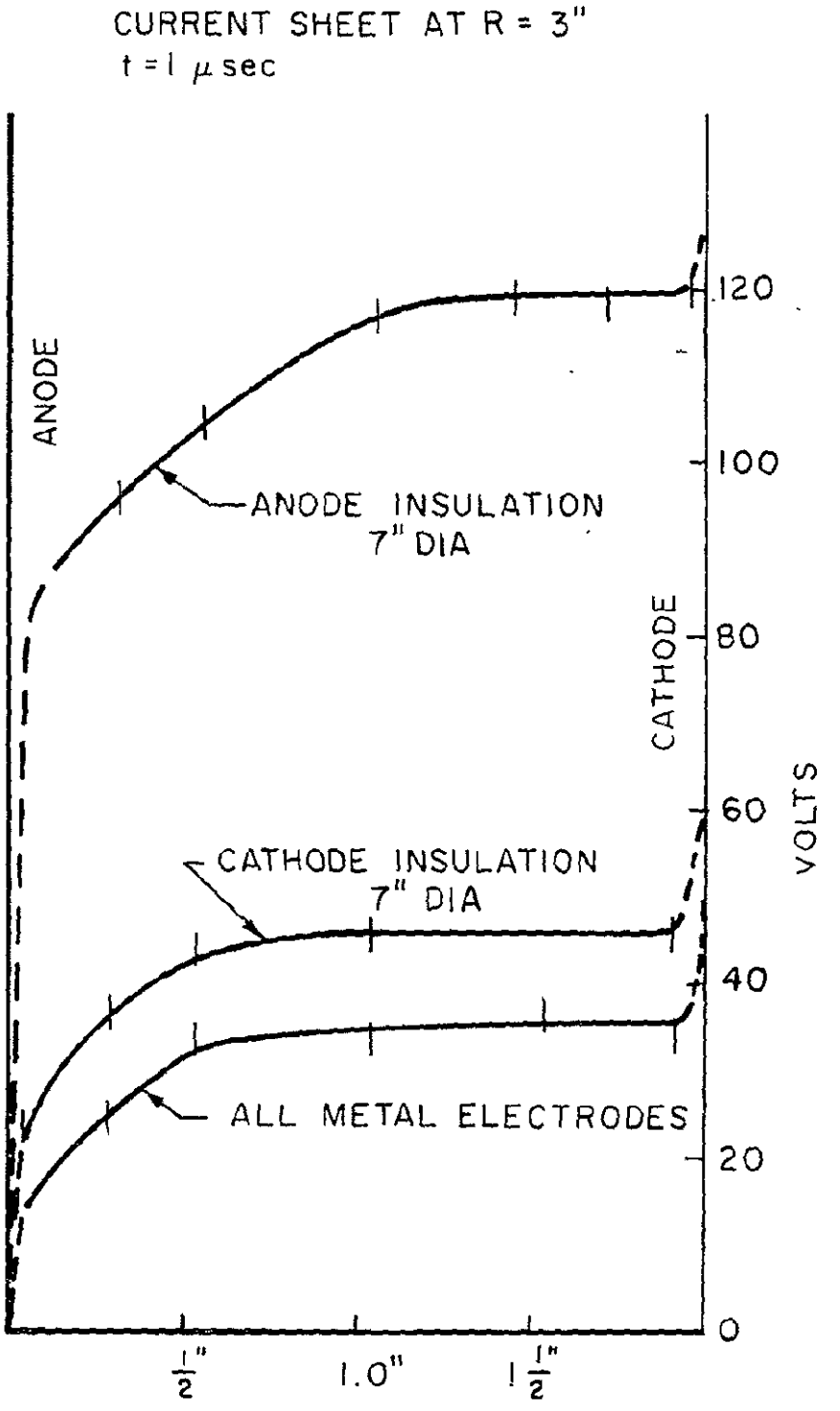

POTENTIAL DISTRIBUTIONS ACROSS DISCHARGE CHAMBER AT R = 1 INCH

FIGURE 4-13

is most likely caused by an electron space charge layer which forms over the insulator surface. The anode precursor conduction, discussed on the previous page, probably involves an electron flux to the anode surface ahead of the current sheet. The presence of insulation prevents electrons from making the transition from the plasma to the metal anode, thus causing the accumulation of electron charge density there.

The above procedures have been carried one step further in attempting to map the potential profiles throughout the 8-in. pinch chamber for the same experimental conditions. This was done for the case with 7-in.-diameter mylar insulation placed concentrically on the anode; probe readings were again taken 1 μsec after discharge initiation with the discharge current at its maximum of 310 kA and the current sheet standing at large radii. Figure 4-14 shows the resulting equipotential profiles. Unfortunately, their interpretation is made somewhat ambiguous by the fact that it is often very difficult to separate the true resistive components of the potential distribution from the inductive contributions associated with the unsteady features of the pinch discharge. This ambiguity, however, does not arise in the interpretation of the central chamber potential data of Figs. 4-12 and 4-13 as the inductive effects are minimal at these central chamber locations. Clearly, then, the utility of the potential profiles displayed in Fig. 4-15 is considerably reduced by this problem. Nevertheless, the profiles appear to indicate a concentration of potential gradients near the insulated portion of the anode with a much weaker field region elsewhere in the chamber. This observation agrees qualitatively with previous results, which indicated the formation of a negative space charge layer and a strong potential gradient at the central region of the insulated anode.

F. SUMMARY

First, magnetic probe and photographic studies have revealed a basic asymmetry in the structure of the cylindrical

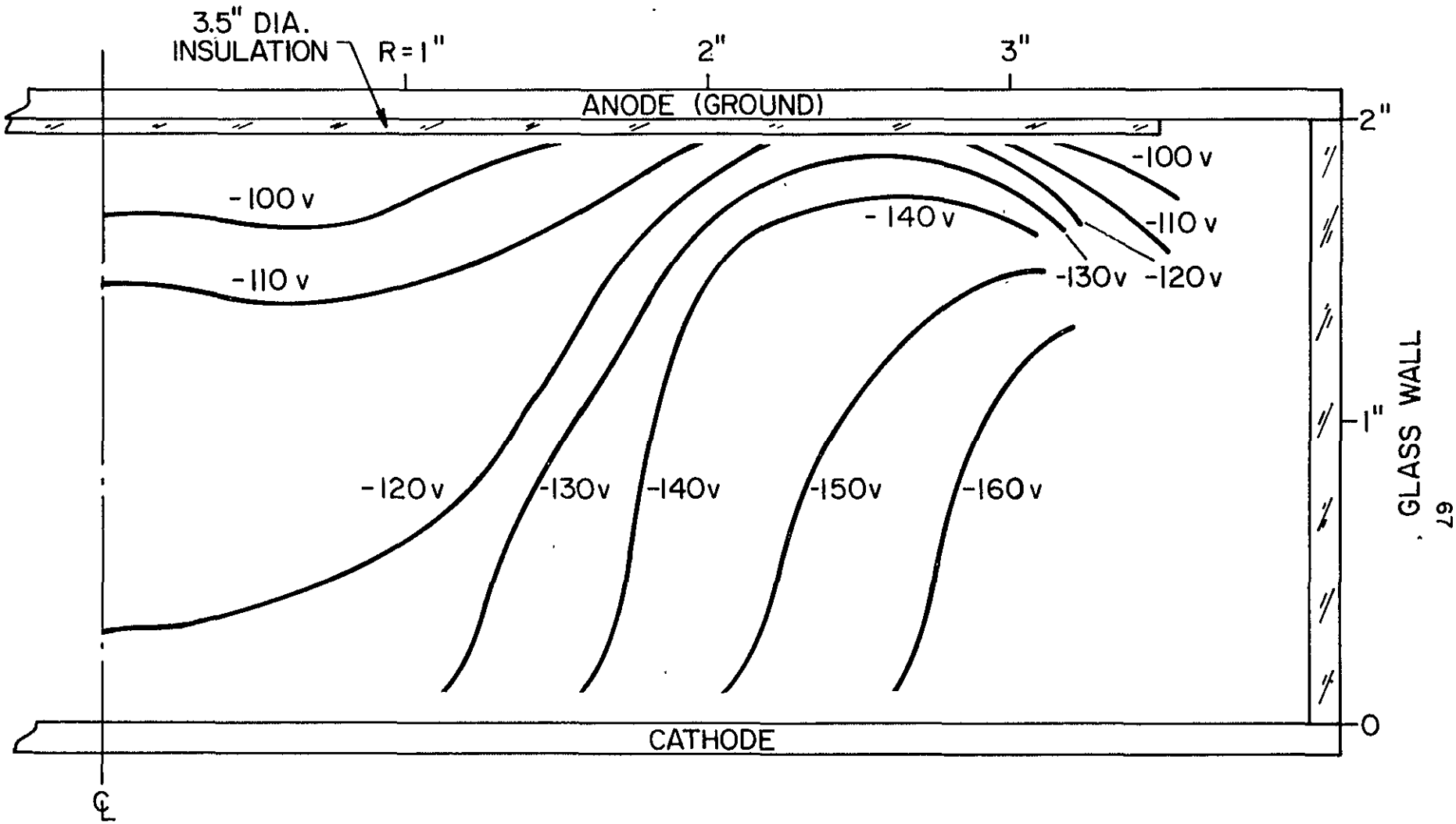

POTENTIAL CONTOURS IN CHAMBER

$t = 1\ \mu sec$

CURRENT SHEET AT R = 3.0"

FIGURE 4-14

current sheet. Namely, the cathode region of the sheet remains narrow and well-defined, whereas near the anode surface the sheet becomes broad, diffuse, and sometimes divided into two or more regions of high-current density as it propagates towards the chamber center. Second, experiments using an inner voltage divider have demonstrated that the discharge arc voltage increases substantially for insulation of the central anode region, but that similar cathode insulation has only a minimal effect on arc voltage. This result has been interpreted to mean that major portions of the anode surface particpate in the initial phase of the pinch discharge; this participation is presumed to be in the form of some sort of anode precursor conduction. The data suggests that no equivalent cathode precursor conduction exists during this initial phase of the discharge. These experiments were next extended to the parallel-plate accelerator (see Chap. V) in an attempt to provide a better distinction between these two anode processes: the spread of the current sheet at the anode producing the broad "anode foot" and the anode current sheet bifurcation, and the apparent anode precursor conduction during the early phases of the discharge.

CHAPTER V

EXPERIMENTS ON THE PARALLEL-PLATE ACCELERATOR

A. PHOTOGRAPHIC STUDIES

Studies of anode phenomena in a parallel-plate accelerator have been carried out in order to determine, which of the effects, observed in the 8-in. pinch event, persist in this geometry and which are modified by it. The electrode dimensions in this device are 6 in. by 48 in., substantially larger than those of the 8-in. pinch device. The discharge is driven into a 100 μ argon ambient fill by a 120 kA square current pulse lasting for 20 μsec. In the first experiments performed on this accelerator,[41] a Kerr-cell photographic system was employed to gather qualitative data on current sheet structure. Figure 5-1 shows a series of such photographs taken through the Plexiglas sidewall of the accelerator for the case of all-metal electrodes. The first photograph shows an essentially planar current sheet standing near the back insulator wall 2 μsec after discharge initiation. After 3 μsec, the sheet has progressed downstream and begins to develop structure in the streamwise direction; namely, the anode attachment is now leading and is more broad and diffuse than the cathode attachment. The third picture, taken at 6 μsec, when the current sheet has progressed about 5 in. downstream from the back wall, displays the familiar "Y"-shaped structure discussed in Chap. IV, Sec. B. However, in addition to the "Y"-shape of the current sheet, the beginnings of a "cathode foot" are also seen in this photograph. The final photograph, taken at 9 μsec, confirms another aspect of the anode bifurcation model proposed earlier; i.e., the so-called "triple point" of the Y-shaped sheet has now progressed towards the cathode such that the

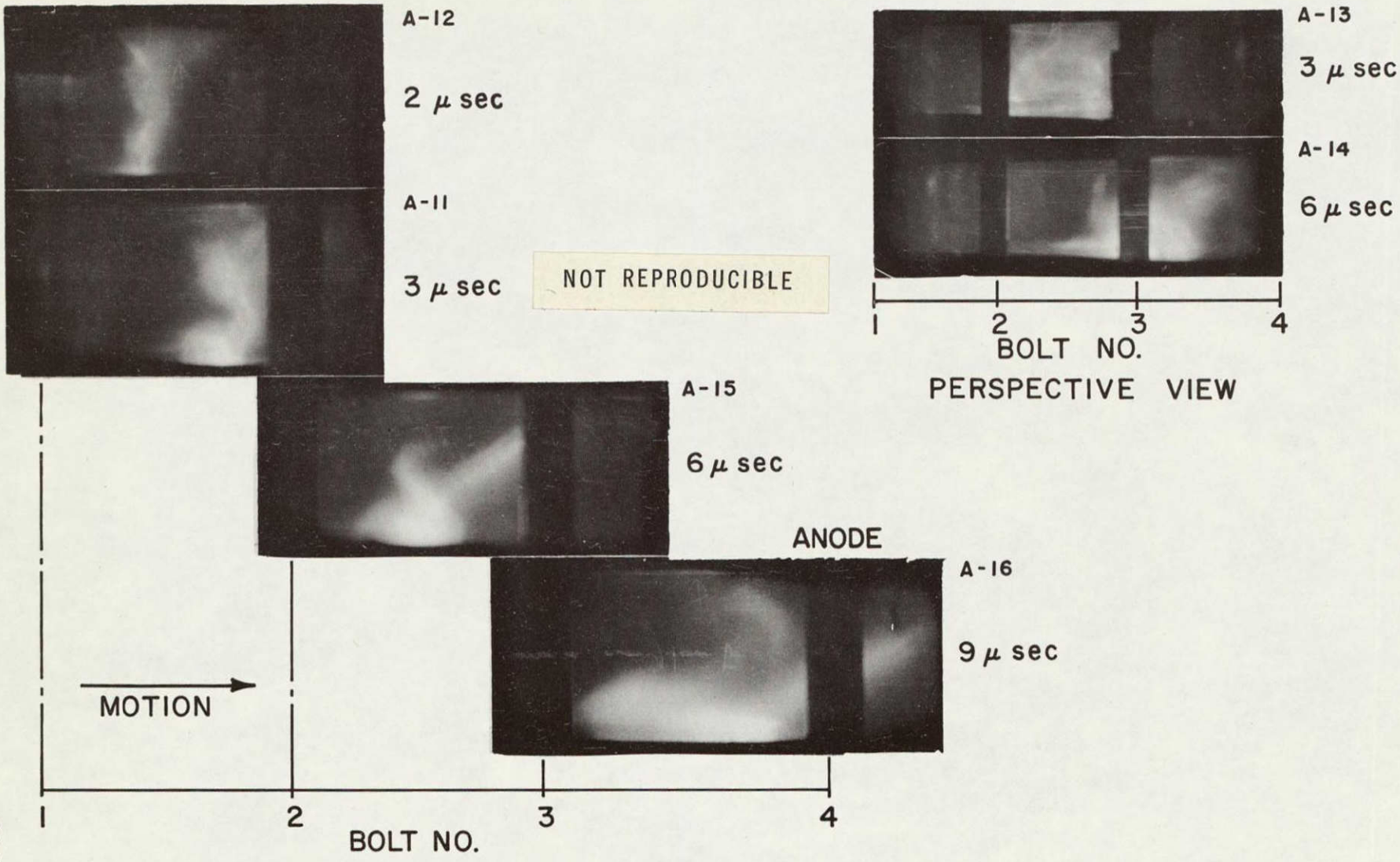

FIGURE 5-1

KERR-CELL PHOTOGRAPHS OF PROPAGATING LUMINOUS FRONT
IN PARALLEL PLATE ACCELERATOR ;
FULL ELECTRODES ; 100 μ ARGON ;
DRIVING CURRENT 120,000 amp × 20 μ sec.
(REF 41)

anode bifurcation consumes almost the entire current sheet. The cathode attachment has also grown more broad and diffuse, a significant departure from the behavior of the 8-in. pinch discharge, where sharply defined cathode attachments persist throughout the short pinch event. This development of a substantial cathode foot, after an elapsed time greater than that available to the pinch discharge, is a significant observation to which reference will be made in Sec. C.

B. ARC VOLTAGE MEASUREMENTS

Inner divider voltage probe measurements, similar to those carried out on the 8-in. pinch device, were undertaken in this new geometry to further examine the importance of so-called precursor conduction in pulsed plasma accelerators. In addition, magnetic probes were inserted at various locations in the accelerator to permit more precise differentiation between this precursor conduction and the broad, diffusing electrode attachments of the main current sheet. A voltage tap was located at the downstream end of the parallel-plate device, at which position it measures only the resistive voltage drop across the electrodes, exclusive of any inductive components. The signals were fed to an oscilloscope via a Tektronix Model 6013 voltage probe of 10^8 ohm impedance. Figure 5-2a displays a schematic of the accelerator and voltage measuring circuit; also shown is the configuration of electrode insulation employed in this experiment. Figure 5-2b shows the driving-current waveform along with a typical response of the inner divider voltage probe for a current sheet propagating along the full length of the electrodes. The arc voltage for this all-metal electrode case is virtually constant at a value of 80 V.

The same measurements have been repeated with varying portions of the anode and cathode insulated by mylar. Typical triple overlayed oscillograms, corresponding to anode insulation, are shown in Fig. 5-3. Figure 5-3a, for 5 1/4 in. of anode exposed, shows an elevated voltage, 180 V in this case, immediately after breakdown followed by an increasing signal

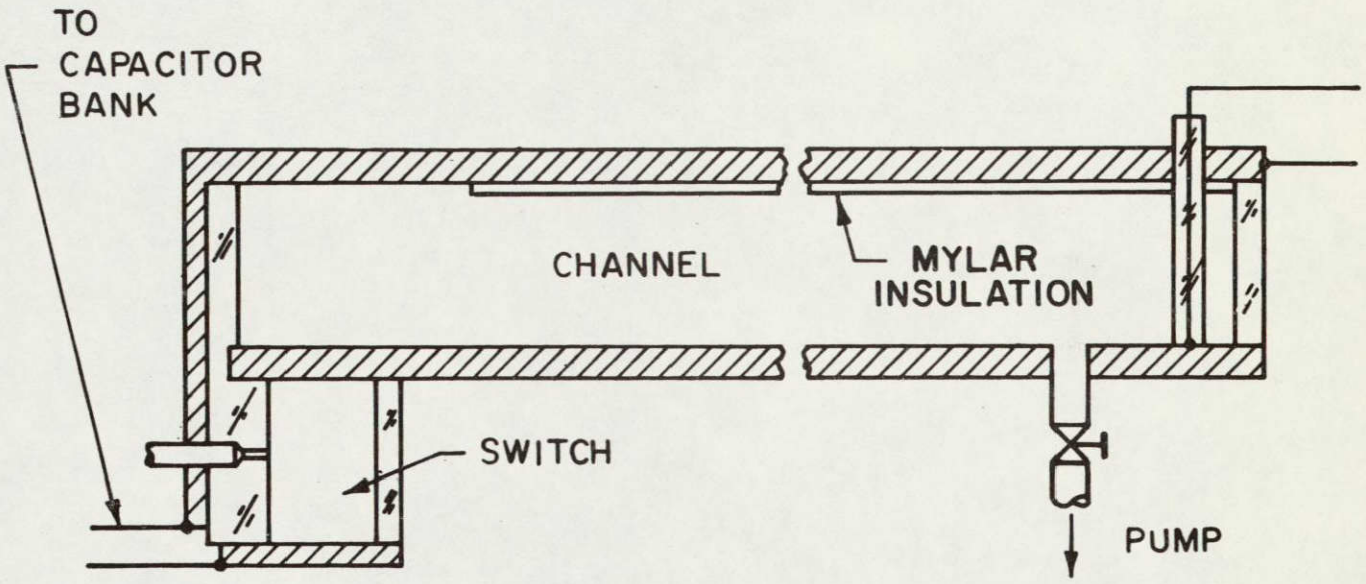

a) SCHEMATIC OF PARALLEL PLATE ACCELERATOR

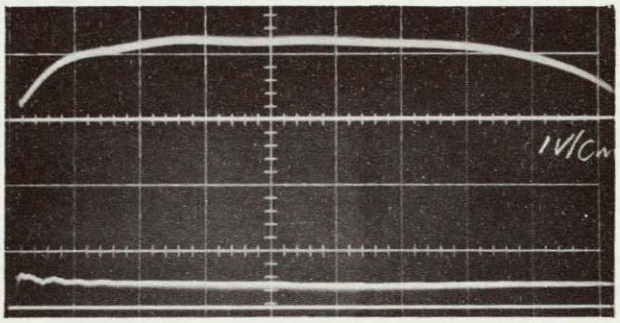

b) ARC VOLTAGE FOR ALL-METAL ELECTRODES

PARALLEL PLATE ACCELERATOR

FIGURE 5-2

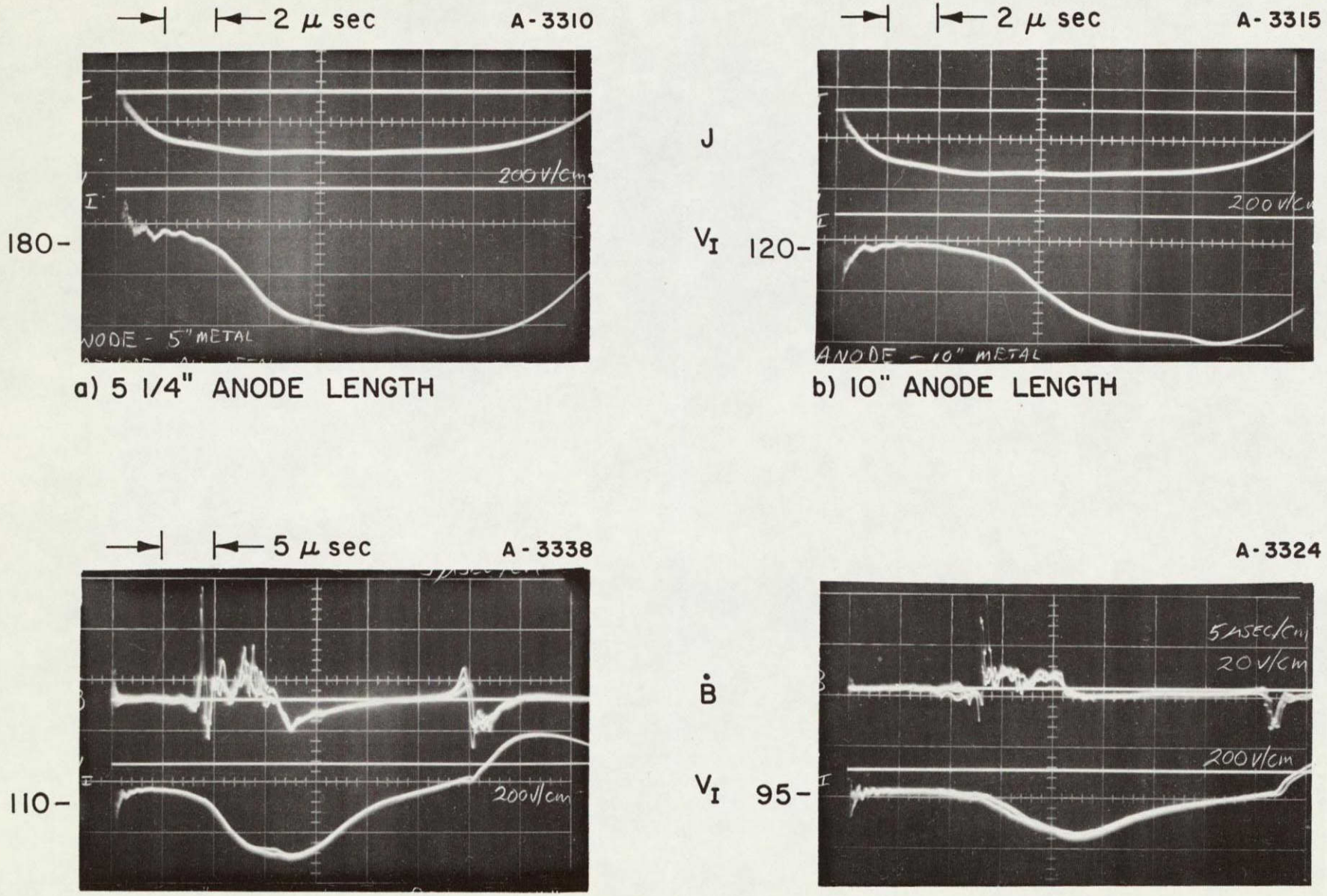

FIGURE 5-3

INNER DIVIDER RECORDS FOR ANODE INSULATION

as the current sheet encounters the insulation and the arc length begins to increase. Figures 5-3b,c,d, for increasing lengths of uninsulated anode, display the same general characteristics but with successively lower initial voltages and later onset of voltage increase. The initial elevated voltages must be again attributed to the interruption of anode precursor conduction by the mylar insulation.

In order to correlate the arrival time of the current sheet anode attachment at the insulation interface with the beginning of the voltage signal increase, a magnetic induction coil was inserted adjacent to the anode at the location where insulation begins. The responses of this magnetic probe are shown in the upper traces of Figs. 5-3c,d for 14 1/2 in. and 21 in. of exposed anode. Observe that the voltage signal begins to increase when the leading edge of the "anode foot" contacts the insulation, and then continues to rise while the lagging parts of the "foot" arrive there. It is not clear whether the voltage increase is caused by constriction of the previously broad and diffuse anode attachment at the insulation edge, or whether it is related to an increase in arc length resulting from the arrest of the anode attachment while the main portion of the sheet continues to propagate downstream. In either case, this voltage increase appears to be independent of the precursor anode conduction mechanisms which were responsible for the elevated voltages observed at the beginning of the discharge.

However, a significant departure from the behavior observed in the pinch event is found when the same measurements are repeated on the cathode. With the machine polarity reversed, so that the cathode now becomes the insulated electrode, the arc voltage traces obtained for various lengths of cathode insulation (Fig. 5-4) are, in most respects, unexpectedly similar to those for corresponding anode insulation. Once again, elevated voltage readings are observed at the beginning of the discharge, followed by increasing voltage when the cathode attachment meets the insulation. In most cases the initial

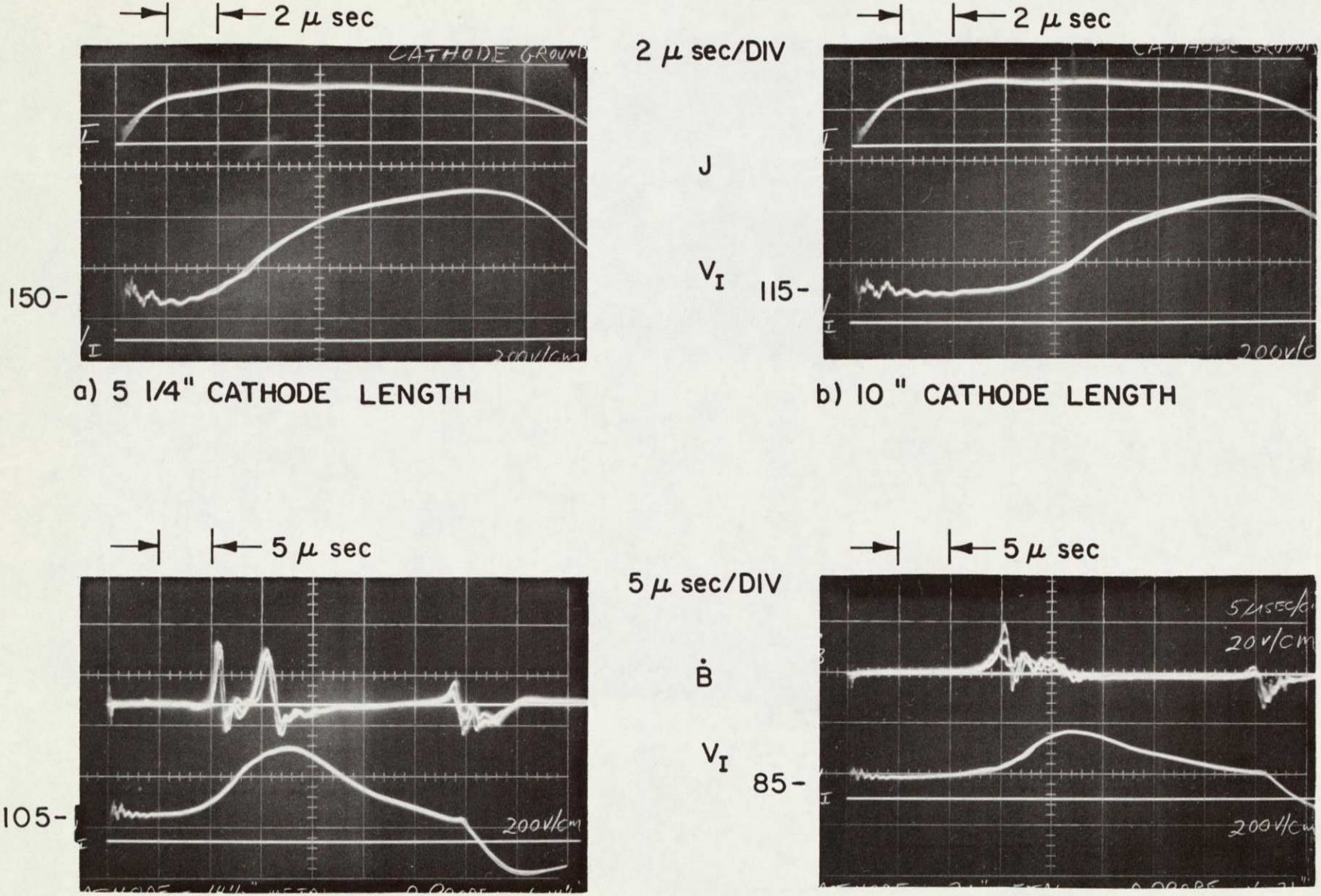

FIGURE 5-4

INNER DIVIDER RECORDS FOR CATHODE INSULATION

arc voltage is essentially the same as that for comparable anode insulation, except for a moderate difference at the 5 1/4-in. electrode situation. Initial arc voltage readings above the all-metal value of 80 V can only be interpreted to mean, for this experimental situation at least, that cathode precursor conduction has assumed an importance comparable to that of anode precursor conduction.

The responses of the magnetic probe, located on the cathode surface at the insulation interface, are displayed in Figs. 5-4c,d along with the accompanying voltage traces. These signatures, in comparison with those of Figs. 5-3c,d, show that the current sheet cathode attachment trails the leading part of the "anode foot." This result confirms the so-called current sheet tilt which has been reported elsewhere,[30,31] and which was also observed in current sheet photographs in the parallel-plate accelerator (Fig. 5-1). In addition, the magnetic probe signals reveal that the cathode attachment, at these downstream locations, is now broad, diffuse, and even divided, thus displaying "cathode bifurcation." This conclusion is partially substantiated by Kerr-cell luminosity photographs (Fig. 5-1). Again, the times of cathode foot arrival at the insulation interface correlate well with the first indications of a voltage increase. The arc voltage then continues to rise while the lagging portions of the broad cathode attachment reach the insulation. The cause of this voltage increase must be attributed, analogously to the anode case, to either the constriction of the broad "cathode foot" at the insulation edge, or to the increasing arc length caused by the arrest of the cathode attachment. On the other hand, it must be assumed that the elevated initial arc voltages are caused by the interruption of precursor cathode conduction by the mylar insulation.

Figure 5-5 summarizes the dependence of the accelerator arc voltage, at 2 μsec after breakdown, on exposed electrode area for the two different types of electrode insulation. The increasing initial arc voltage for decreasing anode area is an

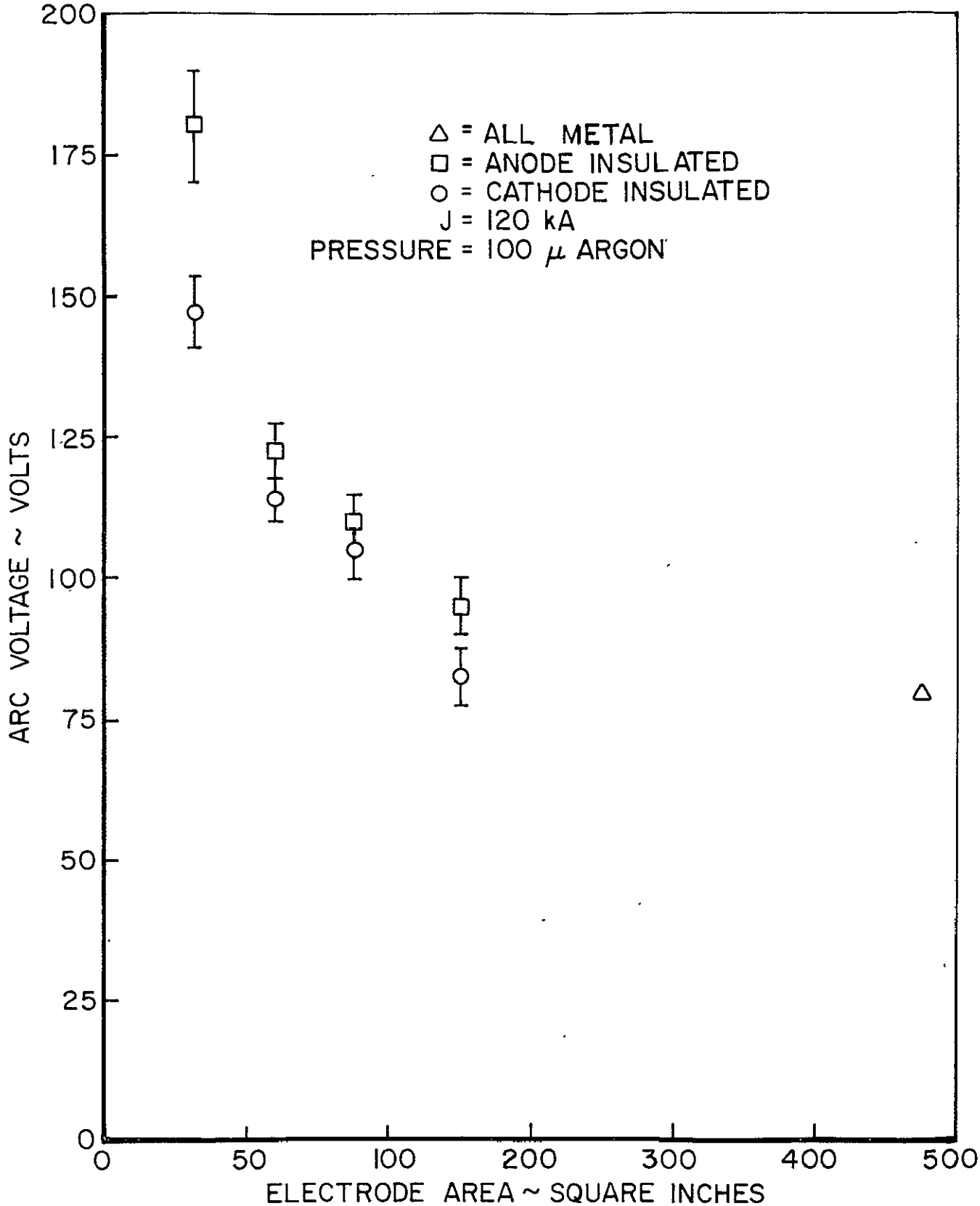

RESISTIVE VOLTAGE DROP AT 2.0 μsec
IN PARALLEL PLATE ACCELERATOR

FIGURE 5-5

expected result, which suggests that the arc voltage again rises because progressively more of the anode precursor conduction is obstructed by increasing amounts of anode insulation. However, the good agreement between the anode insulation curve and the cathode insulation curve represents a marked departure from the arc voltage data for the pinch discharge (see Fig. 4-11). Unlike the previous situation, cathode insulation now has a noticeable influence on initial arc voltage, thus leading to the conclusion that cathode precursor conduction, for this experimental situation, has become of equal importance with anode precursor conduction. This discrepancy between the arc voltage data of the pinch and parallel-plate devices is taken up in the next section.

C. COMPARISON OF PARALLEL-PLATE AND PINCH DATA

Both photographic observations and arc voltage measurements have revealed significant differences between the various electrode processes occurring in the parallel-plate and 8-in. pinch devices. For example, Fig. 5-6, which compares the dependence of arc voltage on electrode area for these two accelerators, shows that the arc voltage of the parallel-plate device is almost equally sensitive to variations of anode or cathode area; whereas the pinch arc voltage responds much more severely to changes in anode area than to changes in cathode area. These data suggest that precursor anode conduction occurs in both devices, but that similar precursor current conduction at the cathode surface is peculiar to the parallel-plate accelerator. A second, related divergence in discharge behavior is that a so-called "cathode foot" is evident in current sheet luminosity photographs of the parallel-plate discharge (Fig. 5-1), but not in those of the pinch event (Fig. 4-5). A well-developed anode foot is clearly exhibited in both cases.

An explanation of this apparent discrepancy is sought by examining the various discharge properties for these two experimental facilities. First, both devices were prefilled to the same argon pressure and the total discharge currents were

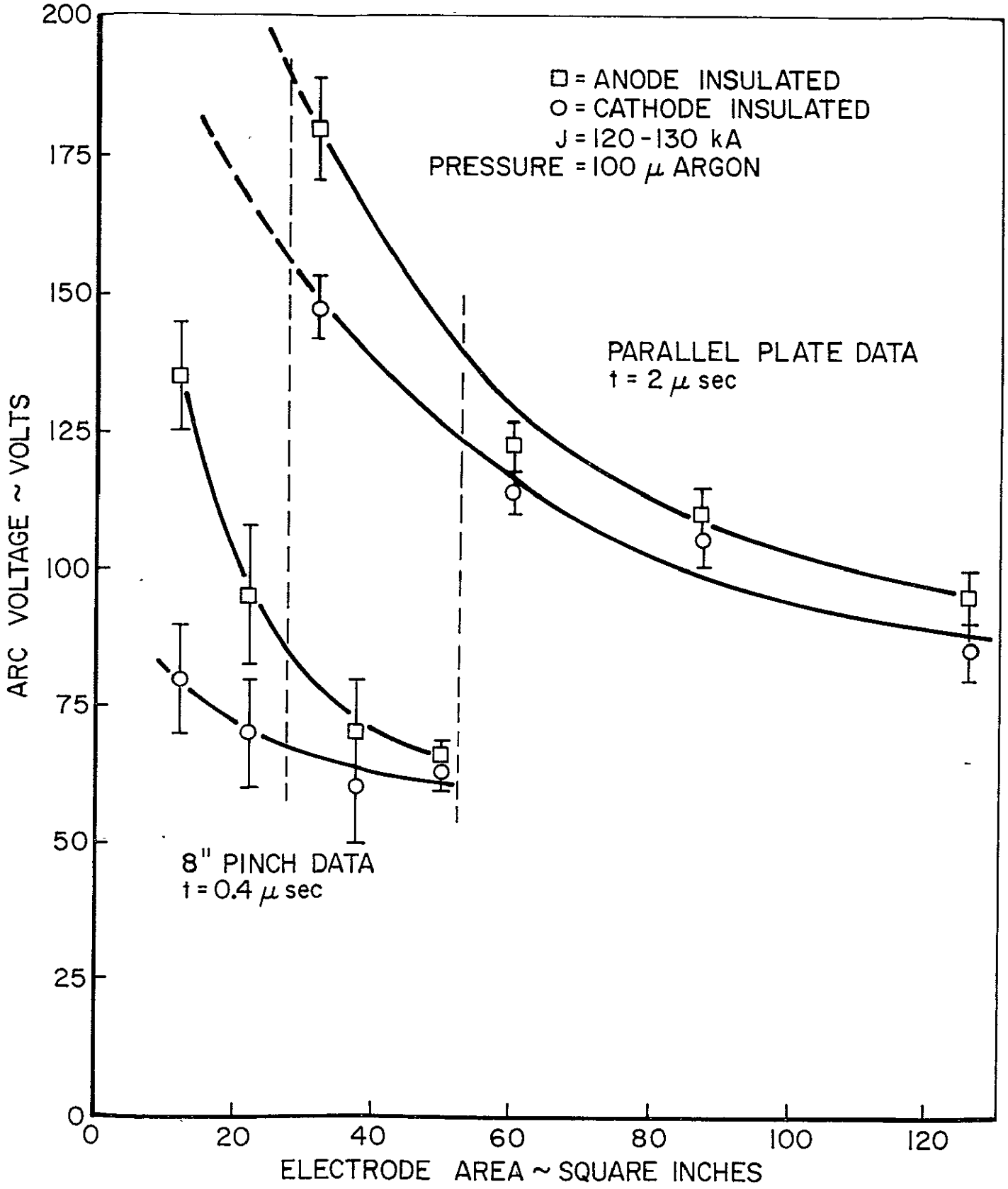

FIGURE 5-6

COMPARISON OF 8-in PINCH AND PARALLEL PLATE VOLTAGE DATA

approximately equal at the respective times of data collection. Second, although the total electrode area is somewhat greater in the parallel-plate accelerator, parallel-plate and pinch data corresponding to the same range of electrode area continue to display a similar dependence on anode area but a noticeably different dependence on cathode area (Fig. 5-6). However, it should be pointed out that the pinch arc voltage measurements were taken 0.4 μsec after discharge initiation, before the cylindrical current sheet contacts the circular electrode insulation; parallel-plate data, not available at this early time because of signal noise (see Fig. 5-4), were taken at 2.0 μsec, still sufficiently early for this measurement due to the larger dimensions of the parallel-plate device. Thus, experimental indications of cathode precursor conduction in the parallel-plate machine, and not in the pinch device, may simply be a result of the difference in the times of data collection. This explanation would follow if the cathode precursor conduction processes develop at a slow enough rate such that they are not yet observable at 0.4 μsec (pinch data), but are well established by 2.0 μsec (parallel-plate data). Anode precursor conduction, on the other hand, since it is indicated by the 0.4 μsec pinch data, must develop at a faster rate.

Further supporting evidence for this claim is obtained by a comparison of current sheet luminosity photographs in the pinch and parallel-plate devices (Figs. 4-5 and 5-1). The photographs, taken at 2 μsec after discharge initiation, display little evidence of a cathode foot in either device, although an anode foot is already clearly visible for both cases. Only at later times, say 6 μsec, does the cathode disturbance become well developed in the parallel-plate accelerator. Since this longer time period is not accessible to the pinch event, a cathode foot is never observed there. Thus, the available data seem to suggest that both cathode precursor conduction and the current sheet cathode disturbance develop at a slower rate than the corresponding processes at the anode.

Lacking more detailed information at the electrode

regions, the following qualitative remarks are given in explanation of the apparent time scale difference between anode and cathode processes in unsteady plasma accelerators. The regions immediately adjacent to the electrodes of a high-current arc discharge are characterized, respectively, by negative and positive space-charge zones, referred to as the anode and cathode falls (see Chap. II, Sec. B). It shall be assumed, for the present situation, that a space-charge layer of electrons forms at the anode-current sheet interface, while a similar ionic space-charge layer exists at the cathode-current sheet interface. It is suggested that the electrons and ions in the respective electrode space-charge layers tend, by some unspecified mechanism, to spread over the electrode surfaces ahead of the propagating current sheet, thereby carrying the anode and cathode precursor conduction currents. Furthermore, following the reasoning of Lie et al,[29] discussed in Chap. II, Sec. G, these proposed streamwise surface currents give rise to $\vec{j} \times \vec{B}$ forces near the current sheet-electrode interface, which are directed both forward and away from the electrode surface, and therefore cause the sheet to deform there. Thus, the development of the anode and cathode current sheet deformations may also be related, in this way, to the proposed motion of electrons and ions in the downstream direction along the electrode surfaces. The apparent difference in the relative growth rates of these anode and cathode phenomena may then be associated with some difference between the mobilities, thermal velocities, or other properties of the electrons and ions in the respective space-charge layers. Therefore, precursor anode conduction and the broad current sheet anode attachments, both associated with fast moving electrons, should become established earlier in the discharge time history than similar cathode phenomena which are controlled by much slower ions.

D. SUMMARY

Experiments on the parallel-plate accelerator have again demonstrated the existence of precursor anode conduction which

is distinct from, but probably not unrelated to, the broad and diffuse current sheet anode foot. Moreover, during the longer time scale of this experiment both cathode precursor conduction and a broad cathode foot were also seen to develop. These latter observations led to a hypothesis wherein faster growth rates are assigned to the electron-controlled anode processes and slower growth rates to the ion-controlled cathode processes.

CHAPTER VI

EXPERIMENTS ON THE QUASI-STEADY MPD ARC

A. BACKGROUND

The previous two chapters described experiments on the pinch and parallel-plate devices and pointed out several interesting aspects of anode phenomena, while making no attempts to explain these curious physical processes. Clearly, a better understanding of anode current sheet bifurcation and anode precursor conduction would require detailed measurement of the local plasma properties in the electrode regions of these pulsed accelerators. Unfortunately, such probing of the anode region plasma by electrical means was precluded by the severe signal noise and irreproducibility which plagued the data. In addition, the unsteady feature of the pinch and parallel-plate discharges makes data collection that much more difficult. In view of these obstacles, it was decided to conclude the experiments on the pulsed closed chamber devices, and to continue the study of anode phenomena in the quasi-steady MPD facility (see Chap. III). This device has the advantage of affording easy access to the anode region for diagnostic purposes, and of providing a steady discharge phase which facilitates the measurement of important plasma properties. Furthermore, the quasi-steady MPD arc appears to be the most promising of contemporary plasma accelerators, and thus is a very appropriate facility in which to carry on these investigations.

First, measurements of floating potential throughout the arc chamber and plume of this accelerator were undertaken in order to determine the dominant plasma acceleration mechanisms, and to investigate various aspects of anode behavior.

The following pages display the resulting equipotential maps for a variety of operating conditions. With reference to the previous experiments on the pulsed devices, the influence of anode size on the quasi-steady MPD discharge is considered; the distribution of anode current density is examined in Chap. VII.

B. FLOATING POTENTIAL MEASUREMENTS

The floating potential maps were constructed by means of point-by-point probing of the discharge with a variety of electrostatic sensors. The probes had three configurations of exposed surface: (1) 1/16-in.-diameter x 1/16-in.-high cone, (2) 1/16-in.-diameter flat disc, (3) 1/16-in.-diameter hemisphere. It can be shown that probe size and shape are unimportant for the measurement of floating potential;[47] this was also demonstrated empirically by comparing the readings of differently shaped probes, placed at the same location in the arc. In most cases the probes were inserted axially upstream into the discharge; in some cases they were inserted radially. One probe was bent to allow access to regions behind the anode lip. All leads to the probe sensing surfaces were coaxially shielded, and the signals were presented to the oscilloscope via a Tektronix Model 6013A voltage probe of 10^8 ohm impedance.

In interpreting the floating potential profiles, it is important to first demonstrate that they are good representations of the more physically significant plasma potential profiles. An electrostatic probe at the floating potential, by definition, draws zero net current, and therefore the electron and ion fluxes to the probe tip must be equal. Hence, in order to inhibit the fast moving electrons and thus balance the electron and ion fluxes to the probe tip, a negative Debye sheath forms over the probe surface. In the case of a quiescent plasma, the following expression relates the floating and plasma potentials via the negative sheath drop[48]

$$V_F - V_p = \frac{kT_e}{e}\left[\ln\left(\frac{m_i}{m_e}\right)^{1/2} - \ln\left(\hat{J}_i\left(\frac{T_i}{T_e}\right)^{1/2}\right)\right] \qquad (6\text{-}1)$$

where $\hat{J}_i$ is the nondimensional ion current which relates the ion current to the probe at a given potential to the ion current at plasma potential. Recent spectroscopic measurements have indicated ion temperatures in excess of 10 eV in the arc chamber of the quasi-steady MPD arc,[49] while Langmuir probe studies in this region confirm that the electron temperatures are relatively uniform at 1.5 eV.[50] Furthermore, $\hat{J}_i$ is taken to be about 1.8 for the given probe dimensions and plasma properties.[48] Hence the floating potential correction is estimated to be

$$V_F - V_P \approx 4.1 \, k T_e / e \qquad (6\text{-}2)$$

Using the value 1.5 eV for the electron temperature at various arc locations and operating conditions, it is seen that the plasma potential values are displaced some 6 V toward anode potential from the floating values. Ion streaming velocities are substantial in most parts of the arc chamber and downstream plume, and these tend to enhance the ion current to the probe tip. The net effect of this is to decrease the magnitude of the electron retarding sheath, and thereby move the floating potential values closer to the true plasma potentials. Thus, the 6 V correction is conservative. In other words, the floating potential contours displayed on the following pages are in fact close representations of the true plasma potentials, and hence shall be interpreted as such.

C. POTENTIAL CONTOURS FOR "MATCHED" OPERATION

Recent experiments on this accelerator have been directed

towards the investigation of the relationship between exhaust velocity and mass flow rate for constant arc currents. The data show that the exhaust velocity increases steadily with decreasing mass flow up to a point, and then remains essentially constant for further decreases in mass flow. This effect can be explained by assuming that the arc, at the low mass flow condition, is beginning to injest mass from the tank region and to erode the Plexiglas insulator. Thus, in effect, the net mass flow to the arc is no longer decreasing and therefore the exhaust velocity should remain constant. Hence, a critical mass flow is reached below which the arc cannot sustain a given current level, and it must therefore seek additional mass through injestion and insulator erosion. For an arc current of 17.5 kA these effects begin to occur at an argon mass flow rate of about 5.9 g/sec; 5.9 g/sec is thus referred to as the critical mass flow rate corresponding to an arc current of 17.5 kA, and when these two conditions coexist the arc operation is said to be "matched."

Figure 6-1 displays the floating equipotential contours for quasi-steady MPD arc operation at the so-called "matched" conditions of 17.5 kA x 5.9 g/sec. Several significant features of these potential contours are immediately evident. First, the downstream potential differs by only 30 V (25 V if the 1.5 eV electron temperature correction is applied) from anode potential, and by only 15 V from the region of gas injection. This is an order of magnitude lower than the observed ion kinetic energy in the exhaust stream,[4] and hence voids any simple collisionless electrostatic acceleration model. Second, the bulk of the potential drop occurs within two diameters of the cathode and is normal to it. Note that this intense field region is directed so as to decelerate ions attempting to flow downstream, hence cannot aid in a direct electrostatic acceleration process. However, in view of the high current densities prevailing in the cathode region, along with the intense electric fields, it is clear that a large fraction of the total arc power is deposited in this

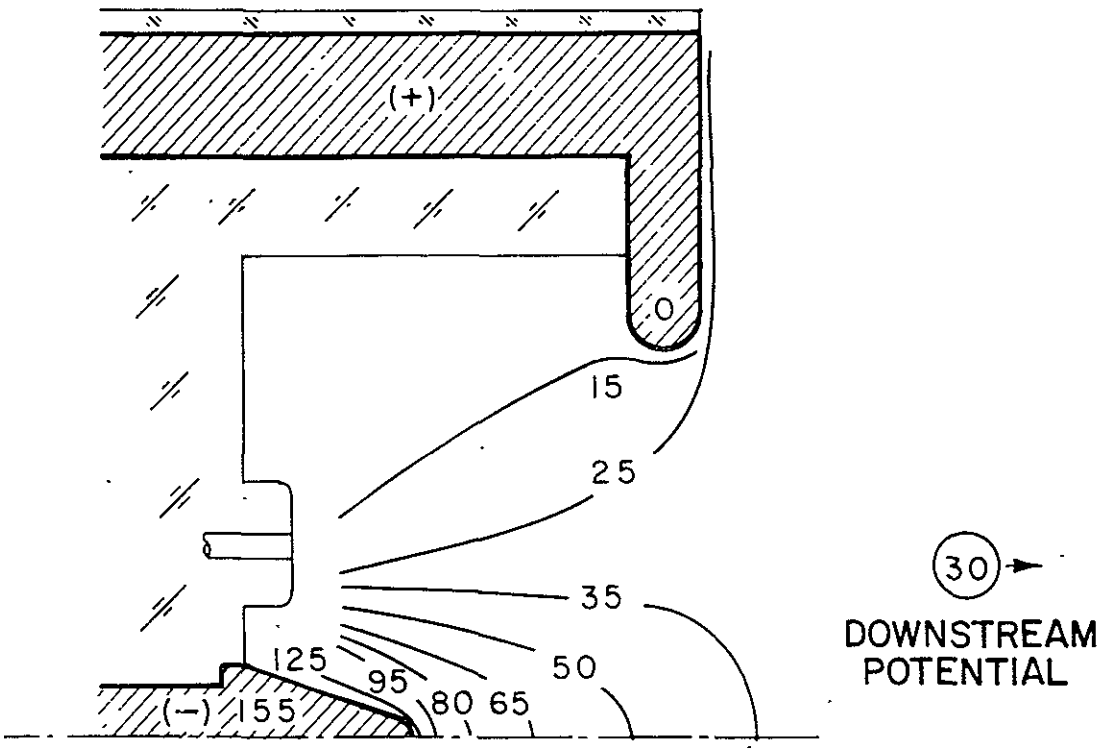

EQUIPOTENTIAL PROFILES FOR
"MATCHED" OPERATION

$J = 17.5$ kA
$\dot{m} = 5.9$ g/sec

FIGURE 6-1

cathode envelope; therefore it must be presumed that this zone is primarily responsible for the high exhaust velocities found downstream. In some portions of the envelope the electric field may reflect a large $\vec{u} \times \vec{B}$ or motional EMF component, but in others, such as near the inlet orifices and along the axis, this component must be small, leaving mainly a resistive component. This, in turn, implies substantial ohmic heating and subsequent electrothermal contributions to the overall acceleration process. Detailed investigations of both the acceleration and current conduction processes prevailing in this cathode envelope are the subject of another Ph.D. thesis from this laboratory.[50]

Turning attention to the anode region of the arc, it is observed that the anode fall voltage is less than 15 V over the upstream lip of the anode and rises to a somewhat higher value at the downstream face. Subsequent measurements of current density distribution around the anode, using magnetic induction coils, have shown that most of the current enters the anode near the upstream portion of the lip where anode fall voltages seem to be lowest. This apparent dependence of anode fall on local current density has important implications for anode heat losses, and hence is the subject of a more detailed investigation (see Sec. F).

D. POTENTIAL CONTOURS FOR LARGE ANODE CONFIGURATION

Earlier experiments with unsteady operation of the plasma pinch and parallel-plate devices (Chap. IV and V) revealed that variations of anode size had a significant effect on the total arc voltage. Briefly, it was found that the arc voltage increased substantially when the effective anode size was reduced so as to obstruct the precursor anode current conduction, presumed to exist downstream of the propagating current sheet. In view of these observations, a large 34-in.-diameter anode was fitted to the quasi-steady MPD arc, and the resulting arc voltage and equipotential profiles were investigated in order to study the effects of anode size on

the operation of this device. Figure 6-2 displays a map of the floating potential contours for the familiar matched operation conditions, 17.5 kA x 5.9 g/sec argon, and with the arc chamber modified by a 34-in.-diameter anode. Note that the arc voltage is 160 V in this case, as compared to 155 V for the previously discussed operation with the small 7 1/2-in.-diameter anode (Fig. 6-1). However, this 5 V discrepancy is most likely caused by operational deterioration of the tungsten cathode, and in any event is too small to merit further discussion. Furthermore, comparison of the overall potential distributions for similar arc operation with the small and large anodes reveals few noticeable differences, and therefore it is apparent that the availability of more anode surface does not influence the behavior of the quasi-steady MPD arc.

Two possible explanations for this apparent disagreement with the previous experiments on the pulsed accelerators are immediately obvious. First, since the effects of anode size variation have only been observed in pulsed or unsteady devices, it seems reasonable to suggest that anode precursor conduction subsides after the transient phase of the discharge has passed, and thereafter ceases to be an important aspect of arc behavior, hence is not found during quasi-steady operation. Second, the quasi-steady MPD arc operates at 17.5 kA, or at almost an order of magnitude lower current than those employed in the pinch and parallel-plate experiments, suggesting that the effects of precursor anode conduction may be insignificant at the low arc current or, more likely, at the low ratio of current to anode area employed in this device. In the parallel-plate insulation experiment (Chap. V), this ratio, J/A, was increased to a value of 15 kA/in.^{2} before any increase in arc voltage was observed, whereas J/A is only 3.7 kA/in.^{2} for the quasi-steady MPD arc employing the small 7 1/2-in.-diameter anode. A careful examination of the arc voltage signals corresponding to arc operation with the small and large anodes reveals that these

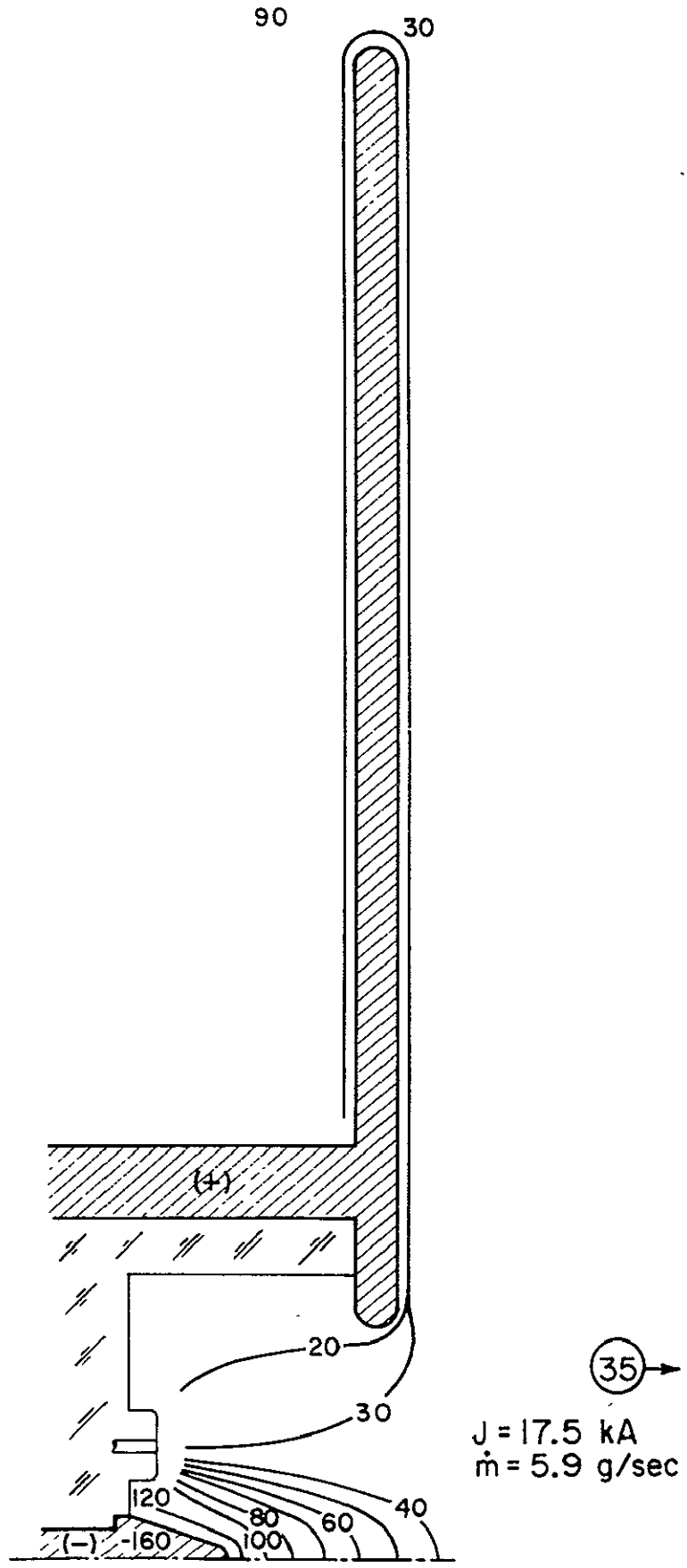

EQUIPOTENTIAL PROFILES
FOR LARGE ANODE

FIGURE 6-2

traces are almost identical, even during the early transient phase of this discharge. This suggests that the second of the above interpretations is the more reasonable in terms of present data. In any case, it is indeed clear that no basic improvement in quasi-steady MPD arc performance has been achieved by the deployment of a larger anode, and certainly the increase in accelerator size and weight, thereby incurred, makes its use undesirable.

Before concluding this discussion, it is noted that a 25 V voltage drop (corrected to the plasma potential value) appears over most of the large anode surface including the back face (Fig. 6-2), implying that the entire anode surface participates, albeit to a very small degree in some places, in the conduction of the total discharge current. However, as was pointed out previously, this small fraction of the arc current, which extends over most of this large anode surface, appears not to influence the quasi-steady operation of the device.

E. VARIATION OF ARC CURRENT AND MASS FLOW RATE

To this point, all the discussion has pertained specifically to quasi-steady operation of the MPD facility at the "matched" conditions of 17.5 kA x 5.9 g/sec. Earlier studies have established the importance of matching the mass flow to the arc current for optimum operation; indeed, the observed characteristics were found to depend qualitatively on the ratio of arc current squared to mass flow, rather than on either separately.[5] In this section, equipotential profiles are presented for arc operation at off-matched conditions, where the ratio $J^2/\dot{m}$ is either greater than (underfed) or less than (overfed) the value corresponding to matched operation.

Figure 6-3 compares the equipotential contours for quasi-steady arc operation at three different mass flow rates, 1.2 g/sec, 5.9 g/sec, 36.0 g/sec, and a constant current of

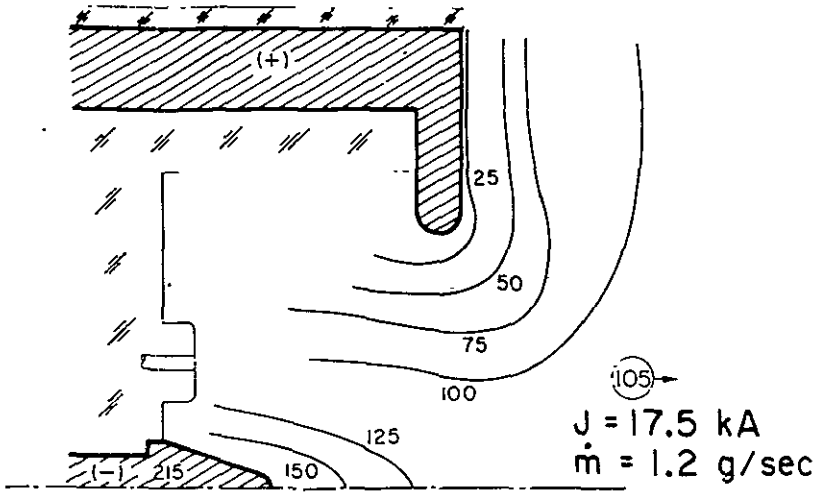

(a)

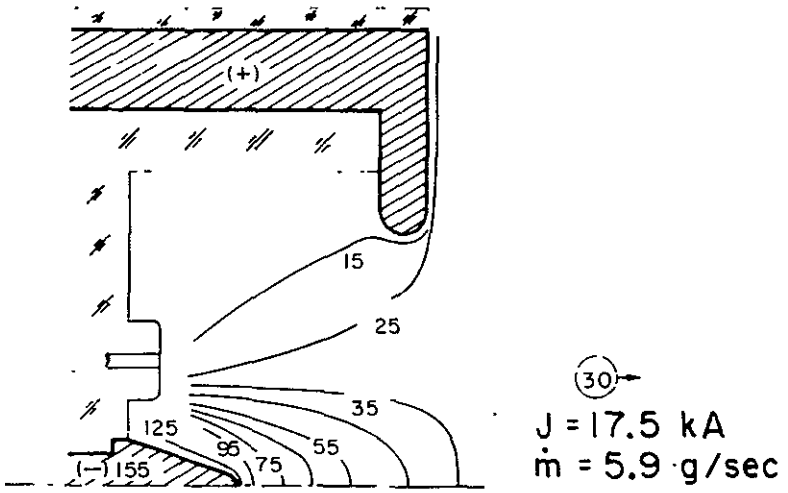

(b)

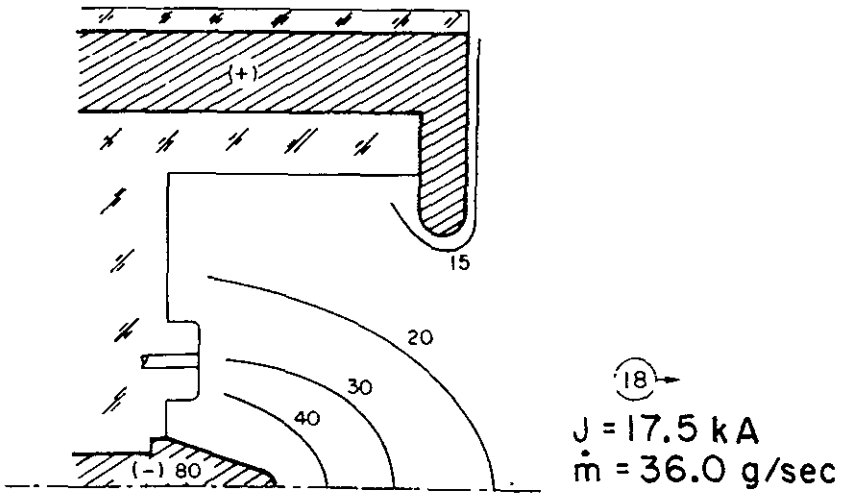

(c)

EQUIPOTENTIAL PROFILES FOR THREE DIFFERENT MASS FLOW RATES

FIGURE 6-3

17.5 kA. In addition to a decrease in the total arc voltage and downstream potential as the argon mass flow rate is increased, certain differences in the potential distribution are readily observable. The most apparent is the development of large voltage gradients in the anode region for the 1.2 g/sec mass flow, the so-called underfed case (Fig. 6-3a). It is not clear at this point whether this anode envelope is simply a very broad anode sheath necessitated by conduction difficulties prevailing in the lower density environment, or whether it is in fact an increased field gradient of the arc column itself formed to counteract lower plasma conductivities. In either event, if all of the power deposited in this region were delivered to the anode the fractional anode loss at this operating condition would be quite high. The importance of this anode field development thus becomes obvious, and therefore the conduction processes participating in this anode envelope are investigated in Chap. VII.

Turning now to the cathode region of the arc chamber, it is observed that a large fraction of the total arc voltage continues to appear across the cathode envelope, regardless of the mass flow rate employed, so that this region continues to be one of large power deposition. The importance of the cathode envelope for plasma acceleration can be readily discovered by noting that in both the underfed and matched cases the voltage drop across this region is approximately 100 V, compared to only 60 V in the overfed case; measurements of downstream ion velocities have found essentially the same values for the first two conditions but return a substantial decrease in downstream velocity at overfed conditions.[4]

Displayed in Figure 6-4 are equipotential profiles for three different arc currents, 42.0 kA, 17.5 kA, and 4.4 kA, at the same argon mass flow rate of 5.9 g/sec, representing underfed, matched, and overfed conditions respectively. As before the underfed condition, 42.0 kA x 5.9 g/sec, possesses a substantial anode envelope of voltage drop which is

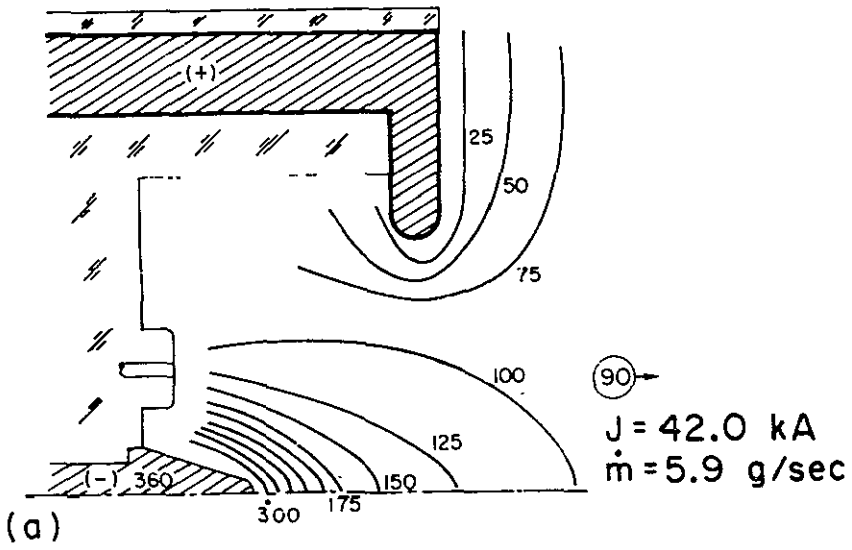

EQUIPOTENTIAL PROFILES FOR THREE DIFFERENT CURRENT LEVELS

FIGURE 6-4

not observed in either the matched or overfed cases. The voltage drop across this region is now only 25% of the total arc voltage; i.e., much less than the 50% fraction observed for the previously discussed underfed condition (17.5 kA x 1.2 g/sec). Since arc performance seems to depend on the ratio of arc current squared to mass flow rate, it follows that the 42.0 kA x 5.9 g/sec case represents a smaller departure from the matched condition, and hence displays milder symptoms of arc underfeeding. The other basic features of the quasi-steady arc potential distribution remain unchanged as the discharge current is varied by an order of magnitude.

F. ANODE FALL VARIATION WITH LOCAL CURRENT DENSITY

In a previous discussion of the potential profiles corresponding to accelerator operation at the matched condition, 17.5 kA x 5.9 g/sec, reference was made to the apparent variation of anode fall voltage with local anode current density. Indeed the term "anode fall" has been rather loosely applied here because the electrostatic probes employed in this experiment were not designed to measure the potential at less than about 0.1 cm from the metal surface, and thus the term "anode fall" describes the total voltage drop over a distance 0.1 cm away from the anode surface. The discussions in Chap. II have pointed out that both the anode fall region (thickness on the order of the electron mean free path) and the anode adjacent ϵ -layer (caused by anode cooling of the plasma) are normally confined to a zone much smaller than the 0.1 cm probing distance. For the present situation, it is possible to approximate the thickness of the anode fall by computing the electron mean free path from Langmuir probe estimates of the electron density near the anode surface (see Chap. VII). At the upstream portions of the anode the electron mean free path is estimated to be about 0.01 cm, whereas at the front face of the anode this value becomes on the order of 1 cm. These figures probably give a rough estimate of the anode fall thickness at the upstream anode locations,

where ion production in the fall is important, and where the electron mean free path is therefore a relevant measure of the fall thickness. However, at the front face of the anode, the drift of ions away from the anode and towards the cathode is not significant, and thus nor is the production of ions in the fall. Therefore, over this portion of the anode surface, the fall thickness is more likely associated with the prevailing Debye length, about 0.001 cm. In any event, measurements of plasma potential at a distance 0.1 cm from the anode surface provide only an upper estimate of the true anode fall voltage since contributions due to possible ϵ-layer fields are included in the probe readings. However, for convenience, the term anode fall shall henceforth refer to the anode voltage drop measured to within 0.1 cm of the metal surface.

In order to establish the general features of the anode fall variation noted above, an experiment was designed in which the anode current density distribution was mapped out using magnetic probes, while anode fall voltages were simultaneously monitored by electrostatic probes. These measurements were carried out during quasi-steady arc operation at the previously discussed matched condition, 17.5 kA x 5.9 g/sec, as well as at two other operating conditions, 8.7 kA x 1.2 g/sec, and 42.0 kA x 36.0 g/sec, both of which are considered to be matched based on their ratios of arc current squared to mass flow rate (see Sec. F). Data were taken at three operating conditions to give more generality to the results and to provide a broader range of anode current densities. The matched cases were chosen because the arc is relatively well-behaved, and the identification of the anode fall is less ambiguous, under these conditions. The measured values of floating potential adjacent to the anode surface were corrected by the amount $-4.1\ kT_e/e$ (see Eq. 6-2), as it is reasonable to assume that the ion streaming energy is negligible over most portions of the anode; as a rough correction the electron temperature was taken to be constant,

1.5 eV, over the entire anode surface for each of the operating conditions. Figure 6-5 was then constructed by plotting the corrected anode fall voltages against the measured values of local current density at the various anode locations and operating conditions.

Within the accuracy of the experiments, the data of Fig. 6-5 appear to indicate an inverse dependence of anode fall on local anode current density. For purposes of engineering calculations it is convenient to seek a reciprocal relationship between these two quantities, since this would imply a constant power density at the anode fall, $p_A = j_A V_A \approx$ constant, which then could be readily integrated over the total anode area to give the power deposited at the anode due to the anode fall voltage. The reciprocal form, $V_A = 1.5 \times 10^3 / j_A$ (volt/amp/cm^2), plotted on Fig. 6-6, defines, along with the ordinate and the abscissa, an envelope within which most of the data lies; thus any calculation of anode power loss based on this relationship would surely be a pessimistic one. If the contributions due to the electron thermal motion and the work function of the metal anode are included, though neglecting convection and radiation (see Sec. H), a more accurate estimate of the anode power density for the 17.5 kA x 5.9 g/sec operating conditions can be calculated, $p_A \approx 2.0 \times 10^3$ W/cm^2. This figure is relatively modest in comparison to recent experimental observations. For example, Shih and Dethlefson[51] have experimentally determined the anode heat flux density in argon and nitrogen arcs operating at currents from 50 to 2000 A; their data shows $p_A \approx 10^4$ to 10^6 W/cm^2; i.e., power densities 5 to 500 times greater than that estimated for the quasi-steady MPD arc.

In conclusion, the observed inverse dependence of anode fall on local anode current density has major implications for the overall efficiency of the accelerator. Steady flow devices operating in much lower power ranges are known to dissipate large portions of their input power--

FIGURE 6-5

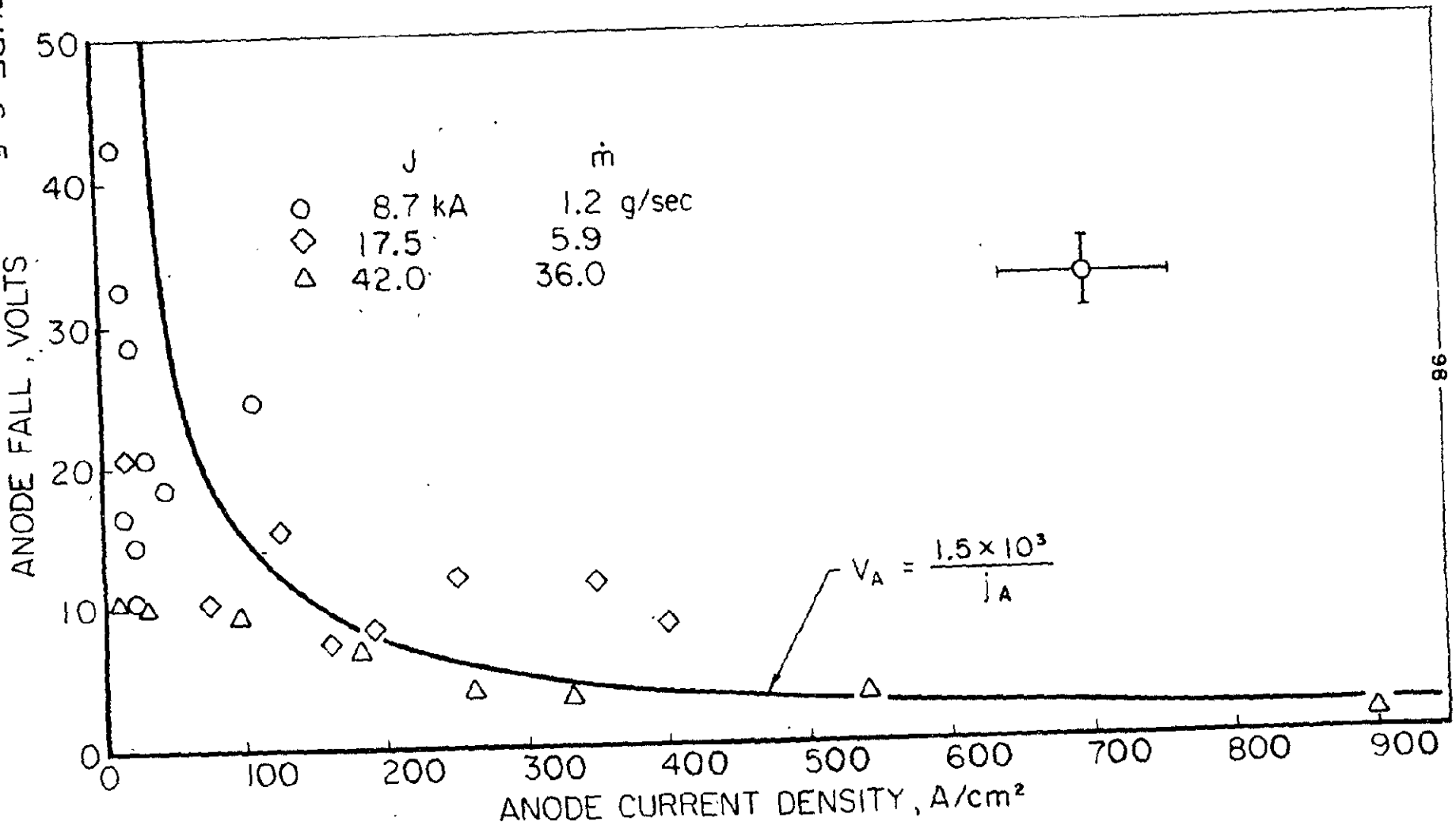

ANODE FALL VARIATION WITH LOCAL CURRENT DENSITY

in some cases 60% or more--into heating of the anode. This dissipation is clearly related to the anode fall established by the arc, and any empirical means for reducing the fall voltage should be reflected in higher overall performance. As will be shown in Sec. H, the inverse dependence of anode fall on local current density results in substantially lower relative power loss to the anode, and hence more efficient accelerator operation at the higher power levels.

G. INTERPRETATION OF ANODE FALL DATA

The inverse dependence of anode fall voltage on local anode current density, for the matched quasi-steady MPD arc (see Fig. 6-5), shall now be related to the anode fall theories of Bez and Höcker,[18,19] see Chap. II, Sec. D. Briefly, they distinguish between two mechanisms by which ions are produced in the anode fall region: field ionization and thermal ionization. In the field ionization case, electrons from the column plasma undergo essentially collisionless acceleration in the anode fall field, and then ionize neutral atoms upon impact. Hence, for this ion production process to occur the anode fall voltage must exceed the ionization potential of the carrier gas. Bez and Höcker have developed a model for this type of ionization, and thereby have derived a relation [see Eq. (2-6)] which fits the experimental anode fall data for low temperature arcs, less than 7000 - 9000 ^{o}K. For nitrogen and argon, the electron collision mean free path begins to decrease sharply at these temperatures (see Fig. 2-3), causing Eq. (2-6) to predict increased anode fall voltages which contradict experimental data. Bez and Höcker claim, therefore, that the conditions for field ionization are violated at arc plasma temperatures above 7000 - 9000 ^{o}K, and that ion production in the fall is then achieved via the thermal ionization mechanism. In this case, the accelerating electrons have their velocities randomized by elastic collisions in the fall zone, and since only electrons in the high energy "tail" of the energy distribution take

part in the ionization process, the anode fall voltage drops below the ionization potential of the gas. The important point of Bez and Höcker is that the transition from field to thermal ionization occurs at some critical arc plasma temperature, and that this critical temperature coincides with a sudden decrease in the electron collision mean free path due to increased ion-electron encounters. Furthermore, it was observed experimentally that the transition from F- to T-ionization in the carbon arc with nitrogen gas takes place at an anode current density of 40 A/cm^2.

For comparison with the above model of the anode fall zone, the anode fall data for the matched quasi-steady MPD arc have been replotted in Fig. 6-6. Also shown on this figure are twin Langmuir probe electron temperature measurements taken at four different anode locations for the 17.5 kA x 5.9 g/sec operating condition. Most of the data corresponding to low anode current densities, less than 60 A/cm^2, lie above the ionization potential of the working gas (argon), whereas the anode fall voltages at current densities greater than this value are generally less than the ionization potential. In addition, the plotted electron temperature data indicate that the high anode fall voltages correspond to temperatures below about 19,000 ^oK, whereas the low voltage drops occur for electron temperatures above this value. Invoking the ionization model of the anode fall zone, it is reasonable to presume that anode fall voltages greater than the ionization potential of argon reflect the field ionization mechanism, while those below it correspond to the thermal ionization process. Consistent with this interpretation, the data define critical values of the near anode electron temperature and the anode current density: 19,000 ^oK and 60 A/cm^2, respectively. This apparent transition anode current density is close to the critical value for the carbon arc, 40 A/cm^2, thus suggesting that the quasi-steady MPD arc data may indeed comply with Bez and Höcker. On the other hand, the electron temperature of 19,000 ^oK is far from the argon critical

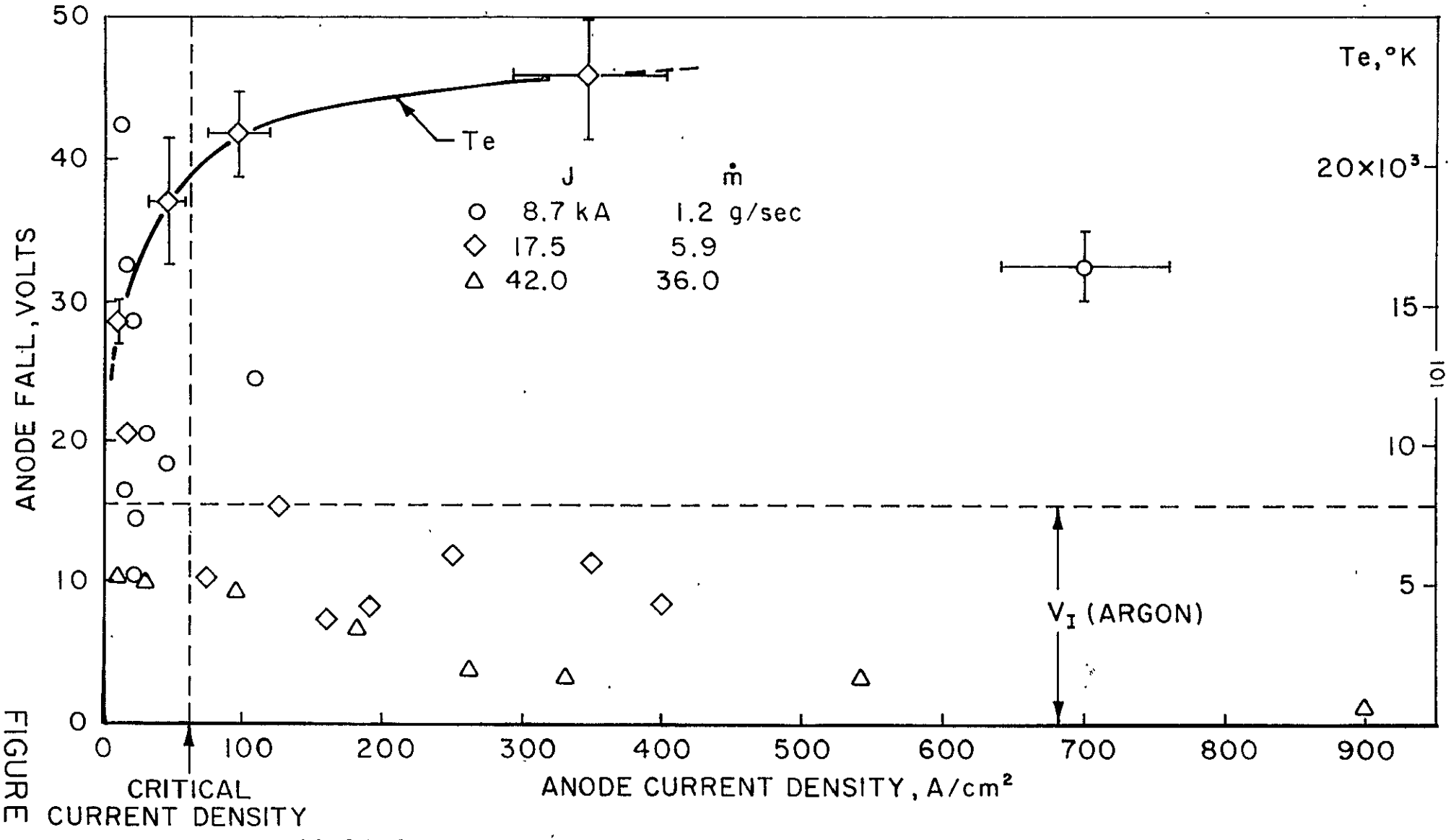

FIGURE 6-6

ANODE FALL VARIATION WITH LOCAL CURRENT DENSITY

temperature which, based on the sudden decrease in electron collision mean free path, is about 7500 °K.[19] Since the electron temperature measurements were taken at about 0.5 cm from the anode surface, one may argue that plasma cooling at the anode surface causes the plasma temperature at the edge of the fall zone to be substantially lower. Conceivably, the electron temperature of 19,000 °K may correspond to a temperature of around 7500 °K for the cooled plasma adjacent to the anode fall. However, from the available data it is not possible to determine, one way or another, whether the matched quasi-steady MPD arc anode fall data agree, even qualitatively, with the anode fall ionization model of Bez and Höcker.

H. POWER LOSSES AT THE ANODE

The total power delivered to the anode of the quasi-steady MPD arc can be written as

$$P_A = P_{cA} + P_{RA} + \int_{\substack{\text{ANODE}\\ \text{SURFACE}}} j_A \left(\frac{5}{2} \frac{kT_e}{e} + V_A + \phi_A \right) da \qquad (6\text{-}3)$$

where P_{cA} and P_{RA} are the contributions due to convection and radiation respectively, and the third term represents the power deposited at the anode by current-carrying electrons, with j_A as the current density at the anode, V_A as the anode fall voltage and ϕ_A as the work function of the anode metal (see Chap. II, Sec. E). The term j_A 5/2(kT_e/e) represents the energy flux at the anode due to the electron thermal energy in the neighboring plasma; the use of the factor 5/2, as opposed to the factor 2 which often appears in this literature, is discussed in the Appendix.

1. Radiative Losses

Recent experiments on the quasi-steady MPD arc have estimated that between 2 and 10% of the total arc input power is lost as radiation from the highly luminous arc plasma.[52] The radiative power delivered to the anode can be estimated by calculating the percentage of this total arc radiation which is absorbed by the anode surface. However, the geometry of this particular accelerator is such that only a small fraction of the arc radiation will be delivered to the anode, and by far the largest portion will be absorbed by either the insulating walls of the chamber or the downstream environment. For this reason, the term P_{RA} in Eq. (6-3) does not represent a substantial anode power loss, and can be shown to be negligible compared with the power loss due to the electron current at the anode; nevertheless, the total radiative power loss of the accelerator may not be insignificant.

2. Convective Losses

Convective power losses may arise at the anode because of the interaction of the streaming plasma with the anode surface. An order of magnitude estimate of this contribution to the total anode loss is attempted by assuming that viscous and thermal boundary layers form at the lip region of the anode, and that heat is convected through the boundary layer to the anode surface (see Fig. 6-7). Heat transfer by conduction from the hot plasma to the remaining portions of the anode will be due primarily to the flux of fast moving thermal electrons. However, the anode current density, j_A, essentially defines this electron flux, and therefore the conductive heat transfer at the anode is included in Eq. (6-3) by the term $j_A \, 5/2(kT_e/e)$.

The convective heat transfer at the anode is expressed in terms of an enthalpy difference after Eckert[27]

$$P_{cA} = h_i A_A (i_s - i_A) \qquad (6\text{-}4)$$

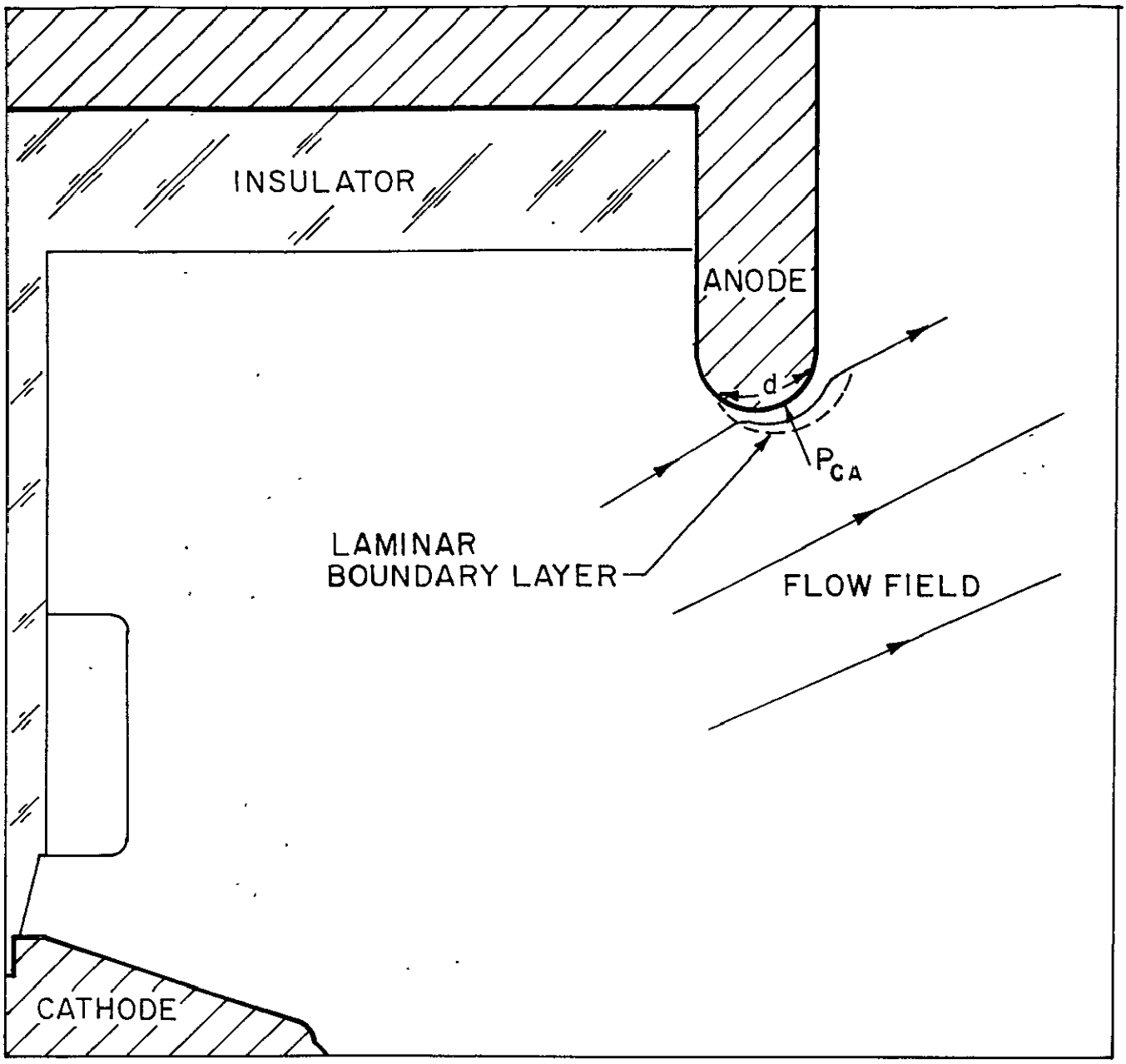

CONVECTIVE HEAT TRANSFER TO THE ANODE OF THE QUASI-STEADY MPD ARC

FIGURE 6-7

where h_i is the convective heat transfer coefficient based on enthalpies, i_s is the stagnation enthalpy of the streaming plasma at the outer edge of the boundary layer, i_A is the enthalpy of the plasma in thermal equilibrium at the anode surface, and A_A is the area of the anode convection zone. The effects of recombination between electrons and ions in the boundary layer is taken into account by writing the convective heat transfer in the above form.

From downstream velocity patterns for the quasi-steady MPD arc,[4] it is clear that the plasma streaming velocity at the anode lip cannot exceed 10^4 m/sec. In addition, Langmuir probe measurements near this region of the arc indicate electron temperatures of about 20,000 ^{o}K and plasma densities of approximately 7×10^{-9} g/cm^2. It is assumed for the present calculation that the plasma under consideration is in local thermodynamic equilibrium at a temperature of 20,000 ^{o}K. Argon at this temperature and at a pressure of 1 atm has a shear viscosity, $\mu \approx 2.2 \times 10^{-4}$ gm/cm-sec.[53] Since shear viscosity depends only on temperature over a wide range of pressures and densities, this value should be appropriate for the present low pressure ($\approx$ 0.001 atm) situation. Using the above estimates of plasma properties along with the characteristic length of the anode lip boundary layer, $d \approx 1$ cm, the flow Reynolds number is determined

$$R_{ey} = \rho u_s d / \mu \approx 32 \qquad (6\text{-}5)$$

This low Reynolds number suggests that the anode boundary layer is laminar. The convective heat transfer coefficient for a laminar boundary layer on a flat plate is given in terms of the Stanton number[27]

$$h_i / \rho u_s = St_i = .332 \Big/ (R_{ey})^{1/2} (P_r)^{2/3} \qquad (6\text{-}6)$$

References 53 and 54 give the following estimates of the thermal conductivity and specific heat at constant pressure for argon at 20,000 ^{o}K and 0.1 – 1 atm: $K \approx 5.7 \times 10^{-3}$ cal/cm-sec-^{o}K and $C_p \approx 1.0$ cal/gm-^{o}K. Both of these quantities are only weakly dependent on pressure and density over a wide range, and therefore the above values should apply reasonably well to the low density argon plasma under consideration. The Prandtl number can now be computed

$$P_r = C_p \mu / K \approx .04 \tag{6-7}$$

The quantities appearing in Eq. (6-6) should be evaluated at a reference enthalpy corresponding to the arithmetric mean of the plasma enthalpy at the outer edge of the boundary layer and the plasma enthalpy corresponding to the surface temperature. However, evaluation at the free stream conditions is sufficient for these approximate calculations. Substituting the above values of R_{ey} and P_r, along with the estimated plasma density and velocity, into Eq. (6-6) yields the following value for the convective heat transfer coefficient

$$h_i \approx 0.0035 \text{ gm/cm}^2\text{-sec}$$

The stagnation enthalpy of argon plasma with a streaming velocity of 10^4 m/sec and a temperature of 20,000 ^{o}K is estimated to be,[55] $i_s \approx 1.5 \times 10^5$ J/gm. Thus, a conservative estimate of the anode power loss due to convective heat transfer at the anode lip boundary layer can now be made with the aid of Eq. (6-4),

$$P_{cA} = h_i A_A (i_s - i_A) \approx h_i i_s A_A \approx 20 \text{ kW} \tag{6-4}$$

where the area of convective heat transfer, A_A, is deduced from the flow field diagram shown in Fig. 6-7.

The total input power to the quasi-steady MPD arc at the matched conditions, 17.5 kA x 5.9 g/sec, is $P_T = JV_T = 2.6 \times 10^3$ kW. Hence, the convective power loss at the anode appears to be on the order of 1% of the input power of the accelerator.

3. Losses Due to the Electron Current

Since it has been demonstrated that both the radiative and convective heat transfer to the anode of the quasi-steady MPD arc are rather insignificant, the expression for the total power loss at the anode reduces to the form

$$P_A \approx \int_{ANODE} j_A \left(\frac{5}{2} \frac{kT_e}{e} + V_A + \phi_A \right) da \qquad (6\text{-}8)$$

Since T_e and ϕ_A are essentially constant over most of the anode surface this expression can be simplified to

$$P_A \approx J\left(\frac{5}{2} \frac{kT_e}{e} + \phi_A \right) + \int_{ANODE} j_A V_A \, da \qquad (6\text{-}9)$$

By restricting this formulation to the case of quasi-steady MPD arc operation at the three matched conditions sighted in Sec. F, the experimentally observed variation of anode fall with current density ($j_A V_A \approx 1.5 \times 10^3$ W/cm^2) can be employed here. The integral on the right-hand side of Eq. (6-9) can now be easily evaluated, and substituting $T_e = 1.5$ eV for average electron temperature at the anode (see Fig. 6-6), and $\phi_A = 3.5$ V, the expression for the total anode power loss becomes

$$P_A \approx 7.25\,J + 4.5 \times 10^5 \quad \text{WATTS} \qquad (6\text{-}10)$$

where J is the total arc current in amps. The fractional anode power loss for quasi-steady arc operation at the matched

conditions is then

$$P_A / P_T \approx 7.25 / V_T + 4.5 \times 10^5 / J V_T \qquad (6\text{-}11)$$

where V_T is the total arc voltage.

Figure 6-8 displays this fractional anode power loss computed for the three matched conditions, 42.0 kA x 36.0 g/sec, 17.5 kA x 5.9 g/sec, 8.7 kA x 1.2 g/sec, during quasi-steady arc operation. The fractional power loss drops from over 50% to less than 10% with an increase in arc power from 1.5 mW to about 10.0 mW. This distribution of data dramatically reflects the observed inverse dependence of anode fall on local anode current density (see Sec. F). The implications of these data are clear; matched operation of the quasi-steady MPD arc in the megawatt range of pulse power should result in thermal efficiencies much higher than those attained by steady, low power MPD arcs which operate in the 40 to 70% range (see Chap. II, Sec. E).

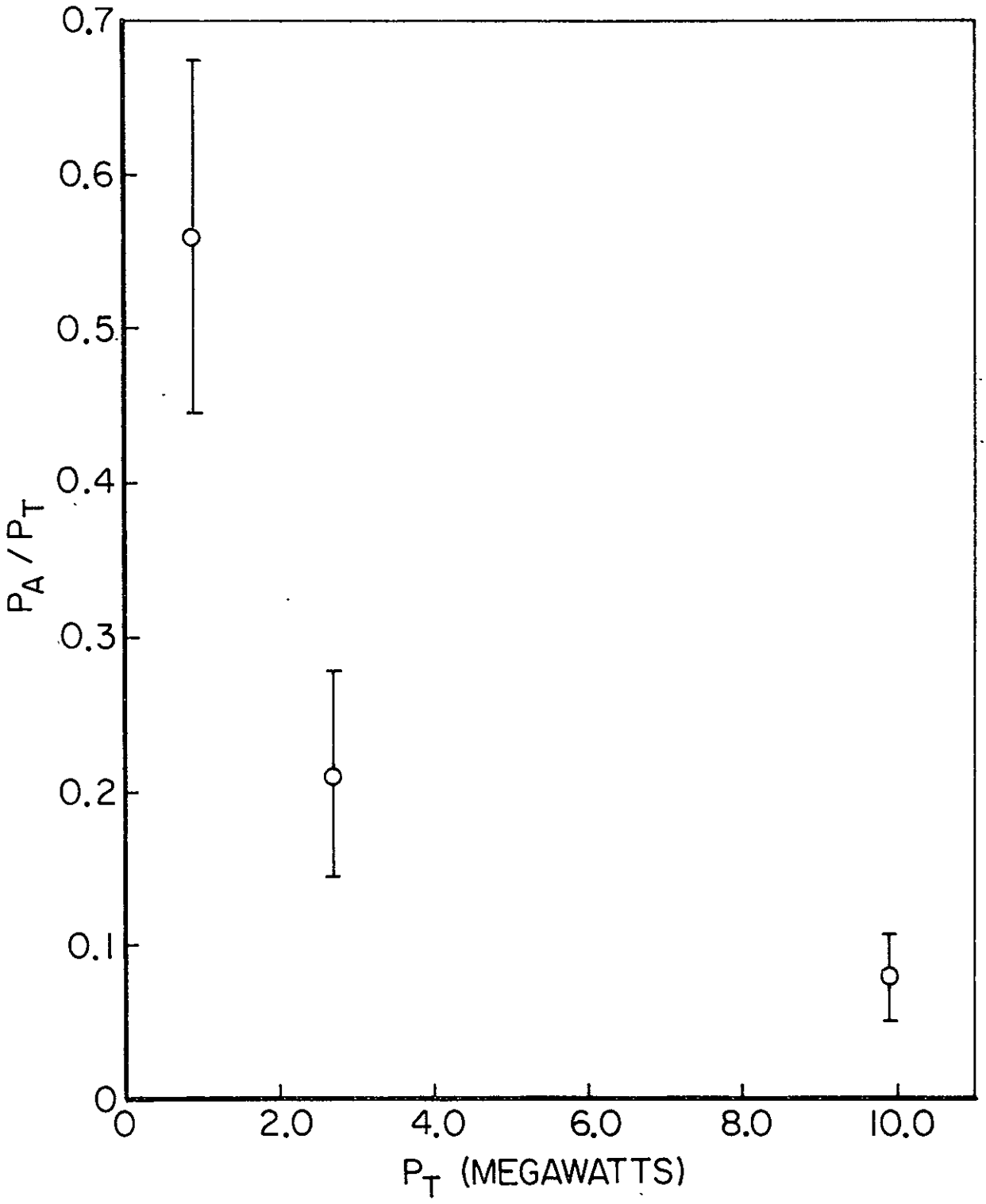

FRACTIONAL ANODE POWER VARIATION WITH TOTAL ARC POWER AT MATCHED CONDITIONS

FIGURE 6-8

CHAPTER VII

ANODE CURRENT CONDUCTION IN A QUASI-STEADY MPD ARC

A. ELECTRON TEMPERATURE AND DENSITY MEASUREMENTS

Measurements of electron temperature and electron number density have aided the understanding of the plasma potential patterns which arise in the quasi-steady MPD discharge, see Chap. VI. In addition, these electron temperature measurements can be used to correct the previously determined floating potential values to the true plasma potentials. A description of the twin Langmuir probes and measurement techniques used in this experiment is given in detail in Chap. III, Sec. G. Briefly, these particular probes consisted of two separately shielded and biased 1/8-in. long exposed tips of 3-mil tungsten wire, oriented parallel to the flow axis to minimize streaming effects. This probe radius is less than the anticipated electron-ion mean free path in the regions to be probed, and larger than the Debye length. One of the probes was bent to allow access to the back portion of the anode. The probe signals were monitored with Tektronix P6006 voltage probes and displayed on an oscilloscope. The electron temperature is obtained from ratios of probe voltage and probe current for differently biased tips, providing both tips operate in the electron retarding region of the probe characteristic. Electron number density is determined, somewhat less precisely, by ascertaining when the probe ceases to operate in the retarding region and goes over to the electron saturation branch of the probe characteristic. The uncertainties quoted with the following probe measurements do not include the effects of magnetic fields and particle collisions, since near the anode these should not be severe. For example,

the electron-ion collision mean free paths, calculated from temperature and density measurements near the anode lip, are approximately 0.01 to 0.1 cm, still at an order of magnitude larger than the probe radius. With the aid of magnetic probe measurements, the mean electron gyro radii near this part of the anode are estimated to be about 0.02 cm, almost a factor of five larger than the probe radius.

Previous measurements with floating electrostatic probes revealed, for argon mass flow rates below the critical or "matched" level corresponding to a given arc current, that substantial electric fields developed in the anode region of the arc (see Chap. VI, Sec. E). At higher mass flows all fields were confined to the cathode region of the discharge, except for a sheath drop immediately adjacent to the anode surface. To explore this effect further, a more precise and detailed series of experiments have been performed. Figures 7-1, 7-2, and 7-3 display the resulting plasma potential and enclosed current contours for three different argon mass flow rates, 36 g/sec, 5.9 g/sec, and 1.2 g/sec, at a common current level of 17.5 kA. In addition to the previously observed electric field growth around the anode for the 1.2 g/sec case, it can be seen that a greater portion of the anode surface participates in the current conduction for this "underfed" condition. These two observations will be referred to later during the development of the physical model.

Electron temperature and number density were measured at the locations marked on these diagrams; those near the cathode, labeled (1) and (2), provide reference data needed for the model below. From these measurements of electron temperature and number density, along with magnetic probe data at the same locations, characteristics of the current conduction mechanism in this region of the arc can be deduced. For example, the electron Hall parameter, Ω_e, can be estimated with the aid of the Spitzer formula[56] for electron

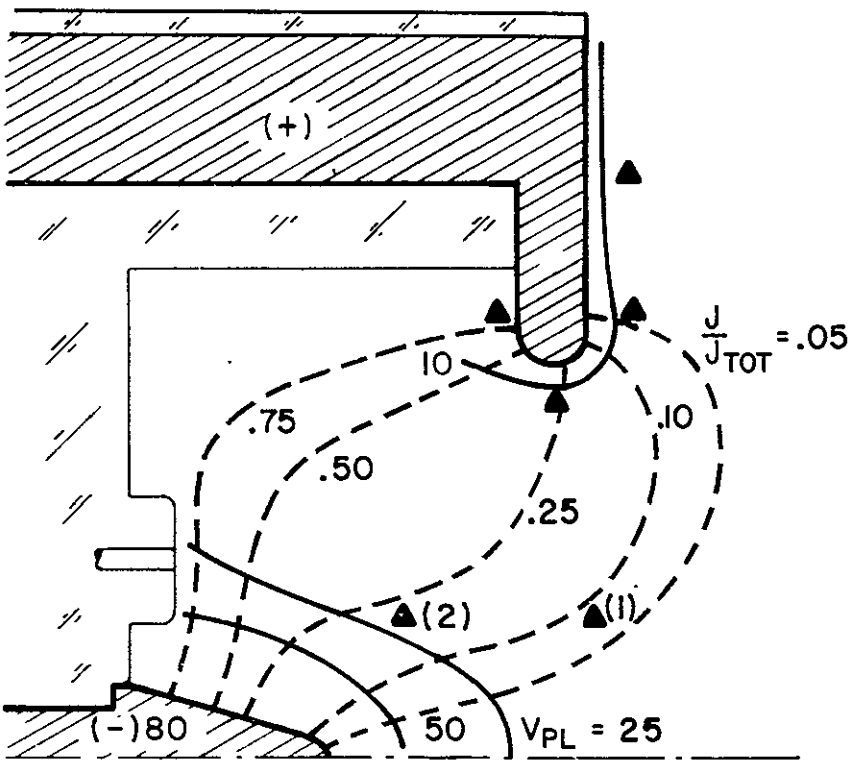

PLASMA POTENTIAL AND ENCLOSED CURRENT CONTOURS

J = 17.5 kA , $\dot{m}$ = 36.0 g/sec

FIGURE 7-1

7A

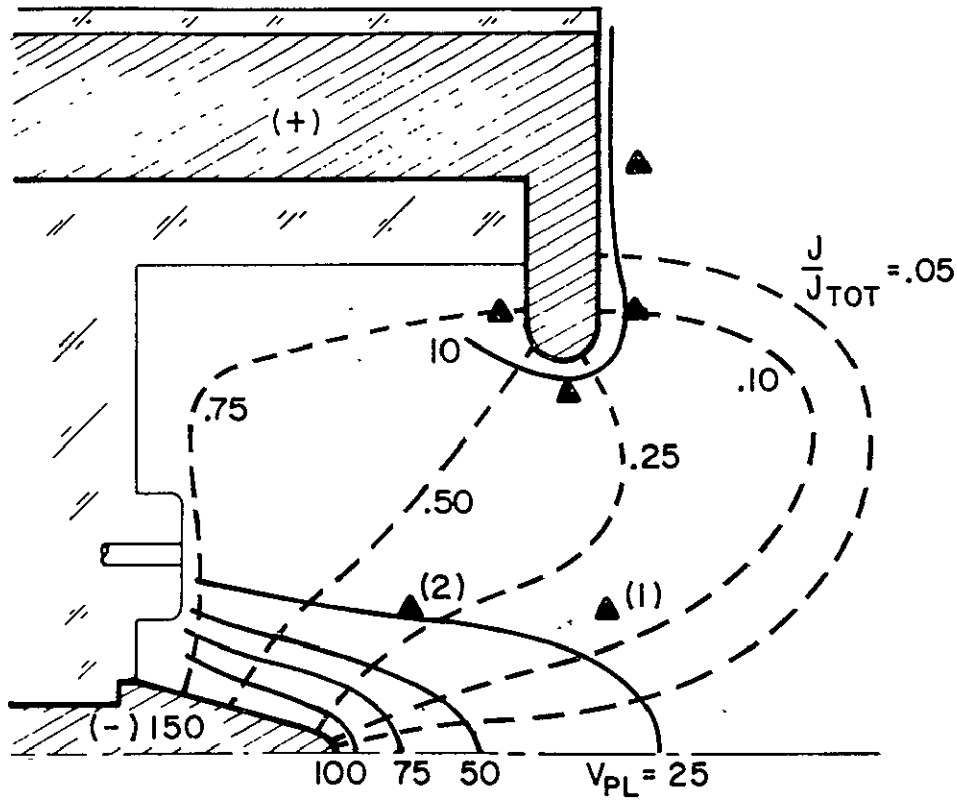

PLASMA POTENTIAL AND ENCLOSED CURRENT CONTOURS

J = 17.5 kA , $\dot{m}$ = 5.9 g / sec

FIGURE 7-2

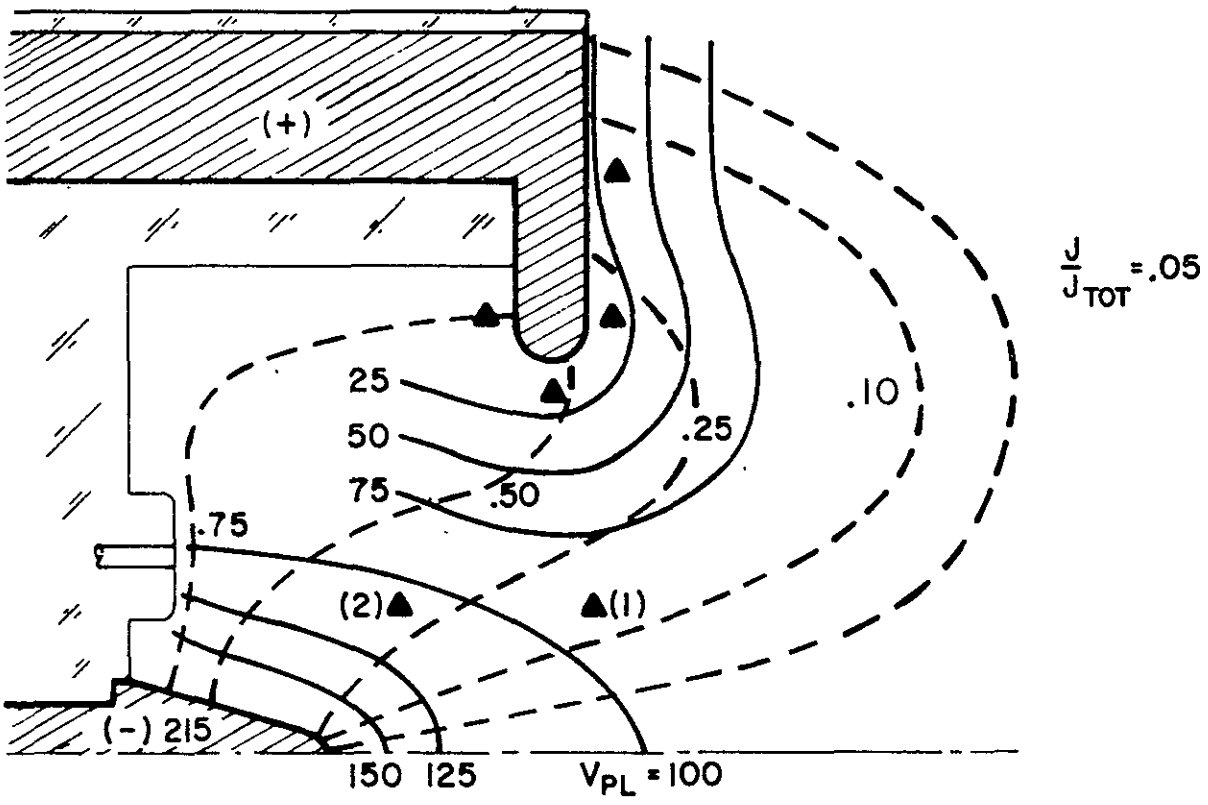

PLASMA POTENTIAL AND ENCLOSED CURRENT CONTOURS

J = 17.5 kA , $\dot{m}$ = 1.2 g/sec

FIGURE 7-3

collision frequency in a fully ionized gas,

$$\nu_{ce} = \frac{8 \times 1.714 \pi m_e e^4 \ln \Lambda}{m_e^{1/2} (3 k T_e)^{3/2}} \qquad (7\text{-}1)$$

$$= 7.2 \times 10^{-5} \; m_e / T_e^{3/2} \quad \text{SEC}^{-1}$$

where n_e is electron number density in cm^{-3} and T_e is the electron temperature in eV. Hence,

$$\Omega_e = e B / m_e \nu_{ce}$$

$$= 2.4 \times 10^{15} \; B T_e^{3/2} / m_e \qquad (7\text{-}2)$$

where B is the magnetic induction field in W/m^2.

Likewise, the scalar conductivity of the plasma, σ, can be computed,[56]

$$\eta = 6.53 \times 10 \ln \Lambda / T_e^{3/2} \quad \text{OHM-M}$$

or

$$\sigma = 2.75 \times 10^{3} \; T_e^{3/2} \quad \text{MHO/M} \qquad (7\text{-}3)$$

where T_e is in eV.

A summary of these measurements and calculations, performed at the two near cathode locations labeled (1) and (2) for three mass flow rates, is listed in Table 7-1. The conduction in this region of the discharge is seen to be

strongly tensor in nature, based on the observations that $\Omega_e \sim 1$ and $j/E < \sigma$, where j/E is computed from measured values of current density and electric field. This mode of conduction, as will be seen later, is in marked contrast to the processes prevailing near the anode.

The symbol $\sim$ in this table implies an accuracy of approximately 25% for the numbers quoted.

Table 7-1 Conduction Parameters at Various Mass Flows (J = 17.5 kA)

$\dot{m}$(g/sec)		36.0	5.9	1.2
T_e(eV)	(1)	1.9 ± 0.1	1.6 ± 0.2	2.0 ± 0.4
	(2)	1.9 ± 0.4	1.4 ± 0.1	2.0 ± 0.4
n_e(cm^{-3})	(1)	$2.0 \pm 0.4 \times 10^{14}$	$1.8 \pm 0.6 \times 10^{14}$	$1.7 \pm 0.7 \times 10^{14}$
	(2)	$1.4 \pm 0.6 \times 10^{14}$	$1.3 \pm 0.4 \times 10^{14}$	$1.7 \pm 0.7 \times 10^{14}$
B(W/m^2)	(1)	$\sim 1.4 \times 10^{-2}$	$\sim 2.5 \times 10^{-2}$	$\sim 3.2 \times 10^{-2}$
	(2)	$\sim 3.9 \times 10^{-2}$	$\sim 6.1 \times 10^{-2}$	$\sim 5.7 \times 10^{-2}$
Ω_e	(1)	~ 0.4	~ 0.7	~ 1.3
	(2)	~ 1.8	~ 1.8	~ 2.4
σ (mho/m)	(1)	$\sim 7.2 \times 10^3$	$\sim 5.5 \times 10^3$	$\sim 7.8 \times 10^3$
	(2)	$\sim 7.2 \times 10^3$	$\sim 4.5 \times 10^3$	$\sim 7.8 \times 10^3$
j/E(mho/m)	(1)	$\sim 1.1 \times 10^3$	$\sim 2.0 \times 10^3$	$\sim 1.0 \times 10^3$
	(2)	$\sim 1.0 \times 10^3$	$\sim 1.5 \times 10^3$	$\sim 1.1 \times 10^3$

B. ANODE CURRENT CONDUCTION PROCESSES

In the anode region of the quasi-steady MPD discharge, both the electric and magnetic fields are generally quite weak, and therefore the plasma conductivity must be sufficiently high to enable the weak electric fields to drive the necessary

current. In addition, current conduction in this region may be augmented by diffusion-dominated electron transport towards the anode surface. Furthermore, from measurements of electron temperature and number density at the four marked anode locations, one may establish, for mass flows above the critical value, that the random thermal flux of electrons from the plasma adjacent to the anode is sufficient to carry the required anode current. Assuming a Maxwell-Boltzmann distribution for the electrons, the electron current density at the anode-plasma boundary due to random flux is simply

$$j_{R.F.} = \frac{e n_e \bar{C}_e}{4} = e n_e \left(\frac{k T_e}{2\pi m_e} \right)^{1/2} \qquad (7\text{-}4)$$

Figures 7-4a,b compare this random flux current density, computed at the four anode locations and two different mass flow rates, with the actual anode current density distribution determined from magnetic probe data. The anode surface has been linearized in these diagrams, so that in going from left to right one progresses from the insulator wall at the back anode around the lip to the front face. The favorable comparison of random electron flux with anode current density in these two cases verifies that the plasma in the vicinity of the anode is sufficiently dense and thermally active that the required discharge current can be passed through it to the anode without the need for local high electric fields. The small potential drop right at the surface may be required to offset the cooling effect of the anode on the plasma, and may also serve to capture those electrons which approach the anode by virtue of their random motion. One may even speculate that it is this match of ambient plasma conditions to the discharge current that identifies the "critical" mass flow for a given arc current operation. This specification of the critical mass flow for a given arc current defines the so-called "matched" operation referred to in Chap. VI.

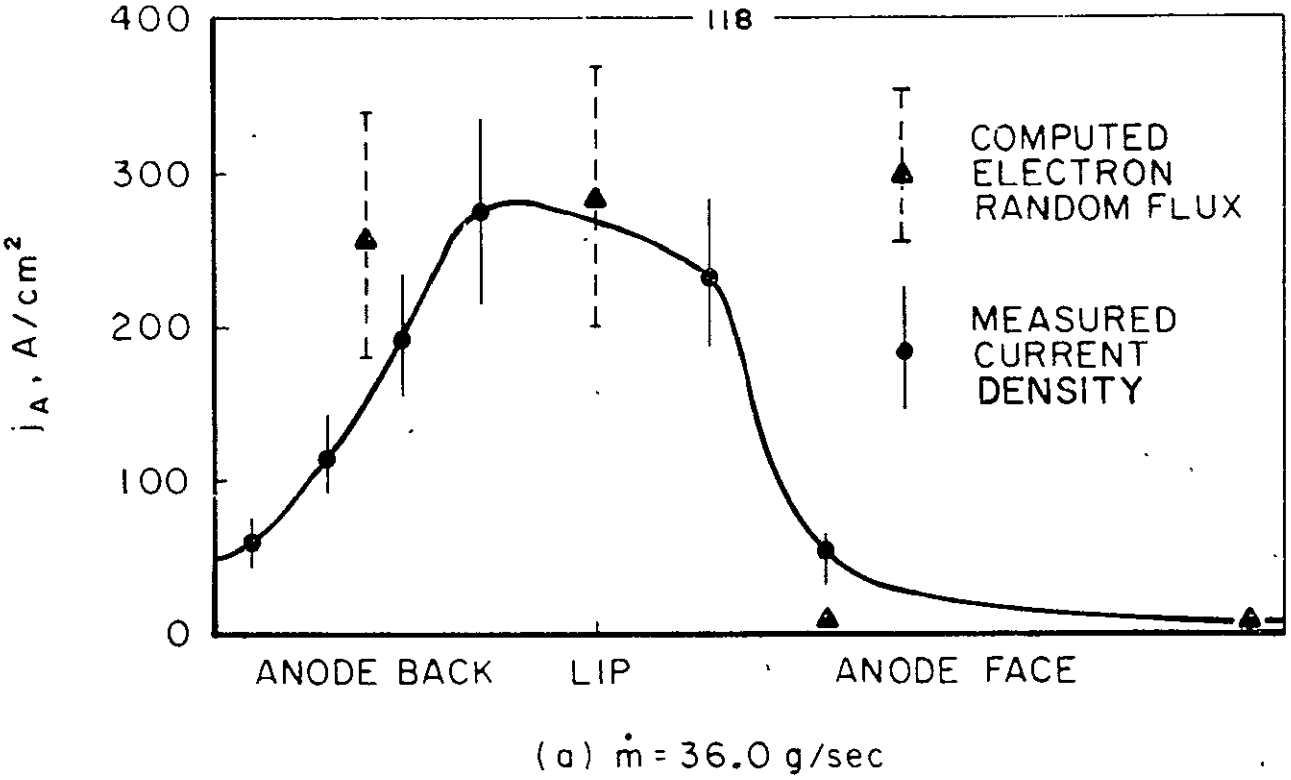

(a) $\dot{m}$ = 36.0 g/sec

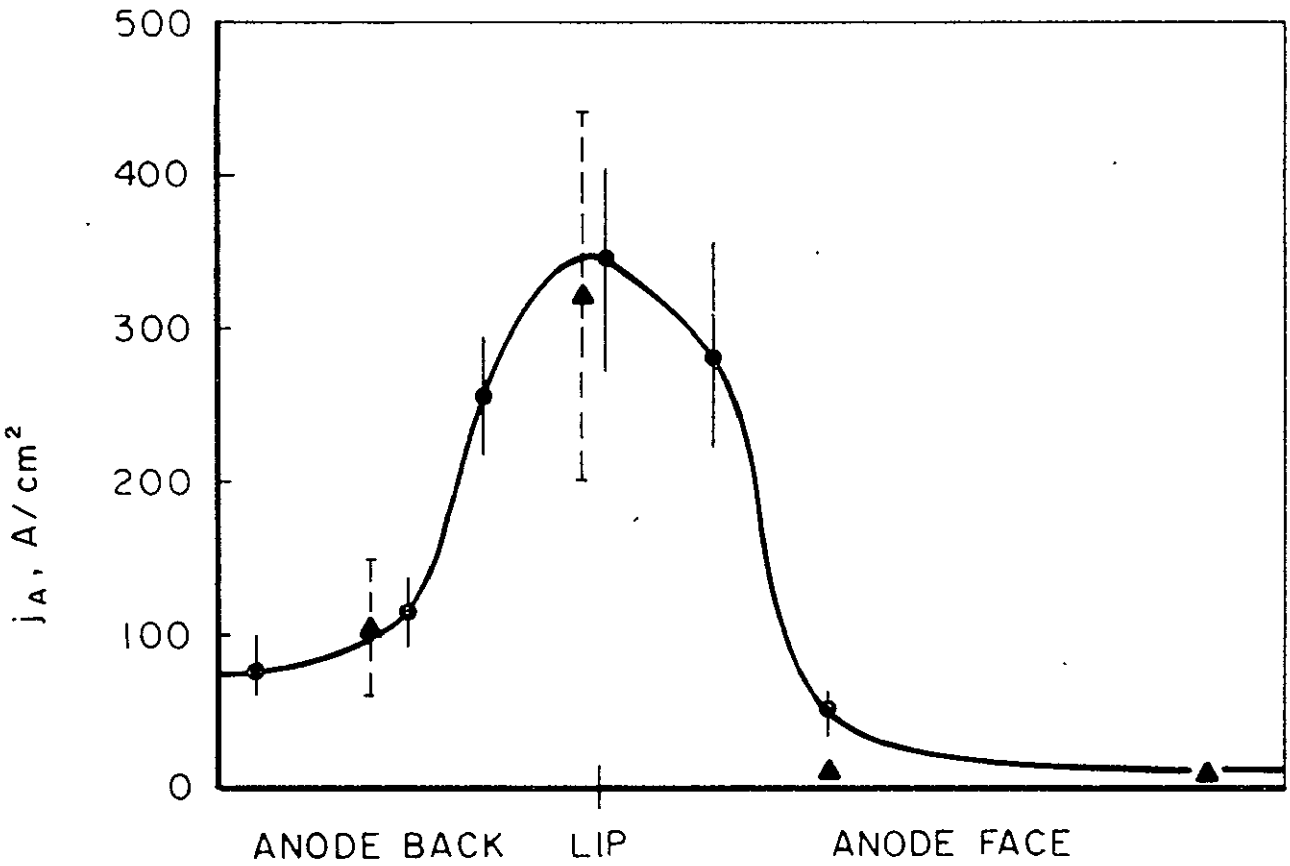

(b) $\dot{m}$ = 5.9 g/sec

COMPUTED ELECTRON RANDOM FLUX COMPARED TO MEASURED CURRENT DENSITY AT ANODE SURFACE

FIGURE 7-4

Regrettably, it has not been possible to make the same comparison for the "starved" condition, $\dot{m} = 1.2$ g/sec. In this case the electrostatic and magnetic probe data in the vicinity of the anode are exceedingly noisy and irreproducible, indicative of an unhappy domain of arc operation, and it is therefore impossible to define characteristic values of the plasma properties and current densities over most of the anode surface other than recalling that, at this condition, a sizable electric field extends far from the anode surface, even to the edge of the cathode region (Fig. 7-3). In the absence of better data at the anode, the following hypothesis is advanced. At the low mass flow rate, the electron number density near the anode is lower than that demanded by the random flux condition invoked above, presumably due to the lower overall density level in the chamber. Hence, in order to satisfy the current demands at the anode, the arc establishes an anode region field whose function is to increase the electron flux at the anode to the proper level. In addition, at this condition the arc current spreads itself over a larger portion of the anode surface (see Fig. 7-3), thereby alleviating somewhat the local demand for electron random flux.

It is possible to distinguish between two means by which this anode region electric field may accomplish the needed increase in electron flux to the anode surface: a) it may heat the plasma locally by means of the Joule-heating component of the total $\vec{E} \cdot \vec{j}$ energy input, thereby increasing the ionization level and possibly also the electron temperature to the point where the random flux of electrons again becomes adequate; b) it may establish an electron conduction current of the required magnitude to just compensate for the deficiency of random electron flux at this low density situation. Two elementary calculations should serve to estimate the relative effectiveness of these two means.

First, the complete expression for the electron flux to the anode is derived by considering a Maxwell-Boltzmann

distribution that has been shifted by the drift velocity of electrons towards the anode, u_e , and by integrating over one-half of the velocity space; i.e., over all those electrons moving towards the anode surface. Taking the x-direction to be perpendicular to the anode surface this has the form:

$$j_{eA} = n_e e \left(\frac{m_e}{2\pi k T_e}\right)^{3/2} \int_0^{\infty}\int_{-\infty}^{\infty}\int_{-\infty}^{\infty} v_x \, e^{-\frac{m_e}{2kT_e}\left[(v_x-u_e)^2+v_y^2+v_z^2\right]} dv_x\, dv_y\, dv_z$$

(7-5)

$$= \frac{n_e e \bar{c}_e}{4} e^{\frac{-m_e u_e^2}{2kT_e}} + \frac{n_e e u_e}{2}\left\{1 + 2\,erf\left[\left(\frac{m_e u_e^2}{kT_e}\right)^{1/2}\right]\right\}$$

where $\bar{c}_e = (8\,kT_e/\pi m_e)^{\frac{1}{2}}$ is the mean thermal velocity of the electrons. For the high temperature plasmas that arise in discharges of this nature, the electron thermal velocities are much greater than their drift velocities, hence $u_e^2 << 2kT_e/m_e$ and $u_e << \bar{c}_e$, and the lowest approximation to j_{eA} is just the expression used earlier for the isotropic electron distribution,

$$j_{eA} \approx j_{R.F.} = e n_e \bar{c}_e / 4 \qquad (7\text{-}6)$$

Now, let $(\Delta j_{eA})_J$ and $(\Delta j_{eA})_C$ define the increases in electron flux to the anode produced by Joule-heating of the plasma and by electron conduction respectively, where

$$(\Delta j_{eA})_J = \left(\frac{\partial j_{eA}}{\partial n_e}\right)\Delta n_e + \left(\frac{\partial j_{eA}}{\partial T_e}\right)\Delta T_e \qquad (7\text{-}7)$$

$$(\Delta j_{eA})_C = \left(\frac{\partial j_{eA}}{\partial u_e}\right)\Delta u_e \qquad (7\text{-}8)$$

The relative importance of the two terms in the expression for $(\Delta j_{eA})_J$ depends strongly on the state of the plasma under consideration. For example, if the plasma is only partially ionized, further energy input will increase the degree of ionization with the electron temperature charging only slightly until full ionization is approached. The addition of energy to a plasma which is almost completely ionized, on the other hand, will be reflected by an increase in the electron temperature rather than by the onset of second ionization because of the high-energy threshold of the latter process. Unfortunately, few data are presently available on the ionization levels in the anode region of the quasi-steady MPD discharge. However, measurements of electron temperature at the back surface of the anode for the three different mass flows have revealed that T_e does not increase at the "starved" case in response to anode field development.

Furthermore, partial differentiation of the expression for the electron flux to the anode, Eq. (7-5), yields the following results:

$$\left(\frac{\partial j_{eA}}{\partial n_e}\right)\Delta n_e = \frac{n_e e \bar{C}_e}{4} e^{-\frac{m_e u_e^2}{2kT_e}} \frac{\Delta n_e}{n_e} \qquad (7\text{-}9)$$

$$\left(\frac{\partial j_{eA}}{\partial T_e}\right)\Delta T_e = \frac{n_e e \bar{C}_e}{4} e^{-\frac{m_e u_e^2}{2kT_e}} \frac{\Delta T_e}{2T_e} \qquad (7\text{-}10)$$

where the assumption, $u_e^2 << 2kT_e/m_e$, has again been employed. These expressions show that the fractional increase in electron temperature must be double that of electron number density in order to achieve the same increase in the electron flux to the anode. Hence, it becomes apparent from both empirical and theoretical arguments that an increase in the level

of ionization, rather than a raising of the electron temperature, is the more likely and more effective means by which Joule-heating of the anode region plasma may serve to raise the flux of electrons to the anode. Therefore the second term in the expression for $(\Delta j_{eA})_J$ may be neglected; and hence a comparison of the relative importance of plasma-heating and electron conduction involves the evaluation of the two partial derivatives: $\partial j_{eA}/\partial n_e$ and $\partial j_{eA}/\partial u_e$.

With reference to Eq. (7-5), the following expressions can be derived:

$$\frac{\partial j_{eA}}{\partial n_e} = \frac{e \bar{C}_e}{4} e^{-\frac{m_e u_e^2}{kT_e}} \tag{7-11}$$

$$\frac{\partial j_{eA}}{\partial u_e} = \frac{n_e e}{2} \left\{ 1 + 2 \, erf \left[\left(\frac{m_e u_e^2}{2kT_e} \right)^{1/2} \right] \right\} \tag{7-12}$$

Employing the usual assumption that $u_e^2 << 2kT_e/m_e$ to simplify the above forms, a ratio is established which compares the relative effectiveness of plasma-heating and electron conduction in terms of their ability to raise the electron flux at the anode to the required level, namely

$$\frac{(\Delta j_{eA})_J}{(\Delta j_{eA})_C} = \left(\frac{2kT_e}{\pi m_e} \right)^{1/2} \frac{\Delta n_e}{n_e \Delta u_e} = \frac{\Delta \bar{n}_e}{2 \Delta \bar{u}_e} \tag{7-13}$$

where $\Delta \bar{n}_e$ is the normalized increment in electron density, and $\Delta \bar{u}_e$ is the increment in electron drift velocity perpendicular to the anode normalized by the electron mean thermal velocity.

The respective increases in electron number density and electron drift velocity, Δn_e and Δu_e , which arise

in response to the anode region field at the starved condition, E_A , must now be related to this field by means of ionization and conduction models. First, the current conduction in the anode region of the discharge is probably tensor in nature, with the components of current parallel and perpendicular to the anode field given by $j_{\parallel} = \sigma E_A/(1+\Omega_e^2)$ and $j_{\perp} = \sigma\Omega_e E_A/(1+\Omega_e^2)$; where the perpendicular component lies in the r-z plane and is directed towards the downstream portions of the anode. Hence, the increase in electron drift velocity perpendicular to the anode surface, i.e., parallel to E_A , is given by

$$\Delta u_e = \Delta\left(j_{\parallel}/m_e e\right) = \sigma\Delta E_A/(1+\Omega_e^2)m_e e \qquad (7\text{-}14)$$

where ΔE_A is the increase in the anode region field, which results because of the "starved" mass flow rate, and the ratio σ/m_e is assumed to be only weakly dependent on m_e .

The rate of Joule-heating in the anode field region is simply j^2/σ ,[57] where j is the total current density given by $j = \sigma E_A/(1+\Omega_e)^{1/2}$. Thus, the rate of ionization, or in other words, the rate of electron production due to the increased anode field, E_A , is given by

$$\frac{dm_e}{dt} = \frac{j^2/\sigma}{eV_I^*} = \frac{\sigma E_A^2}{(1+\Omega_e^2)\,eV_I^*} \qquad (7\text{-}15)$$

where it is assumed that all of the Joule-heating energy goes into ionization and V_I^* is the effective or mean ionization potential of argon. In order for the steady state level of electron density at the anode to increase by the amount Δm_e over the value it would assume in the absence of ionization, Δm_e new electrons must be produced in the anode field region over the time interval taken for all of the electrons in that

region at a given moment to reach the anode. In other words, the time interval, $\Delta\tau_I$, used to compute Δm_e, must be approximately equal to the transit time for electrons drifting across the anode field region. If the average thickness of this region is d_A, then the time interval during which Δm_e electrons are produced must be $\Delta\tau_I = d_A / u_e$, where u_e is again related to the current component parallel to E_A, $u_e = j_{\parallel} / n_e e$. Hence the increase in electron number density at the anode, due to Joule-heating of the plasma in the anode field region, is given by

$$\Delta n_e = \frac{j^2/\sigma}{e V_I^*}\,\Delta\tau_I = \frac{j^2}{\sigma e V_I^*}\cdot\frac{d_A}{u_e} \qquad (7\text{-}16)$$

which reduces to the simple form

$$\Delta n_e = n_e\,\Delta E_A\, d_A / V_I^* \qquad (7\text{-}17)$$

Substituting the expressions for Δu_e and Δn_e given by Eqs. (7-14) and (7-17) into the ratio of Joule-heating to electron conduction defined by Eq. (7-13) yields

$$\frac{(\Delta j_{eA})_J}{(\Delta j_{eA})_C} = \left(\frac{2kT_e}{\pi m_e}\right)^{1/2}\frac{n_e e\, d_A\,(1+\Omega_e^2)}{\sigma V_I^*} \qquad (7\text{-}18)$$

Using the formula for σ given by Eq. (7-3), and substituting $d_A = 2$ cm for the approximately uniform thickness of the anode field region, and $V_I^* = 33$ V for the effective or mean ionization potential of argon,[58] the ratio takes the simplified form,

$$\frac{(\Delta j_{eA})_J}{(\Delta j_{eA})_C} \approx 1.0\times10^{-14}\, n_e(1+\Omega_e^2)/T_e \qquad (7\text{-}19)$$

where n_e is in cm^{-3} and T_e is in eV.

The above ratio is strongly dependent upon local plasma properties; hence must be evaluated at several representative anode locations in order to determine whether Joule-heating or electron conduction is the more effective means of increasing the electron flux to the anode surface. As mentioned earlier, considerable noise and irreproducibility are associated with Langmuir probe signals at this "starved" condition, thus precluding the measurement of electron temperature and number density in the anode region of the arc. Lacking better data, the value $T_e = 2$ eV (see Table 7-1) shall be assumed for the plasma at the lip region of the anode. Measurements of electron density at this same location for the 5.9 g/sec mass flow yield $n_e \approx 1 \times 10^{14}$ cm^{-3} (see Fig. 7-4b). Presumably, the electron densities are lower at the starved case because of the lower overall plasma density at the decreased mass flow, and as a first approximation, it is assumed that the electron densities are lowered by the ratio of the respective mass flow rates; hence $n_e \sim 2 \times 10^{13}$ cm^{-3} is predicted at the anode lip for the 1.2 g/sec mass flow case. The magnetic fields at the lip region are estimated from the enclosed current contours of Fig. 7-3, thus $B \approx 3.5 \times 10^{-2}$ W/m^2. However, when these values of T_e, n_e, and B are inserted into the formula for the electron Hall parameter,

$$\Omega_e = 2.4 \times 10^{15} \, B \, T_e^{3/2} / n_e \qquad (7\text{-}2)$$

the result is $\Omega_e \approx 12$. A Hall parameter of this magnitude implies that the current near the anode must flow essentially perpendicular to the electric field. This is clearly in disagreement with the current and potential contours for the starved condition (Fig. 7-3), suggesting that the first order approximation for n_e based on the ratio of mass flow rates is not valid. Magnetic probe data, used in constructing the

enclosed current contours for the starved case, were not available at less than about 1 cm from the anode surface because of excessive signal noise there, and hence the current lines close to the anode are very approximate. Nevertheless, by comparing the direction of current flow near the anode surface, as indicated by the enclosed current contours, with the direction of the anode region field, Hall parameters between 0.5 and 2 are estimated over much of the anode region.

Looking first at the lip region of the anode where n_e should be approximately 10^{14} cm^{-3} and T_e is about 2 eV, the ratio of Joule-heating to electron conduction becomes

$$\left[\frac{(\Delta j_{eA})_J}{(\Delta j_{eA})_c}\right]_{\text{ANODE LIP}} \approx (1+\Omega_e^2)/2 \qquad (7\text{-}20)$$

Thus, it appears that $\Omega_e \approx 1$, which characterizes the transition regime between scalar and Hall conduction, also implies a condition at the anode lip wherein the Joule-heating and electron conduction mechanisms assume almost equal importance in maintaining the required electron flux to the anode surface at the starved condition.

At the front face of the anode, the magnetic fields drop off by factors of at least two to seven, depending on the distance from the anode lip; since Ω_e is relatively constant over most of the region in question (see Fig. 7-3), Eq. (7-2) requires that the electron density must decrease by similar amounts. The electron temperature may also decrease at the front anode but not sufficiently to compensate for the substantial decrease in n_e; therefore the ratio $(\Delta j_{eA})_J/(\Delta j_{eA})_c$, given by Eq. (7-19), yields at the front face of the anode,

$$\left[\frac{(\Delta j_{eA})_J}{(\Delta j_{eA})_c}\right]_{\text{ANODE FACE}} \approx .3$$

This result implies, for this low density, low magnetic field region of the anode, that an increase in the electron flux to the anode surface at mass starvation is more effectively accomplished by the process of electron conduction than by that of Joule-heating. This conclusion is also physically intuitive since the low plasma densities tend to discriminate against the ionization mechanism, while the weak magnetic fields encourage current conduction in a direction parallel to the anode field, i.e., towards the anode surface.

An analogy between the quasi-steady MPD arc anode, whose current demands are satisfied simply by random thermal electron flux from the adjacent arc plasma, and a Langmuir probe, which is operating at the electron saturation point of the probe characteristic, is suggested. Several elaborate collisionless theories have been developed to describe the sheath growth around a probe tip which is forced to draw more than the saturation, or random thermal, electron current.[44] One may speculate that the anode field growth observed at the starved mass flow, or low plasma density, condition is in fact an electron capture sheath similar to that formed around an electron attracting probe tip. Should this be true, Langmuir probe theories could be used to describe the anode field region of the starved quasi-steady MPD arc. However, calculations of Debye length and collision mean free paths in the MPD arc plasma reveal that both are several orders of magnitude smaller than the anode field envelope. Hence, the process of anode field growth at mass starvation is in no way similar to the collisionless Debye sheath which grows around Langmuir probe tips attempting to draw more than the saturation electron current.

C. SUMMARY

It has been shown, for the quasi-steady MPD arc at matched and overfed mass flows, that anode current conduction is accomplished by the random thermal flux of electrons from the adjacent arc plasma. At conditions of mass starvation,

substantial electric fields develop around the anode. It is proposed that the random thermal electron flux is insufficient, at this low mass flow, low plasma density situation, to carry the necessary anode current, and hence these anode region fields are formed to maintain the electron flux to the anode surface at values consistent with the arc current demands. In the anode lip region of the arc, the processes of electron tensor conduction and Joule-heating of the plasma both contribute to this task, whereas at the front face of the anode, the electron conduction mechanism appears to dominate.

CHAPTER VIII

SUMMARY AND CONCLUSIONS

A study of anode phenomena in high-current arc discharges has been carried out under several different experimental situations employing various electrode geometries, arc current levels, and current pulse durations. The unifying aspect of these experiments, on several rather different plasma accelerators, has been the common goal of achieving more effective plasma acceleration through the understanding of the various physical processes occurring at the anode of these devices. Specifically, the pulsed or unsteady mode of gas acceleration was studied in both cylindrical pinch and parallel-plate geometries at current levels from 120 to 300 kA, pulse durations from 3.5 to 20 μsec, and ambient argon pressures of 100 μ. The quasi-steady mode of accelerator operation, in a coaxial MPD arc geometry at current levels from 4.4 to 42.0 kA and argon mass flows from 1.2 to 36.0 g/sec, was also examined in detail.

First, investigations of current sheet behavior in the large-radius pinch discharge and parallel-plate accelerator have revealed that the narrow current distribution begins to deform at the anode surface into a broad, diffuse, and sometimes divided "anode foot." At later times, a similar structure, though somewhat less pronounced, develops at the cathode, and this "cathode foot" lags behind the anode attachment as the current sheet propagates inward or along the electrode channel. A random, filamentary "current spoke" has been observed at the anode of the pinch discharge, and combined with irreproducible probe signals in this part of the chamber, indicates an uncertain or unstable domain of current conduction. A similar con-

duction difficulty is encountered, at underfed mass flows, in the anode region of the quasi-steady MPD arc, as indicated by excessive noise and irreproducibility of magnetic and electric probe data. These observations may also imply substantial power dissipation in the anode region of both the pinch and MPD discharges.

In addition to the main current distribution in the pulsed accelerators, a less obvious but equally important region of current conduction appears to form at the electrode surfaces considerably downstream of the current sheet. The pinch discharge experiments show that this precursor conduction occurs mainly at the anode surface, but the longer time scale parallel-plate experiments reveal that the cathode also participates in this downstream current conduction, although to a lesser degree. A qualitative argument, based on the relative mobilities of electrons and ions, was presented to explain the slower growth rates of cathode conduction processes compared to those at the anode. However, the real significance of precursor current conduction is its apparent relation to the power dissipation of pulsed accelerators. More explicitly, the resistive arc voltage of both the pinch and parallel-plate devices was found to increase sharply when precursor anode conduction was impeded by mylar insulation; similar interruption of precursor cathode conduction in the parallel-plate device induced a somewhat less severe increase in resistive voltage drop. From results of this nature, it can be proposed that the thermal efficiencies of pulsed plasma accelerators should decrease with a decrease in electrode area, with the effect being more strongly dependent on a decrease in anode area. A very different result was discovered from experiments on the quasi-steady MPD arc wherein the anode fall voltage tends to decrease with increasing local anode current density, thus implying that higher thermal efficiencies may, in fact, be achieved by decreasing the anode size.

Floating potential measurements on the 8-in. pinch discharge revealed that almost all of the resistive arc voltage

drop occurs within about 1/2 in. of the anode surface, with a sizable portion of this voltage appearing adjacent to the surface. These data imply that most of the power dissipation in this device takes place near the anode; this observation carries over to the quasi-steady MPD arc, where detailed potential patterns indicate that the anode is a major source of power loss, while most of the actual plasma acceleration takes place in the cathode region of the arc.

As pointed out in Chap. I, high power quasi-steady MPD arcs appear to promise high efficiency, high specific impulse, high thrust density plasma acceleration; certain results of the present study speak directly to the high thermal efficiency of these devices. For example, an apparent inverse dependence of anode fall voltage on local anode current density was observed for matched quasi-steady operation of the MPD facility at current levels of 8.7, 17.5, and 42.0 kA. When the empirical relationship, $V_A \approx 1.5 \times 10^7/j_A$ (mks), was used in a computation of the fractional anode power loss, the results predict a decrease from over 50% to less than 10% when the total arc power is increased from 1 to 10 mW. These calculations were based on the assertion that the electron current is the major cause of anode heat transfer, whereas convective and radiative losses at the anode are much less significant.

Finally, the importance of mass flow rate to the overall characteristics of the quasi-steady MPD discharge, in particular to the arc behavior in the anode region, was determined. Namely, at matched and overfed argon mass flows, the electric fields, except for those in the acceleration region near the cathode, are confined to a narrow region at the anode surface; and anode current conduction is accomplished simply by random thermal electron flux from the adjacent arc plasma. However, at underfed mass flows substantial fields develop around the anode. Approximate calculations indicate that these fields help to maintain the required electron flux to the lip region of the anode by establishing both Joule-heating of the plasma and tensor electron conduction; at the front face of the anode,

electron conduction appears to be the dominant mechanism for producing the requisite electron flux. The power deposited in this anode field envelope probably appears as an increase in fractional anode power loss; in any event, it is responsible for a decrease in the thermal efficiency of the accelerator at the underfed condition. Hence, the available data imply that high-efficiency plasma acceleration can be accomplished by quasi-steady MPD operation in the megawatt range of pulse power, provided that sufficiently high propellant mass flow is supplied to avoid the formation of electric fields in the anode region of the arc.

Appendix

CONTRIBUTION OF ELECTRON THERMAL ENERGY TO ANODE HEAT TRANSFER

For some time there have been conflicting opinions regarding the magnitude of one of the terms appearing in the anode heat transfer expression generally applied to MPD arcjets.[59–62,13] The expression is usually written in the following form,

$$Q_A = Q_{RA} + Q_{CA} + J(5kT_e/2e + V_A + \Phi_A) \qquad (A\text{-}1)$$

where Q_A is total heat transferred to the anode and Q_{RA}, Q_{CA} are the heat transferred by radiation and convection. The third term represents the energy carried to the anode by the electrons which are presumed to carry most of the current and V_A is anode fall voltage, Φ_A is work function of metallic anode, and T_e is electron temperature.

In question is the numerical coefficient of the first term in the bracket which represents the thermal energy transported to the anode, per current-carrying electron. Some authors prefer the value $2kT_e/e$, arguing that the electron pressure contributes only $1/2kT_e$ to the enthalpy term because only one-half of the electron distribution is absorbed by the anode. Hence

$$Q_{Ae} = \frac{J}{e} h_e = \frac{J}{e} (\mathcal{E} + P_e/\delta_e) \qquad (A\text{-}2)$$

$$= \frac{J}{e} (3/2kT_e + 1/2kT_e)$$

$$= J\ (2kT_e/e)$$

where h_e is electron specific enthalpy and P_e, δ_e are electron pressure and density.

We shall now look at this problem from a particle flux point of view and discover that both of these forms have some supporting evidence but that the stronger arguments point to $5kT_e/2e$ as the correct form.

First, let us assume that the electrons have a normal Maxwell-Boltzmann distribution at the edge of the anode sheath, and that all electrons having velocities directed towards the anode are captured by the voltage drop of the fall and absorbed by the anode. Defining the positive x-direction as the inward normal to the anode surface, we can write the energy per unit area carried to the anode by electrons:

$$q_{Ae} = \int_0^\infty \int_{-\infty}^{\infty} \int_{-\infty}^{\infty} \left(\frac{m_e}{2} v_e^2\right) v_x \, dn_e$$

$$= \frac{m_e}{2} n_e \left(\frac{m_e}{2\pi kT_e}\right)^{3/2} \int_0^\infty \int_{-\infty}^{\infty} \int_{-\infty}^{\infty} v_x (v_x^2 + v_y^2 + v_z^2) \tag{A-3}$$

$$\cdot e^{-m_e/2kT_e (v_x^2 + v_y^2 + v_z^2)} \, dv_x dv_y dv_z$$

With reference to standard integral tables the result is

$$q_{Ae} = \frac{\pi n_e m_e}{2} \left(\frac{2kT_e}{\pi m_e}\right)^{3/2} \tag{A-4}$$

The flux of electrons to the anode is given by a similar

integral

$$\frac{j_{Ae}}{e} = n_e\left(\frac{m_e}{2\pi kT_e}\right)^{3/2} \int_0^{\infty}\int_{-\infty}^{\infty}\int_{-\infty}^{\infty} v_x e^{-m_e/2kT_e(v_x^2 + v_y^2 + v_z^2)}\, dv_x dv_y dv_z \tag{A-5}$$

$$= \frac{n_e \bar{c}}{4} = \frac{n_e}{2}\left(\frac{2kT_e}{\pi m_e}\right)^{\frac{1}{2}}$$

Using this result in our previous expression we then find that

$$q_{Ae} = j_{Ae}(2kT_e/e) \tag{A-6}$$

which can be integrated over the anode area to give

$$Q_{Ae} = J(2kT_e/e) \tag{A-7}$$

In the second approach we employ a Maxwellian distribution for the electrons that has been shifted by the electron drift velocity so that there is now a net average motion of electrons towards the anode. The particle integration is carried out at a surface near the anode sheath edge but nevertheless in a region where electrons can cross the surface in both directions. If one assumes that there is no electron heat flux through the side boundaries of the arc then the heat flux across the surface equals that entering the anode. The positive x-direction is defined in the same way as before, but the integration is now carried out over <u>all</u> particles. The electron heat flux is now given by

$$q_{Ae} = \frac{m_e}{2} m_e\left(\frac{m_e}{2\pi kT_e}\right)^{3/2} \int_{-\infty}^{\infty}\int_{-\infty}^{\infty}\int_{-\infty}^{\infty} v_x(v_x^2 + v_y^2 + v_z^2) \cdot e^{-m_e/2kT_e[(v_x - u)^2 + v_y^2 + v_z^2]}\, dv_x dv_y dv_z \tag{A-8}$$

$$= 1/2m_e n_e \left(\frac{m_e}{2\pi kT_e}\right)^{\frac{1}{2}} \int_{-\infty}^{\infty} v_x^3 \, e^{-m_e/2kT_e (v_x - u)^2} \, dv_x + kT_e n_e u$$

After making the change of variables $\eta = v_x - u$ the integral transforms to

$$q_{Ae} = 1/2m_e n_e \left(\frac{m_e}{2\pi kT_e}\right)^{\frac{1}{2}} \int_{-\infty}^{\infty} (\eta^3 + 3u\eta^2 + 3u^2\eta + u^3) \, e^{-m_e/2kT_e \eta^2} \, d\eta + kT_e n_e u \tag{A-9}$$

Again referring to the tables and employing symmetry arguments, the final form becomes

$$\begin{aligned} q_{Ae} &= 3/2kT_e n_e u + 1/2 n_e m_e u^3 + kT_e n_e u \\ &= 5/2 \frac{kT_e}{e} n_e eu + 1/2 \frac{m_e u^2}{e} n_e eu \end{aligned} \tag{A-10}$$

By physical reasoning or by carrying out the integration for electron flux density across the imaginary surface

$$\frac{j_e}{e} = \int_{-\infty}^{\infty} \int_{-\infty}^{\infty} \int_{-\infty}^{\infty} v_x \, dn_e = n_e u \tag{A-11}$$

Hence our expression for the electron energy flux density becomes,

$$q_{Ae} = j_{Ae} \left(5/2 \frac{kT_e}{e} + 1/2 \frac{m_e u^2}{e} \right) \tag{A-12}$$

Realizing that electron thermal energies are much greater than their drift energy for our plasma, and integrating

this expression over the surface area we arrive at

$$Q_{Ae} = J(5kT_e/2e) \qquad \text{(A-13)}$$

which is the most frequently quoted form of the electron energy flux to the anode.

As derived, the difference between the two calculated forms of Q_{Ae} is seen to arise from the presumption of the first method that an isotropic Maxwellian distribution exists at the edge of the anode sheath. In view of the steady demand for delivery of electrons of one velocity sign to the sheath, this assumption is untenable in this geometry in the steady state. To maintain such a condition, the sheath edge would need to recede from the anode surface as time progressed. The second method makes no such presumption, hence yields the proper result.

REFERENCES

[1]Jahn, R. G., Physics of Electric Propulsion, McGraw-Hill Book Company, New York (1968), Chap. 1.

[2]Black, N. A. and R. G. Jahn, "On the Dynamic Efficiency of Pulsed Plasma Accelerators," AIAA Journal, Vol. 3, No. 6, June 1965, pp. 1209-1210.

[3]Clark, K. E. and R. G. Jahn, "Quasi-Steady Plasma Acceleration," AIAA Journal, Vol. 8, No. 2, Feb. 1970, pp. 216-220.

[4]Jahn, R. G., K. E. Clark, R. C. Oberth, and P. J. Turchi, "Acceleration Patterns in Quasi-Steady MPD Arcs," AIAA Paper 70-165, AIAA 8th Aerospace Sciences Meeting, New York, N. Y., 19-21 Jan. 1970.

[5]Clark, K. E., "Quasi-Steady Plasma Acceleration," Ph.D. thesis, May 1969, Princeton Univ., Princeton, N. J.

[6]Schoeck, P. A., "An Investigation of the Energy Transfer to the Anode of a High Intensity Arc in Argon," Ph.D. thesis, 1961, Univ. of Minnesota, Minneapolis, Minn.

[7]Schneiderman, A. M. and R. M. Patrick, "Optimization of the Thermal Efficiency of the Magnetic Annular Arc," AIAA Paper 66-115, AIAA 3rd Aerospace Sciences Meeting, New York, N. Y., 24-26 Jan. 1966.

[8]Ducati, A. C., E. Muehlberger, and R. P. Treat, "Arcjet Efficiency in an Insulated Test Environment," AIAA Paper 67-677, AIAA Electric Propulsion and Plasmadynamics Conference, Colorado Springs, Colo., 11-13 Sept. 1967.

[9]Shih, K. T., E. Pfender, W. E. Ibele, and E. R. G. Eckert, "Experimental Studies of the Electrode Heat Transfer in a MPD Arc Configuration," AIAA Paper 67-673, AIAA Electric Propulsion and Plasmadynamics Conference, Colorado Springs, Colo., 11-13 Sept. 1967.

[10]Nerheim, N. M. and A. J. Kelly, "A Critical Review of the State-of-the-Art of the MPD Thruster," AIAA Paper 67-688, AIAA Electric Propulsion and Plasmadynamics Conference, Colorado Springs, Colo., 11-13 Sept. 1967.

[11]Ecker, G., "Electrode Components of the Arc Discharge," Ergebnisse Der Exakten Naturwissenschaften, Vol. XXXIII, Springer-Verlag, Berlin, 1961.

[12]Shih, K. T. and E. Pfender, "Electrode Energy Transfer Mechanisms in a MPD Arc," AIAA Journal, Vol. 8, No. 2, Feb. 1970, pp. 211-215.

REFERENCES

[13]Bose, T. K. and E. Pfender, "Direct and Indirect Measurements of the Anode Fall in a Coaxial Arc Configuration," AIAA Journal, Vol. 7, No. 8, Aug. 1969, pp. 1643-1645.

[14]Shih, K. T., "Anode Current and Heat Flux Distribution in an MPD Engine," AIAA Journal, Vol. 8, No. 2, Feb. 1970, pp. 377-378.

[15]Black, N. A., "Dynamics of a Pinch Discharge Driven by a High-Current Pulse-Forming Network," Ph.D. thesis, May 1966, Princeton Univ., Princeton, N. J.

[16]Jahn, R. G. et al., "Pulsed Electromagnetic Gas Acceleration," NASA NsG-306-63 progress report for the period 1 Jan. 1967 to 30 June 1967, Aerospace and Mechanical Sciences Rept. No. 634i, July 1967, Princeton Univ., Princeton, N. J.

[17]Somerville, J. M., The Electric Arc, Methuen and Co. Ltd., London, 1959, Chap. 3.

[18]Bez, W. and K. H. Höcker, "Theorie Des Anodenfalls I," Zeitschrift Fur Naturforschung, Vol. 9a, 1954, pp. 72-81.

[19]Höcker, K. H. and W. Bez, "Theorie Des Anodenfalls II," Zeitschrift Fur Naturforschung, Vol. 10a, 1955, pp. 706-714.

[20]Bez, W. and K. H. Höcker, "Theorie Des Anodenfalls III," Zeitschrift Fur Naturforschung, Vol. 10a, 1955, pp. 714-717.

[21]Bez, W. and K. H. Höcker, "Theorie Des Anodenfalls IV," Zeitschrift Fur Naturforschung, Vol. 11a, 1956, pp. 118-123.

[22]Bez, W. and K. H. Höcker, "Theorie Des Anodenfalls IV," Zeitschrift Fur Naturforschung, Vol. 11a, 1956, pp. 192-196.

[23]Block, M. J. and W. Finkelnburg, "Uber Die Axiale Ausdehnung Des Anodenfallgebiets Beim Kohlelichtbogen," Zeitschrift Fur Naturforschung, Vol. 8a, 1953, p. 758.

[24]Busz-Peuckert, G. and W. Finkelnburg, "Thermische Lichtbogen Hoher Temperatur Und Niedriger Brennspannung," Zeitschrift Fur Physik, Vol. 139, 1954, p. 212.

[25]Schoeck, P. A., E. R. G. Eckert, and S. A. Wutzke, "An Investigation of the Anode Losses in Argon Arcs and Their Reduction by Transpiration Cooling," ARL Rept. 62-341, April 1962.

[26]Finkelnburg, W. and H. Maecker, "Electric Arcs and Thermal Plasmas," Handbuch Der Physik, Vol. XXII, Springer-Verlag, Berlin, 1956.

REFERENCES

[27]Eckert, E. R. G., "Survey on Heat Transfer at High Speeds," WADC Tech. Rept. 54-70, April 1954.

[28]Pfender, E., G. D. Raithby, and E. R. G. Eckert, "An Anode Comparison Study in a Wall Stabilized Argon Arc," ARL Rept. 65-232, Nov. 1965.

[29]Lie, T. N., A. W. Ali, and C. C. Chang, "Diagnostics of Accelerating Plasma," Dept. of Space Science and Applied Physics Rept. 67-029, Aug. 1967, Catholic Univ. of America, Washington, D. C.

[30]Johansson, R. B., "Current Sheet Tilt in a Radial Magnetic Shock Tube," The Physics of Fluids, Vol. 8, No. 5, May 1965, pp. 866-871.

[31]McLelland, J. R., A. S. V. MacKenzie, and J. Irving, "Schlieren Photography of Rail-Tube Plasmas," The Physics of Fluids, Vol. 9, No. 8, Aug. 1966, pp. 1613-1615.

[32]Lovberg, R. H., "Investigation of Current Sheet Microstructure," AIAA Journal, Vol. 4, No. 7, July 1966, pp. 1215-1222.

[33]Lovberg, R. H., "Acceleration of Plasma by Displacement Currents Resulting From Ionization," Proceedings of VI International Conference on Ionization Phenomena in Gases, Paris, 1963, Vol. IV, pp. 235-239.

[34]Kislov, A. Ya., A. I. Morozov, and G. N. Tilinin, "Distribution of Potential in a Quasi-Stationary Coaxial Injector," Soviet Physics-Technical Physics, Vol. 13, No. 6, Dec. 1968, pp. 736-738.

[35]Kovrov, P. E., A. I. Morozov, L. G. Tokarev, and G. Ya. Shchepkin, "Magnetic Field Distribution in a Coaxial Plasma Injector," Soviet Physics-Doklady, Vol. 12, No. 2, Aug. 1967, pp. 155-157.

[36]Karkosak, J. J. and M. A. Hoffman, "Electrode Drops and Current Distributions in an MGD Channel," AIAA Journal, Vol. 3, No. 6, June 1965, pp. 1198-1200.

[37]Damman, H., G. Kleist, U. Kogelschatz and W. Botticher, "Anodennahe Vorlaufer Elektromagnetisch Angetriebener Konvergenter Zylinderstosswellen," Zeitschrift Fur Naturforschung, Vol. 24a, Dec. 1969, pp. 1931-

[38]Jahn, R. G. and W. F. Von Jaskowsky, "Current Distributions in Large-Radius Pinch Discharges," AIAA Journal, Vol. 2, No. 10, Oct. 1964, pp. 1749-1753.

REFERENCES

[39]Jahn, R. G., W. F. Von Jaskowsky, and A. L. Casini, "Gas-Triggered Pinch Discharge Switch," The Review of Scientific Instruments, Vol. 36, No. 1, Jan. 1965, pp. 101-102.

[40]Leonard, S. L., "Basic Macroscopic Measurements," Plasma Diagnostic Techniques, edited by Huddlestone, R. H. and S. L. Leonard, Academic Press, New York, 1965, pp. 8-15.

[41]Eckbreth, A. C., "Current Pattern and Gas Flow Stabilization in Pulsed Plasma Accelerators," Ph.D. thesis, Dec. 1968, Princeton Univ., Princeton, N. J.

[42]Eckbreth, A. C. and R. G. Jahn, "Current Pattern and Gas Flow Stabilization in Pulsed Plasma Accelerators," AIAA Journal, Vol. 8, No. 1, Jan. 1970, pp. 138-143.

[43]Jahn, R. G. and K. E. Clark, "A Large Dielectric Vacuum Facility," AIAA Journal, Vol. 4, No. 6, June 1966, p. 1135.

[44]Chen, F. F., "Electric Probes," Plasma Diagnostic Techniques, edited by Huddlestone, R. H. and S. L. Leonard, Academic Press, New York, 1965.

[45]Burton, R. L., "Structure of the Current Sheet in a Pinch Discharge," Ph.D. thesis, Sept. 1966, Princeton Univ., Princeton, N. J.

[46]Kolpin, M. A., "Experimental Study of the Dynamics of a Large Inverse Pinch," AIAA Journal, Vol. 5, No. 6, June 1967, pp. 1159-1167.

[47]French, J. B., "Langmuir Probes in a Flowing Low Density Plasma," U.T.I.A. Rept. 79, Aug. 1961.

[48]Laframboise, J. G., "Theory of Spherical and Cylindrical Langmuir Probes in a Collisionless, Maxwellian Plasma at Rest," U.T.I.A.S. Rept. 100, June 1966.

[49]Jahn, R. G. et al., "Pulsed Electromagnetic Gas Acceleration," NASA NGL 31-001-005 progress report for the period 1 Jan. 1970 to 30 June 1970, Aerospace and Mechanical Sciences Rept. 634o, July 1970, Princeton Univ., Princeton, N. J.

[50]Turchi, P. J., "The Cathode Region of the Quasi-Steady MPD Arcjet," Ph.D. Thesis, Sept. 1970, Princeton Univ., Princeton, N. J.

[51]Shih, K. T. and R. Dethlefsen, "Anode Heat Flux Density of High-Current Arcs," A.S.M.E. Paper 69-WA/HT-57, A.S.M.E. Winter Annual Meeting, Los Angeles, Calif., 16-20 Nov. 1969.

REFERENCES

[52]Cory, J. S., Princeton University, private communication.

[53]Devoto, R. S., "Transport Coefficients of Partially Ionized Argon," The Physics of Fluids, Vol. 10, No. 2, Feb. 1967, pp. 354-364.

[54]Drellishak, K. S., C. F. Knapp, and A. B. Cambel, "Partition Functions and Thermodynamic Properties of Argon Plasma," AEDC Rept. TDR-63-146, Aug. 1963.

[55]Bosnjakovic, F., W. Springe, K. F. Knoche, and P. Burgholte, "Mollier Enthalpy-Entropy Charts for High-Temperature Plasmas," Thermodynamics and Transport Properties of Gases, Liquids, and Solids, ASME, McGraw-Hill, New York, 1959, pp. 465-472.

[56]Spitzer, Jr., L., Physics of Fully Ionized Gases, Interscience Publishers, New York, 1962, Chap. 3.

[57]Kalikhman, L. E., "Elements of Magnetogasdynamics, W. B. Saunders Co., Philadelphia, Pa., 1967, pp. 9-16.

[58]von Engel, A. and M. Steenbeck, Electrische Gasentladungen, Springer-Verlag, Berlin, 1932.

[59]Hassan, H. A. and G. W. Garrison, "Anode Losses in Coaxial Hall Current Accelerators," AIAA Journal, Vol. 5, No. 2, May 1967, pp. 840-843.

[60]Aisenberg, S., P. Hu, V. Rohatgi, and S. Ziering, "Plasma Boundary Interactions," NASA CR-868, Aug. 1967.

[61]Shih, K. T., E. Pfender, W. E. Ibele, and E. R. G. Eckert, "Experimental Anode Heat-Transfer Studies in a Coaxial Arc Configuration," AIAA Journal, Vol. 6, No. 8, Aug. 1968, pp. 1482-1487.

[62]Seikel, G. R. et al., "Plasma Physics of Electric Rockets," in "Plasmas and Magnetic Fields in Propulsion and Power Research," NASA SP-226, Oct. 1969, pp. 1-64.